REPORT DOCUMENTATION PAGE

AFRL-SR-AR-TR-04-

0218

1. REPORT DATE *(DD-MM-YYYY)*	2. REPORT TYPE	3. DATES COVERED *(From - To)*
	Final Report	1/1/00 - 1/31/04

4. TITLE AND SUBTITLE
Electrodeposition of Transition Metal-Aluminum Alloys from Chloroaluminate Molten Salts

5a. CONTRACT NUMBER

5b. GRANT NUMBER
F49620-00-1-0123

5c. PROGRAM ELEMENT NUMBER

6. AUTHOR(S)
Dr. Charles L. Hussey
Professor and Chairman

5d. PROJECT NUMBER

5f. WORK UNIT NUMBER

7. PERFORMING ORGANIZATION NAME(S) AND ADDRESS(ES)
Department of Chemistry and Biochemistry
The University of Mississippi
P.O. Box 1848
University, MS 38677

8. PERFORMING ORGANIZATION REPORT NUMBER

20040423 032

9. SPONSORING / MONITORING AGENCY NAME(S) AND ADDRESS(ES)
Air Force Office of Scientific Research
4015 Wilson Blvd
Arlington, VA 22203-1954

10. SPONSOR/MONITOR'S ACRONYM(S)
AFOSR

11. SPONSOR/MONITOR'S REPORT NUMBER(S)

12. DISTRIBUTION / AVAILABILITY STATEMENT
Approve For Public Release: Distribution unlimited.

13. SUPPLEMENTARY NOTES

14. ABSTRACT
The electrodeposition of transition metal aluminum alloys was investigated in the room-temperature chloroaluminate ionic liquid, aluminum chloride-1-methyl-3-ethylimidazolium chloride. Alloys that were investigated include the binary systems, Cu-Al, Ag-Al, Al-Ti, Al-V, Al-Mo, Al-Zr, Al-Nb, and Al-W, and the ternary system Al-Mo-Mn. Those alloys in which the transition metal predominates, Ag-Al and Cu-Al, were thermodynamically unstable in the plating bath and did not form chloride-free, compact coatings during electrodeposition. However, those alloys in which the transition metal was a minor component, e.g., Al-Ti, Al-V, Al-Mo, Al-Zr, Al-Nb, and Al-W, were electrodeposited as compact, nearly specular films. Many of these alloys, notably Al-Mo and Al-W, exhibited outstanding resistance to chloride-induced pitting corrosion, making them useful corrosion protective coatings for Air Force applications in high-salt environments.

15. SUBJECT TERMS

16. SECURITY CLASSIFICATION OF:			17. LIMITATION OF ABSTRACT	18. NUMBER OF PAGES	19a. NAME OF RESPONSIBLE PERSON
a. REPORT	b. ABSTRACT	c. THIS PAGE			19b. TELEPHONE NUMBER *(include area code)*
N/A	N/A	N/A		26+appendices	

FINAL REPORT
AFOSR Grant F49620-00-1-0123
(2000-2004)

Electrodeposition of Transition Metal-Aluminum Alloys from Chloroaluminate Molten Salts

Principal Investigator:

Charles L. Hussey
Chair and Professor
Department of Chemistry and Biochemistry
University of Mississippi
P.O. Box 1848
University, MS 38677

Phone: 662-915-7301
FAX: 662-915-7300
E-mail: chclh@chem1.olemiss.edu

Table of Contents

2. Project Objectives

Aluminum is a reactive metal that survives in the environment by the formation of a passive surface film. Anions such as chloride can adsorb on this film and accelerate is dissolution, leading to the formation of pits in the underlying metal surface, i.e., chloride pitting corrosion. The corrosion resistance of aluminum can be greatly enhanced by alloying with solute metals, especially the transition elements, at concentrations greatly exceeding their normal equilibrium solubilities. A variety of non-equilibrium alloying techniques, e.g., melt spinning, ion implantation, reactive plasma spraying, and sputter deposition, have been devised to prepare these "stainless" aluminum alloys as they are sometimes called, but these techniques are inferior to electrodeposition methods because they are difficult to apply to objects with three dimensional surfaces.

Aluminum cannot be electrodeposited from aqueous solutions because hydrogen is generated before aluminum can be deposited. Thus, aluminum and its alloys can only be electroplated from nonaqueous solutions or molten salts. Some of the solvent systems that are used for this purpose include mixtures of aluminum hydrides such as AlH_4 or $LiAlH_3$ and $AlCl_3$ dissolved in aliphatic ethers and mixtures of aluminum trialkyl compounds and either alkali metal or tetraalkylammonium halides dissolved in aromatic hydrocarbons. These latter plating solutions are toxic and pyrophoric. Chloroaluminate molten salts, which consist of aluminum chloride mixed with an inorganic chloride salt such as sodium chloride (~ 175 °C) or an organic chloride salt such as 1-ethyl-3-methylimidazolium chloride (~ 25 °C), constitute a concentrated reservoir of reducible aluminum. Aside from their sensitivity to moisture, these ionic solvents are relatively non-toxic and easy to handle.

The broad objective of this project was to investigate the electrodeposition of transition metal-aluminum alloys from chloroaluminate molten salts, particularly those that are liquid at room temperature. Included in this objective were the following goals: to identify and characterize new alloys that can be prepared in these melts, to understand the electrochemical mechanism by which aluminum-transitional metal alloys are formed, to determine the factors that affect the structure, morphology, and composition of these alloys, to examine the corrosion resistance of alloys that show promise for industrial applications, and to improve the in-situ

electrochemical methods that are used to analyze electrodeposited alloys. To this end we have succeeded in preparing a number of binary aluminum-transition metal alloys that show considerable resistance to chloride-induced pitting corrosion compared to aluminum, we have developed pulse-plating technology that can be used to electroplate compact aluminum alloy deposits, and we have further refined a rotating-ring disk voltammetry technique for the in situ analysis of electrodeposited alloys that was invented in our laboratory. The main DoD payoff for this project is the development of a low temperature method for making corrosion-resistant aluminum coatings on aircraft parts that are frequently exposed to chloride environments, e.g., aircraft landing gear and structural parts.

3. Publications

a. Q. Zhu and C. L. Hussey, "Electrodeposition of Silver-Aluminum Alloys from a Room-Temperature Chloroaluminate Molten Salt," *J. Electrochem. Soc.*, **148**, C88 (2001).

b. Q. Zhu and C. L. Hussey, "Galvanostatic Pulse Plating of Cu-Al Alloy in a Room-Temperature Chloroaluminate Melt. Rotating Ring-Disk Electrode Studies," *J. Electrochem. Soc.*, **148**, C395 (2001).

c. G. R. Stafford and C. L. Hussey, "Electrodeposition of Transition Metal-Aluminum Alloys from Chloroaluminate Molten Salts," in *Advances in Electrochemical Science and Engineering*, Vol. 6, R. C. Alkire and D. M. Kolb, Editors, Wiley-VCH Publishers, Weinheim, (2002).

d. Q. Zhu, C. L. Hussey, and G. R. Stafford, "Galvanostatic Pulse Plating of Bulk Cu-Al Alloys on Nickel Electrodes from Room-Temperature Chloroaluminate Molten Salts Containing Benzene," *J. Electrochem. Soc.*, **149**, C268 (2002).

e. G. R. Stafford, V. D. Jovic, T.P. Moffat, Q. Zhu, S. Jones, and C. L. Hussey, "The Electrodeposition of Al-Cu Alloys from Room-Temperature Chloroaluminate Electrolytes,"

Proc. Twelfth Intl. Symp. Molten Salts, **PV 99-41**, 535-548 (2000), The Electrochemical Society, Inc., Pennington, NJ.

f. T. Tsuda, C. L. Hussey, G. R. Stafford, and J. Bonevich, "Electrochemistry of Titanium and the Electrodeposition of Ti-Al Alloys in the Lewis Acidic Aluminum Chloride-1-Ethyl-3-methylimidazolium Chloride Melt," *J. Electrochem. Soc.*, **150**, C234 (2003).

g. T. Tsuda and C. L. Hussey, "Electrochemistry of Vanadium(II) and the Electrodeposition of Aluminum-Vanadium Alloys in the Aluminum Chloride-1-Ethyl-3-methylimidazolium Chloride Molten Salt," *Journal of Mining and Metallurgy,* **39B**, 3 (2003).

h. T. Tsuda and C. L. Hussey, "Electrodeposition of Aluminum-Vanadium Alloys from the from the Aluminum Chloride-1-Methyl-3-ethylimidazolium Chloride Molten Salt," *Proc. Symp. Magnetic Materials, Processes, and Devices VII and Electrodeposition of Alloys*, **PV 2002-27** (2003), The Electrochemical Society, Inc., Pennington, NJ.

i. G. R. Stafford, T. Tsuda, and C. L. Hussey, "Order/Disorder in Electrodeposited Aluminum-Titanium Alloys," *Journal of Mining and Metallurgy,* **39B**, 23 (2003).

j. T. Tsuda, C. L. Hussey, G. R. Stafford, and O. Kongstein, "Electrodeposition of Aluminum-Molybdenum Alloys from a Low-Temperature Organic Chloroaluminate Salt," *J. Electrochem. Soc.*, **151**, xx (2004).

k. T. Tsuda, C. L. Hussey, and G. R. Stafford, "Electrodeposition of Aluminum-Zirconium Alloys from the Lewis Acidic Aluminum Chloride-1-Ethyl-3-methylimidazolium Chloride Molten Salt," *J. Electrochem. Soc.*, **151**, xx (2004).

l. T. Tsuda, C. L. Hussey, and G. R. Stafford, "Electrodeposition of Aluminum-Manganese-Molybdenum Alloys from the Lewis Acidic Aluminum Chloride-1-Ethyl-3-methylimidazolium Chloride Melt", *Electrochim. Acta,* in preparation

m. T. Tsuda, C. L. Hussey, and G. R. Stafford, "Electrodeposition of Aluminum-Hafnium Alloys from the Lewis Acidic Aluminum Chloride-1-Ethyl-3-methylimidazolium Chloride Molten Salt," *Electrochim. Acta,* in preparation.

n. T. Tsuda, W. E. Cleland, C. L. Hussey, and G. R. Stafford, "Electrochemistry of Tungsten Species and Electrodeposition of Al-W Alloys from the Lewis Acidic Aluminum Chloride-1-Ethyl-3-methylimidazolium Chloride Melt," *J. Electrochem. Soc.,* in preparation.

4. Invited and Contributed Presentations

a. "Galvanostatic Pulse Plating of Cu-Al Alloy in a Room-Temperature Chloroaluminate Melt. Rotating Ring-Disk Electrode Studies," 52nd Southeast/56th Southwest Combined regional Meeting of the American Chemical Society, New Orleans , LA, December 6-8, 2000. **(Abstract # 43)**

b. "Galvanostatic Pulse Plating of Cu-Al Alloy from the Lewis Acidic Aluminum Chloride-1-Ethyl-3-methylimidazolium Chloride Melt," 199th Meeting of the Electrochemical Society, Washington, DC, March 25-29, 2001.

c. "Electrodeposition of Titanium-Aluminum Alloys from Lewis Acidic $AlCl_3$-1-Ethyl-3-methylimidazolium Chloride Melts," 201st Meeting of the Electrochemical Society, Philadelphia, PA, May 12-17, 2002.

d. "Electrodeposition of Vanadium-Aluminum Alloys in Lewis Acidic $AlCl_3$-EtMeImCl Melt Containing $EtMeImBF_4$," Symposium on Magnetic Materials, Processes, and Devices VII and Electrodeposition of Alloys, 202nd Meeting of The Electrochemical Society, Salt Lake City, Utah, October 20-24, 2002 (invited).

e. "Electrode Reactions of Group 4 Transition Metal Ions in Lewis Acidic $AlCl_3$-EtMeImCl Ionic Liquids," 204th Meeting of the Electrochemical Society, Orlando, Florida, October 12-16, 2003 (invited).

5. Theses and Dissertations

a. Qun Zhu, "Electrodeposition of Transition Metal-Aluminum Alloys from Room-Temperature Ionic Liquids," Ph.D., May, 2001.

b. Zhaoxia Liu, "Pulse-Plating of Co-Al Alloys from Chloroaluminate Melts," M.S., May 2003.

5. Personnel

a. Dr. Charles L. Hussey, Professor and Chair, Department of Chemistry and Biochemistry, The University of Mississippi. (PI)

b. Dr. Gery R. Stafford, Group Leader for Electrochemical Processing, National Institute of Standards and Technology. (principal collaborator)

c. Dr. Tetsuya Tsuda, Postdoctoral Research Associate, Department of Chemistry and Biochemistry, The University of Mississippi.

d. Dr. Lianyong Su, Postdoctoral Research Associate, Department of Chemistry and Biochemistry, The University of Mississippi.

e. Dr. Qun Zhu, Ph.D. Student, Department of Chemistry and Biochemistry, The University of Mississippi, graduated in May of 2001.

f. Ms. Zhaoxia Liu, M.S. Student, Department of Chemistry and Biochemistry, The University of Mississippi, graduated in May of 2003.

g. Mr. Stacy Jones, D.A. Student, Department of Chemistry and Biochemistry, The University of Mississippi, projected to graduate in May of 2004.

h. Ms. Melissa Ann Gronemeyer, B.S. Forensic Chemistry Student, senior undergraduate research student, graduated in August 2001.

6. Summary of Research Results

a. *Galvanostatic pulse-plating of copper-aluminum alloy.*- The electrodeposition of transition metal-aluminum alloys from room-temperature chloroaluminate melts can be divided into two classes. The first class consists of those systems where the transition metal electrodeposits at potentials proximate to aluminum, e.g., Al-Cr and Al-Mn. In this class of alloys, the concentration of aluminum greatly exceeds that of the transition metal. The second class consists of those systems where the transition metal is reduced at potentials several hundred millivolts positive of the aluminum reduction potential, e.g., Ag-Al, Co-Al, Cu-Al, Fe-Al, and Ni-Al. In this case, there often exists a potential window wherein the pure transition metal can be reduced at the mass transport-limited rate before the co-deposition of Al commences. Hence the concentration of the transition metal component greatly exceeds the concentration of the aluminum component. Furthermore, if these types of alloys are allowed to sit in the plating solution without the benefit of cathodic protection, they experience rapid displacement of Al by the transition metal, i.e., they are thermodynamically unstable. Unfortunately, these complications usually lead to practical electrodeposits with very poor morphologies, embedded chloride, and less Al than predicted from transient electrochemical techniques. The use of periodic current waveforms has been demonstrated to produce electrodeposits from aqueous solutions with reduced porosity, improved surface topography, and reduced internal stress. Therefore, we have carried out such investigations with the Cu-Al alloy system.

The electroplating of Cu-Al alloy (aluminum-bronze) was examined by using pulse current, superimposed-pulse current, and reverse-pulse current methods. The composition of the electrodeposited alloy was determined by using rotating ring-disk anodic linear sweep voltammetry (RRDE-ALSV). As mentioned above, the electrodeposition of Cu-Al is complicated by the instability of the alloy in solutions containing Cu^+. If the alloy is removed from cathodic protection while immersed in the plating bath, a condition that occurs during the pulse plating "off-time," t_{off}, Cu^+ in the plating solution oxidizes Al from the electrodeposit. The rate of this displacement reaction is greatest for small values of t_{off}, but decreases as t_{off} becomes longer, suggesting that a copper-rich layer forms on the electrodeposit that blocks the displacement reaction. The displacement reaction can be minimized by lowering the Cu^+ concentration at the electrode surface through the application of a superimposed current during t_{off}, whose magnitude is comparable to that of the limiting current for Cu^+. A simple analytical model incorporating the peak-pulse current, Cu^+ limiting current, peak-pulse current on-time, and superimposed-current on-time, provided a reasonable representation of the experimental data. Reverse-pulse current experiments indicated that the alloy composition can be controlled by manipulating the peak-pulse current, duty cycle, and reverse current with changes in the former having by far the greatest effect. Based on these results, reverse-pulse current and superimposed-pulse current are the plating methods of choice for use in these melts. The results of this investigation were reported in Q. Zhu and C. L. Hussey, *J. Electrochem. Soc.*, **148**, C395 (2001).

b. *Bulk deposition of Cu-Al alloys.*-The pulse plating of bulk Cu-Al alloy films was investigated in the $AlCl_3$-EtMeImCl melt containing 45.4% (v/v) benzene at a demountable nickel rotating disk electrode by using pulse current, superimposed-pulse current, and reverse-pulse current methods. The resulting alloy films were characterized by using SEM/EDS and were compared to those prepared by using conventional DC plating methods. Generally, the as-deposited surface morphology was greatly improved and the chloride contamination was decreased in those alloy electrodeposits prepared by using periodic current waveforms. This was especially true for reverse-pulse current plating, which led to deposits with no detectable chloride contamination. Cu-Al electrodeposits with specular surfaces containing approximately 4 % atomic fraction aluminum were obtained by using superimposed-pulse current plating in which

the superimposed current was equal in magnitude to the limiting current for the reduction of copper (I). This Al content should be sufficient to impart corrosion resistance to the Cu. The use of 1 % (w/w) methyl *t*-butyl ether as a leveling agent to improve the surface morphology of the deposit was also investigated. Although this additive was found to improve the overall deposit quality, it led to an unfortunate decrease in the Al content of the alloy. The bottom line of this work is that it is possible to prepare a good quality chloride-free aluminum bronze plating from room-temperature chloroaluminates by using pulse-plating techniques. The results of this investigation were reported in Q. Zhu, C. L. Hussey, and G. R. Stafford, *J. Electrochem. Soc.*, **149**, C268 (2002).

c. *Electrodeposition of silver-aluminum alloy*.-The electrodeposition of silver-aluminum alloy was investigated at platinum and tungsten electrodes in the Lewis acidic aluminum chloride-1-ethyl-3-methylimidazolium chloride molten salt containing electrogenerated silver(I) at 25 °C. This system was investigated for its possible utility as a corrosion-resistant coating for other metals. Sampled-current voltammetry indicated that it is possible to electrodeposit Ag-Al alloys at potentials positive of that where the bulk deposition of aluminum is normally observed (~0 V). The aluminum content of these alloys varied with the applied potential and displayed an inverse dependence on the silver(I) concentration, indicating that the alloy formation process was kinetically limited. Experiments conducted in melts with different compositions revealed that at a fixed potential and silver(I) concentration, the atomic fraction of aluminum in the alloy is virtually independent of the melt composition. At high concentrations, silver(I) adsorbs on platinum and tungsten, but this process is inhibited by the addition of benzene. This phenomenon is very unusual in that the adsorption of inorganic electroactive species on metal electrodes in molten salts is seldom observed. However, the adsorption process does not appear to affect the co-deposition of aluminum with silver. X-ray diffraction analysis of bulk Ag-Al alloy electrodeposits prepared in melt containing benzene as a co-solvent indicated the presence of both fcc Ag and hcp δ-Ag_2Al. Further work on this system will be directed at improving the morphology of bulk deposits through the application of the pulse current techniques described above. The results of this investigation were reported in Q. Zhu and C. L. Hussey, *J. Electrochem. Soc.*, **148**, C88 (2001).

d. *Electrodeposition of magnetic alloys containing iron and aluminum.*-The electrodeposition of iron was investigated in solutions of Fe(II) in the Lewis acidic aluminum chloride-1-ethyl-3-methylimidazolium chloride molten salt with and without benzene co-solvent under ambient temperature conditions. Chronoamperometry was used to study the nucleation of iron on a Pt substrate. The electrodeposition of iron on Pt agrees very well with the progressive three-dimensional diffusion-controlled nucleation/growth model. The density of intrinsic active sites available for nucleation is estimated to be on the order of 10^5 cm^{-2}, which is an extremely low value. Sampled current voltammetry indicated that it is possible to electrodeposit Fe-Al alloys at potentials positive of that where the bulk deposition of aluminum is normally observed (about 0 V). Because Fe(II) is reduced at potentials several hundred millivolts positive of the aluminum reduction potential, the Al in the Fe-Al alloy is displaced rapidly if the deposit is allowed to sit in the plating solution in the absence of cathodic protection. This results in poor deposit morphologies and less Al than predicted from transient electrochemical techniques. As described above, the use of pulse current plating methodology has been demonstrated to produce smooth, Cl-free Cu-Al alloy films from room- temperature chloroaluminates. Based on this information, we attempted to do an initial survey of the pulse current plating of Fe-Al alloy films on copper substrates in the molten salt with and without benzene co-solvent. SEM/EDS analysis of the resulting deposits indicated that smooth Fe-Al alloy films can be obtained by pulse-current plating and that the alloy composition can be easily controlled by changing the pulse-plating parameters (such as current density, pulse time and pulse frequency). However, it did not prove possible to prepare good quality deposits of Fe-Al alloy from these melts, and so we did not pursue this research further.

e. *Electrochemistry of titanium and the deposition of titanium-aluminum alloy.*- The electrochemical behavior of titanium was examined in acidic $AlCl_3$-EtMeImCl at 80 °C. The anodic dissolution of a titanium wire electrode results in the formation of Ti(III) as a reddish, sparingly-soluble film of $TiCl_3$ on the electrode surface. This film eventually passivates the titanium electrode. However, if the $TiCl_3$ precipitate is stirred with titanium metal, it dissolves and the solution becomes greenish-yellow. A UV-vis spectrum of this solution was identical to

that obtained by the direct dissolution of $TiCl_2$. The rate of dissolution of Ti could be greatly enhanced by adding Ti metal to the cell because Ti(III) produced during the electrolysis is immediately converted to Ti(II)

$$Ti + 2Ti(III) \rightleftharpoons 3Ti(II)$$

Ti(II) is converted to $TiCl_3$ by reaction with adventitious O_2 in the glove box; however, Ti(II) solutions are easily stabilized by adding a small amount of Ti metal. The electrochemistry of Ti(II) was investigated with cyclic voltammetry at a stationary Pt disk electrode. These experiments revealed that Ti(II) can be oxidized to Ti(III) and eventually Ti(IV) in quasireversible one-electron reactions, but at slow scan rates the Ti(II)/Ti(III) electrode reaction is complicated by the precipitation of Ti(III) as $TiCl_3$ in a classical E_rC_i reaction mechanism. Assuming that Ti(II) is complexed by three bidentate $AlCl_4^-$ ions according to the EXAFS study reported by Kenneth Seddon's group, this mechanism may take the following form

$$Ti[(AlCl_4)_3]^- \rightleftharpoons Ti[(AlCl_4)_3] + e^-$$

$$3AlCl_4^- + Ti[(AlCl_4)_3] \rightarrow TiCl_3(s) + 3Al_2Cl_7^-$$

The Ti(II)/Ti(III) and Ti(III)/Ti(IV) electrode reactions are independent of the source of Ti(II). That is, the direct dissolution of Ti(II) and the electrolytic dissolution of Ti in the presence of Ti metal produces solutions with identical electrochemical and spectroscopic characteristics. The reduction of Ti(II) occurs at potentials negative of the Al(III)/Al electrode reaction, producing Ti-Al alloy. Ti-Al alloy samples containing ~12 a/o Ti were prepared on the surface of a Cu rotating-disk electrode at a current density of 10 mA cm^{-2} over a wide range of rotation rates.

Electrodeposits containing 7.0 a/o to 18.4 a/o Ti metal were examined by x-ray diffraction methods. All of the diffraction patterns were indexed to a disordered face-centered cubic (fcc) structure and were very similar to that of pure aluminum. Two distinct changes in the diffraction patterns with increased Ti metal content of the alloy were observed. The first was a 0.33 % decrease in the aluminum lattice parameter over this range of composition. This is to be

expected as the smaller Ti atoms substitute for Al in the fcc lattice. The second change was significant broadening of the x-ray reflections with increasing Ti metal content, suggesting a decrease in the deposit grain size. This latter result supports the SEM analysis that showed a decrease in grain size with an increase in the Ti metal content.

A typical diffraction pattern taken on the [001] zone axis from a deposit containing 18.4 a/o Ti metal was consistent with single phase fcc Al-Ti having a lattice parameter close to 0.405 nm. No superlattice reflections were found in any of the diffraction patterns indicating that the detected phase has a random ordering of Al and Ti atoms. For comparison, the diffraction patterns from films containing 16.0 a/o Ti and 24.0 a/o Ti, both deposited from $AlCl_3$-NaCl at clearly show the 100 and 110 superlattice reflections and their intensities grow progressively relative to the fundamental 200 spots as the titanium concentration is increased. The presence of superlattice reflections indicates that the crystal structure of the 423.2 K deposits is not disordered fcc because the 100 and 110 reflections are forbidden for the fcc lattice. It is also clear that the chemical disorder of the room temperature melt deposit is not simply due to the low Ti content. These results strongly suggest that the Al-Ti alloy deposits in the disordered state and that ordering occurs in the solid state, subsequent to the charge transfer step and adatom incorporation into the lattice. The results of this investigation were reported in T. Tsuda, C. L. Hussey, G. R. Stafford, and J. Bonevich, *J. Electrochem. Soc.*, **150**, C234 (2003).

f. *Electrodeposition of Al-V alloys*.-The electrochemical behavior of vanadium(II) was examined in VCl_2-saturated 66.7−33.3 m/o $AlCl_3$-EtMeImCl at 353 K. Voltammetry experiments revealed that V(II) could be oxidized to V(III) and eventually V(IV) in quasi-reversible, one-electron reactions. However, at slow scan rates the V(II)/V(III) electrode reaction is complicated by the rapid precipitation of V(III) as VCl_3. The reduction of V(II) occurs at potentials considerably negative of the Al(III)/Al electrode reaction, and Al-V alloys can not be electrodeposited from this melt. However, electrodeposition experiments conducted in VCl_2-saturated melt containing the additive, 1-ethyl-3-methylimidazolium tetrafluoroborate, resulted in the production of Al-V alloys. The vanadium content of these alloys increased with increasing cathodic current density or more negative applied potentials.

Bulk Al-V samples were electrodeposited on Cu-wire substrates using galvanostatic and potentiostatic techniques. In all cases, the Al-V alloys appear to nucleate along the striations of the drawn copper wire surface. The surface morphology is clearly dependent on the applied current density; as the cathodic current density is increased, the resulting electrodeposits assume a more compact, nodular structure and become relatively smooth and compact at the highest practical current density. Thus, grain refinement is apparently driven by the incorporation of vanadium into the aluminum deposit because an increase in the deposition current density would ordinarily lead to an increase in grain size. Similarly, both of the samples that resulted from potentiostatic electrodeposition experiments exhibited a reasonably smooth, compact surface morphology. EDS elemental compositional maps were prepared for the Al-V electrodeposit with the highest vanadium content, and these maps show a very uniform micro distribution of aluminum and vanadium. EDS analysis of the various Al-V alloy samples prepared during the course of this study indicated that all were free from chloride contamination.

An XRD pattern collected for an Al-V sample containing 9.1 a/o V gave peaks that could be identified with aluminum or with the copper substrate. Reflections for α-$Al_{10}V$, an intermetallic compound that might be expected based on the Al/V elemental ratio of this deposit did not match any of these reflections. The lack of any reflections that can be assigned to discrete Al-V intermetallic compounds, suggests that vanadium has alloyed substitutionally with aluminum in this deposit to form a non-equilibrium or metastable solid solution. Similar results were found for Al-Ti alloys prepared in the Lewis acidic $AlCl_3$-EtMeImCl melt as described above.

The corrosion resistance of the Al-V alloys was investigated by recording potentiodynamic anodic polarization curves in N_2-saturated aqueous NaCl. The Al-V alloy samples display a stable passive region characterized by a very small potential-independent current followed by a sudden rise in current at the pitting potential. This same result was also noted for electrodeposited Al-Ti alloys. The addition of ~ 10 a/o V increases the pitting potential of the alloy by about +0.3 V. This increase is only about 50 % that seen for Al-V alloys with the same composition that were prepared by sputter deposition, but it is comparable to the improvement in pitting potential seen for Al-Ti alloys containing ~ 10 a/o Ti that were prepared in this same molten salt by using similar techniques. One possible explanation for the difference in the pitting potentials of the electrodeposited and sputter-deposited Al-V alloys is the fact that the latter were aged for about 2

years before they were tested whereas the pitting potentials for these electrodeposited samples were measured within a few weeks of their preparation. The results of this investigation were reported in T. Tsuda and C. L. Hussey, *Journal of Mining and Metallurgy,* **39B**, 3 (2003) and in T. Tsuda and C. L. Hussey, *Proc. Symp. Magnetic Materials, Processes, and Devices VII and Electrodeposition of Alloys*, **PV 2002-27** (2003), The Electrochemical Society, Inc., Pennington, NJ.

g. *Electrodeposition of Al-Zr alloys*.-The electrochemistry of Zr(IV) and Zr(II) and the electrodeposition of Al-Zr alloys were examined in the Lewis acidic 66.7–33.3 mole percent aluminum chloride–1-ethyl-3-methylimidazolium chloride molten salt at 353 K. The electrochemical reduction of Zr(IV) to Zr(II) is complicated by the precipitation of $ZrCl_3$; however, solutions of Zr(II) can be prepared by reducing Zr(IV) with Al wire. Al-Zr alloys can be electrodeposited from plating baths containing either Zr(IV) or Zr(II), but for a given concentration and current density, baths containing Zr(IV) lead to Al-Zr alloys with the higher Zr content. This result was traced to the diminutive concentration-dependent diffusion coefficient for Zr(II). It was possible to prepare Al-Zr alloys containing up to ~17 percent atomic fraction (a/o) Zr. The structure of these deposits depended on the Zr content. Alloys containing less than 5 a/o Zr could be indexed to a disordered fcc structure similar to pure Al, whereas alloys containing ~17 a/o Zr were completely amorphous (metallic glass).

Two-phase regions are often observed in electrodeposited aluminum-transition metal alloys when the concentration of the transition metal exceeds the limit of supersaturation in the fcc Al solid solution. The appearance of the second phase, which often has an amorphous structure, generally causes a relaxation in the supersaturation of the solid solution. This has been observed in Al-Cr and Al-Mn alloys electrodeposited from $AlCl_3$-NaCl electrolytes. The two-phase region observed in electrodeposited Al-Zr is clearly different from that that reported in alloys deposited from the high-temperature melt. We have not observed the fine-grained duplex structure that is typically observed in homogeneous two-phase alloys, nor have we observed a relaxation in the supersaturation of Zr in the fcc phase when the amorphous phase is present. This suggests that the two-phase Al-Zr deposits are not intimately co-deposited but consist of large, discrete regions of single-phase material. The non-uniform distribution of Zr and the

resultant inhomogeneous surface morphology revealed by SEM is consistent with this conclusion. The phase distribution appears to follow the composition distribution that appears to be the result of a non-uniform current distribution along the copper wire electrode.

The corrosion resistance of the electrodeposited Al-Zr alloys was investigated by recording potentiodynamic anodic polarization curves in N_2-saturated aqueous 0.1 M NaCl. As noted for Al-Mn alloys examined under similar conditions Al-Zr alloys display a stable passive region characterized by a very small potential-independent current followed by a sudden rise in current at the pitting potential as the deposit undergoes electrodissolution. The addition of 8 a/o or more Zr increases the pitting potential of the alloy by about +0.3 V versus pure Al. This increase is close to the value for the $Al_{97}Zr_3$ alloy that was prepared by sputter deposition. The chloride pitting potentials of alloys with more than 8 a/o Zr were approximately +0.3 V relative to pure Al. The results of this investigation were reported in a manuscript submitted to the *Journal of The Electrochemical Society*. This article has been accepted for publication and will appear in 2004. A copy of the revised manuscript that has been accepted appears in Appendix I.

h. *Electrodeposition of Al-Mo alloys.*-The electrodeposition of aluminum-molybdenum alloys was examined at copper rotating disk and wire substrates in the Lewis acidic 66.7-33.3 mole percent aluminum chloride–1-ethyl-3-methylimidazolium chloride molten salt containing Mo(II) in the form of dissolved $(Mo_6Cl_8)Cl_4$. The molybdenum content of the electrodeposits depended on the electrode rotation rate, Mo(II) concentration, and the bath temperature. Because the cathodic current for the reaction

$$4Al_2Cl_7^- + 3e^- \rightleftharpoons Al + 7AlCl_4^-$$

rises sharply with small negative changes in potential, it was found impractical to investigate the electrodeposition of bulk Al-Mo alloys with any degree of precision by using controlled-potential techniques. Therefore, we used controlled-current techniques to prepare alloy samples for detailed compositional and morphological analysis. During previous investigations involving the electrodeposition of Al-Ti alloys on rotating electrode substrates, the alloy composition was found to depend on the electrode rotation rate below a certain threshold value. Because some of the Al-

Mo alloy samples were to be electrodeposited on Cu RDE and RWE substrates, we examined the electrodeposition of bulk Al-Mo alloys on the former by using dc galvanostatic methods at a current density of -10 mA cm^{-2}. The results of this investigation indicate that the Mo content of these deposits becomes approximately independent of rotation rate above 500 rpm. Therefore, rotation rates exceeding 500 rpm were employed when preparing electrodeposited samples for further analysis.

The Al-Mo alloy composition depends on the applied current density, with the Mo content of the alloy decreasing as the applied current density is increased. This result is expected because the concentration of the reducible Mo(II) species in the plating solution is much smaller than the concentration of $Al_2Cl_7^-$. Thus, the limiting current density for the electrodeposition of Mo only becomes a significant fraction of the total cathodic current density when the latter is small. That is, the partial current density for $\{Mo_6Cl_8\}^{4+}$ reduction is fixed and small, and an increase in the total cathodic current density simply amplifies the Al partial current density, leading to deposits with less Mo.

The effects of temperature and $(Mo_6Cl_8)Cl_4$ concentration on the Al-Mo alloy composition were also investigated. Figure 4 shows the relationship between the current density and the alloy composition for deposits plated at a fixed temperature from melt solutions containing three different $(Mo_6Cl_8)Cl_4$ concentrations and for deposits plated from solutions with the same $(Mo_6Cl_8)Cl_4$ concentration at two different temperatures. The results from both sets of experiments can be explained by considering the effects of each variable on the limiting current for Mo deposition. For example, increasing the $(Mo_6Cl_8)Cl_4$ concentration increases the limiting current density for $\{Mo_6Cl_8\}^{4+}$ reduction (or the partial current density for Mo deposition). Thus, at a fixed cathodic current density, the Mo partial current density increases as the $(Mo_6Cl_8)Cl_4$ concentration is increased, leading to alloy deposits with a greater Mo content. Increasing the plating bath temperature also seems to increase the partial current for Mo deposition relative to that for Al deposition, leading to electrodeposits with larger amounts of Mo. Thus, increasing the temperature of the plating bath has the same net effect as raising the $(Mo_6Cl_8)Cl_4$ concentration.

It was possible to produce non-equilibrium alloys containing more than 10 atomic percent Mo. All of these alloy deposits were compact and chloride-free. Electrodeposits containing 2.6 to 10.2 a/o Mo were examined by x-ray diffraction. Deposits containing less than 5 a/o Mo have

diffraction patterns that can be indexed to a face-centered cubic (fcc) structure very similar to that of pure aluminum, indicating that the Al-Mo alloy is a single phase, supersaturated solid solution. These patterns indicate that the Al grains are randomly oriented and have no preferred crystallographic texture. The primary change in the diffraction patterns with increased Mo composition is the disappearance of the fcc reflections and the development of a broad reflection centered on a 2θ of about 41°, which indicates the presence of an amorphous phase. This broad reflection first appears in deposits containing about 6.5 a/o Mo. The diffraction pattern of the 7.5 a/o Mo deposit indicated that this was a two-phase deposit, consisting of fcc and amorphous material. As the Mo content of the deposit was increased, the amount of fcc phase in the alloy decreases whereas that of the amorphous phase increases. Deposits containing slightly more than 10 a/o Mo are completely amorphous

The level of supersaturation in the two-phase deposits can only be estimated because the Mo content, as measured by EDS, is partitioned between the fcc and amorphous phases. An extrapolation of the lattice parameter data from single-phase deposits places the maximum supersaturation at about 6 to 7 a/o Mo. This level of supersaturation matches that reported in mechanically alloyed materials and is at least twice that observed in rapidly quenched alloys reported to date. In addition to the level of supersaturation obtained in the fcc phase, it is interesting to note that the supersaturation is maintained when the amorphous phase is co-deposited. Similar behavior was also noted for Al-Zr alloys electrodeposited at ambient temperature from $AlCl_3$-EtMeImCl. Aluminum alloys electrodeposited from higher temperature $AlCl_3$-NaCl melts show very different behavior in that the appearance of the amorphous phase results in a relaxation in the supersaturation of the solid solution to levels closer to equilibrium values.

The pitting potentials of electrodeposited Al-Mo alloys were determined by carrying out potentiodynamic anodic polarization experiments in deaerated aqueous NaCl. These experiments were conducted with alloy samples that were deposited on copper wire substrates. As noted for some other electrodeposited stainless aluminum alloys in aqueous chloride media, the Al-Mo alloys are spontaneously passive at the rest potential of the solution. During anodic polarization, they display a stable passive region characterized by a very small potential-independent current followed by a sudden rise in current at the pitting potential. The addition of ~ 10 a/o Mo increases the pitting

potential of the alloy by about +0.800 mV. This increase in the pitting potential is comparable to that found for Al-Mo alloys prepared by sputter deposition. These materials are the most corrosion resistant aluminum-transition metal alloys that have been deposited from chloroaluminate molten salts to date. A manuscript reporting the results of this investigation has been submitted to the *Journal of The Electrochemical Society*. This article has been accepted and will appear in 2004. A copy of the galley proof appears in Appendix II.

i. *Electrodeposition of Al-Hf alloy.*- The electrochemistry of Hf(IV) and the electrodeposition of Al-Hf alloy was examined in the Lewis acidic 66.7–33.3 mole percent (m/o) aluminum chloride–1-ethyl-3-methylimidazolium chloride ($AlCl_3$–EtMeImCl) molten salt containing $HfCl_4$. When cyclic staircase voltammetry was carried out at a platinum electrode in this melt containing $HfCl_4$, the deposition and stripping waves for Al shifted to negative and positive potentials, respectively, suggesting that the aluminum stripping is more difficult due to the formation of Al-Hf alloy. The Hf content of the Al-Hf deposits depended on the $HfCl_4$ concentration in the melt and the applied current density. Al-Hf alloy samples containing ~ 11 atomic percent (a/o) Hf were obtained on the surface of a Cu rotating wire electrode. The alloy surface was covered with dense crystals, the alloy was completely chloride free, and the morphology did not depend on the Hf content of the samples, but on the applied current density. The pitting potential of the Al-Hf alloys was approximately +0.30 V against pure aluminum when the Hf content was above 10 a/o. A manuscript describing these results is in preparation for submission to *Electrochimica Acta*. A draft copy of this manuscript appears as Appendix III.

j. *Electrodeposition of Al-W alloys.*-The electrochemistry and spectrochemistry of tungsten was examined in the Lewis acidic 66.7–33.3 m/o $AlCl_3$–EtMeImCl molten salt. UV-visible spectroscopic data for a solution of WCl_6 changed over a period of several hours at 353 K. We concluded that this anomalous phenomenon is caused by transformation of the W(VI) monomer, $W(AlCl_4^-)_6$, to a dimer, $W_2(AlCl_4^-)_{10}$. The transformation process proceeds with an increase in the bath temperature. The electrode reaction for W(VI)/W(V) and W(V)/W(IV) is reversible one-electron charge transfer process in the solution of WCl_6. In the solutions of WCl_4, the W(IV)/W(III) electrode reaction involves a following irreversible chemical step in which W(III) is converted to

insoluble WCl_3. Melt solutions containing $K_3W_2Cl_9$ were suitable for electroplating of Al-W alloy. It was possible to prepare electrodeposits containing more than 14 a/o W. In these alloys, the pitting potential is shifted to approximately + 1150 mV against pure aluminum. The chloride pitting potential of this alloy is superior to that of all aluminum transition metal alloys that have been prepared in this room-temperature molten salt. A manuscript describing these results is in preparation for submission to the *Journal of The Electrochemical Society*. A draft copy of this manuscript appears in Appendix IV.

k. *Electrodeposition of Al-Mn-Mo alloys.*- The electrodeposition of aluminum-manganese-molybdenum alloy was examined in the Lewis acidic 66.7-33.3 mole percent (m/o) aluminum chloride-1-ethyl-3-methylimidazolium chloride ($AlCl_3$-EtMeImCl) molten salt containing $MnCl_2$ and $(Mo_6Cl_8)Cl_4$ under various conditions. The ratio of these two components in the melt strongly affected both the electrodeposition behavior and the surface morphology of the resulting Al-Mn-Mo alloys. The addition of Mo to the Al-Mn alloy resulted in a considerable improvement in its resistance to chloride-induced pitting corrosion. The pitting potential of the Al-Mn-Mo alloys shifted to approximately +500 and +800 mV against $Al_{95.8}Mn_{4.2}$ alloy and pure Al, respectively, and depended on the total Mo content. This increased resistance to chloride-induced pitting corrosion is comparable to that found for pure Al-Mo alloys electrodeposited from the 66.7 m/o melt. Thus, the addition of Mo into the Al-Mn alloy is an effective method to improve its chloride-induced pitting potential and may have other beneficial effects as well A manuscript describing these results is in preparation for submission to *Electrochimica Acta*. A draft copy of this manuscript is attached as Appendix V.

7. Conclusions

The primary goal of this project was attained. Corrosion-resistant, non-equilibrium binary aluminum alloy films such as Al-Ti, Al-V, Al-Zr, Al-Mo, Al-Hf, and Al-W were prepared by electrodeposition from the room-temperature chloroaluminate molten salt, aluminum chloride-1-ethyl-3-methylimidazolium chloride. It was also possible to electrodeposit the ternary alloy, Al-Mn-Mo, from this ionic solvent. In every case, those alloys that are supersaturated

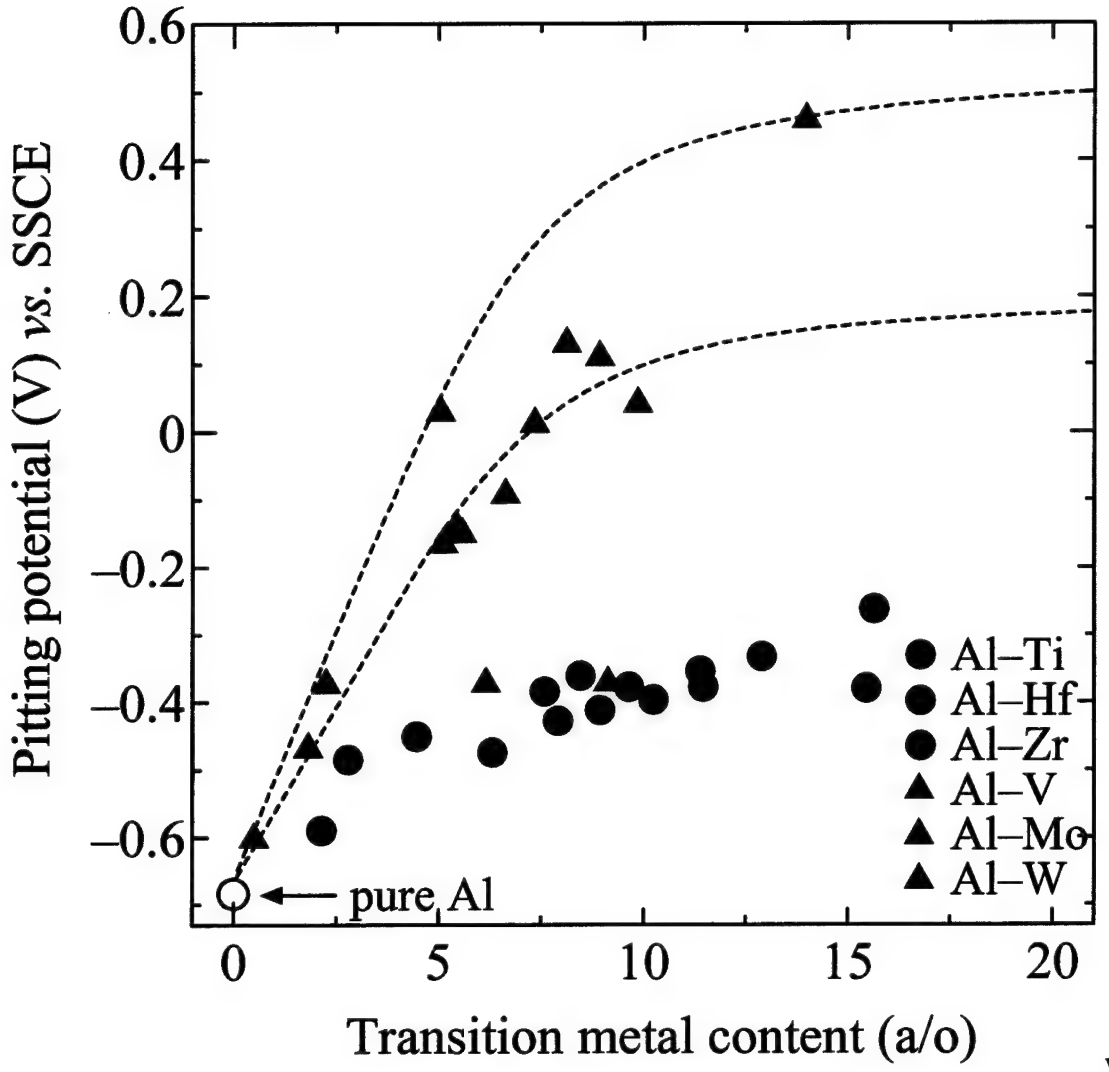

with transition metal solutes exhibited greatly enhanced resistance to chloride-induced pitting corrosion compared to pure aluminum, especially Al-Mo ad Al-W. In most cases, the corrosion resistance of these alloys increases with increasing solute concentration and is comparable to that observed for their counterparts that were prepared by using conventional nonequilibrium alloying methods such as melt spinning, ion implantation, reactive plasma spraying, sputter deposition, and thermal evaporation. The results of this project also suggest that isothermal electrodeposition in chloroaluminate ionic liquids may be a more facile route to these nonequilibrium alloys. Future investigations should be directed at the development of an inexpensive pilot-scale process for electroplating these alloys in an industrial setting.

The principal investigator and his students wish to express their profound gratitude to the Air Force Office of Scientific Research and to Lieutenant Colonel Paul C. Trulove for their support of this research project.

APPENDIX I

T. Tsuda, C. L. Hussey, G. R. Stafford, and O. Kongstein, "Electrodeposition of Al-Zr Alloys from the Lewis Acidic Aluminum Chloride–1-Ethyl-3-methylimidazolium Chloride Melt", *J. Electrochem. Soc.*, in press.

Revised
Accepted

Electrodeposition of Al-Zr Alloys from the Lewis Acidic Aluminum Chloride–1-Ethyl-3-methylimidazolium Chloride Melt

Tetsuya Tsuda,[a,*] Charles L. Hussey,[a,,z] Gery R. Stafford,[b,*] and Ole Kongstein[b]**

[a]*Department of Chemistry and Biochemistry, The University of Mississippi, P.O. Box 1848, University, Mississippi 38677, USA*

[b]*Materials Science and Engineering Laboratory, National Institute of Standards and Technology, Gaithersburg, Maryland 20899, USA*

The electrochemistry of Zr(IV) and Zr(II) and the electrodeposition of Al-Zr alloys were examined in the Lewis acidic 66.7–33.3 mole percent aluminum chloride–1-ethyl-3-methylimidazolium chloride molten salt at 353 K. The electrochemical reduction of Zr(IV) to Zr(II) is complicated by the precipitation of $ZrCl_3$; however, solutions of Zr(II) can be prepared by reducing Zr(IV) with Al wire. Al-Zr alloys can be electrodeposited from plating baths containing either Zr(IV) or Zr(II), but for a given concentration and current density, baths containing Zr(IV) lead to Al-Zr alloys with the higher Zr content. This result was traced to the diminutive concentration-dependent diffusion coefficient for Zr(II). It was possible to prepare Al-Zr alloys containing up to ~17 percent atomic fraction (a/o) Zr. The structure of these deposits depended on the Zr content. Alloys containing less than 5 a/o Zr could be indexed to a disordered fcc structure similar to pure Al, whereas alloys containing ~17 a/o Zr were completely amorphous (metallic glass). The chloride pitting potentials of alloys with more than 8 a/o Zr were approximately +0.3 V relative to pure Al

*Electrochemical Society Active Member
**Electrochemical Society Fellow
[z] E-mail: chclh@chem1.olemiss.edu

Introduction

The maximum solubility of zirconium in face-centered cubic (fcc) aluminum is 0.08 % atomic fraction (a/o). This occurs at the peritectic transformation point at 660.5 °C. At room temperature, zirconium has negligible solubility in aluminum.[1] However like most aluminum-transition metal alloys, supersaturated solid solutions greatly exceeding the equilibrium solubility can be obtained by non-equilibrium processing methods. For example, solid solutions containing up to 3.0 a/o zirconium have been produced by rapid solidification [2-6] and vapor deposition.[7] The Al-Zr solid solution, although metastable, shows good thermal stability up to temperatures of ~400-450 °C. This observation is consistent with the general trend that the thermal stability of the solid solution is related to the melting point of the alloying addition; i.e., the higher the melting point, the more stable the solid solution.[8] The thermal decomposition of the supersaturated solid solution results in the nucleation of a metastable Al_3Zr phase having an ordered cubic $L1_2$ structure (Cu_3Au-type)[5, 6, 9-13] and eventually the equilibrium Al_3Zr phase having a tetragonal structure. These two phases, namely cubic Al_3Zr and tetragonal Al_3Zr, have also been observed in supersaturated Al-Zr solid solutions produced by rapid quenching.[14]

The properties of aluminum and its alloys are significantly altered by the addition of zirconium. The rapid solidification of binary Al-Zr alloys with more that 0.15 a/o zirconium produces considerable grain refinement,[15, 16] resulting in aluminum grain sizes typically less than 10 μm. The general explanation for this phenomenon is that $L1_2$ Al_3Zr acts as a low energy nucleation site for fcc Al due to the similar crystal structures. Rapid quenching is required to ensure that the Al_3Zr solidifies with the metastable $L1_2$ structure rather than the equilibrium tetragonal structure. The presence of these fine Al_3Zr

precipitates also raises the recrystallization temperature of aluminum, extending the good mechanical properties of the alloy to more elevated temperatures. Zirconium is also added to commercial high-strength aluminum alloys to improve toughness, stress-corrosion resistance, and quench sensitivity.[12, 14] The addition of about 0.15 a/o Zr to several of the commercial aluminum alloys makes them superplastic due in part to the resulting grain refinement.[14, 17-19] Typical elongations of 1000 % can be consistently obtained with $Al_{97.6}Cu_{2.2}Zr_{0.2}$ alloys, whereas identically processed binary $Al_{97.4}Cu_{2.6}$ is comprised of large grains and has limited plasticity.

Although Al-Zr alloys with many interesting properties can be obtained by standard non-equilibrium processing methods as noted above, the industrial application of these materials requires a processing method such as isothermal electrodeposition that can be used to produce alloy coatings of uniform thickness with reproducible composition and structure. A number of corrosion-resistant aluminum-transition metal alloys similar to Al-Zr have been electrodeposited from Lewis acidic chloroaluminate molten salts. These well-known melts are obtained by mixing a molar excess of anhydrous aluminum chloride with an appropriate chloride salt. Typical salts that have been used to prepare these melts include alkali chlorides such as NaCl or quaternary ammonium chloride salts such as 1-(1-butyl)pyridinium chloride (BuPyCl) or 1-ethyl-3-methylimidazolium chloride (EtMeImCl). Chloroaluminate molten salts have been used as baths for the electrodeposition of several corrosion resistant aluminum-transition metal alloys; some examples of these alloys include Al-Cr,[20, 21] Al-Mn,[22, 23] Al-Ti,[24, 25] and Al-V.[26] Progress in this area was recently reviewed.[27] Recently, Kawase and Ito[28] reported the electrodeposition of Zr and Al-Zr alloy films on carbon-coated ceramic substrates from solutions of electrogenerated Zr(II) in the LiCl-KCl

eutectic molten salt at 823 K. Al(III) was the source of Al during the deposition of the Al-Zr alloys, and it was generated by the chemical oxidation of Al metal with Zr(II).

The electrochemistry of zirconium has been investigated in the Lewis acidic $AlCl_3$–NaCl melt.[29] In this study, insoluble green crystals of $ZrCl_3$ resulted from the electrochemical reduction of Zr(IV) in melt containing 51-52 m/o $AlCl_3$ at 448 K. It was possible to reduce Zr(IV) to soluble Zr(III) in very acidic melt (60 m/o $AlCl_3$) if the temperature was raised to 523 K or more, but the Zr(III) thus produced rapidly disproportionated to Zr(IV) and Zr(II). The precipitation of Zr(III) as $ZrCl_3$ was used to efficiently separate hafnium from zirconium in $AlCl_3$-NaCl melts of low acidity.[30] The electrochemistry of hexanuclear zirconium halide clusters was investigated in the $AlCl_3$-EtMeImCl melt containing 60 m/o $AlCl_3$.[31] However, no evidence for the electrodeposition of zirconium metal or Al-Zr alloy was obtained during this or any of the investigations described above. In this article, we report the electrodeposition of Al-Zr alloys on Cu substrates from the Lewis acidic $AlCl_3$–EtMeImCl molten salt and the electrochemistry of Zr(IV) and Zr(II) in this melt as it pertains to the electrodeposition of these alloys.

Experimental[a]

The procedures used for the synthesis of EtMeImCl, the purification of $AlCl_3$ by sublimation, and the preparation and purification of the $AlCl_3$–EtMeImCl molten salt were identical to those described in a previous article.[26] Anhydrous $ZrCl_4$ (Aldrich, 99.9 + %) was used as received. The preparation of the molten salt and all electrochemical experiments were carried out in a nitrogen gas-filled glove box (VAC Atmospheres NEXUS system) with O_2 and H_2O concentrations < 5 ppm.

The UV-visible spectra of dissolved Zr ions were obtained by using a Varian CARY 5 spectrometer employing a Wilmad No. 107-7 closed type quartz cells. The path length of these cells was 0.10 cm.

Electrochemical experiments were conducted by using an EG&G Model 273 potentiostat/galvanostat controlled with EG&G PARC M270 software running on a Pentium III computer. Electronic resistance compensation was employed during all staircase voltammetry experiments. The step size used for staircase voltammetry, 2 mV, was small enough to permit the analysis of these resulting voltammograms with the conventional theories developed for linear scan voltammetry.[32]

A three-electrode Pyrex glass cell with a Teflon cap similar to that described in a previous article[33] was used for all experiments. A Pine Instruments Teflon-sheathed platinum rotating disk electrode (geometrical area = 0.099 cm^2) was used for the working electrode during voltammetry experiments. Coils of 0.10 cm diameter aluminum wire (Alfa Aesar, 99.999 %) were used for the counter and reference electrodes. These electrodes were immersed in pure melt with the same composition as the bulk melt, but

[a] Certain trade names are mentioned for experimental information only; in no case does it imply a

were separated from the bulk melt by a porosity E glass frit (Ace Glass). The aluminum electrodes were cleaned with a mixture of concentrated aqueous H_2SO_4- HNO_3-H_3PO_4, rinsed with distilled H_2O, and dried under vacuum before use. All electrochemical experiments were carried out at 353 K unless noted.

The electrodeposition of Al-Zr alloys was performed with an EG&G PARC Model 173 potentiostat/galvanostat equipped with a Model 179 digital coulometer plug-in module. Alloy samples of approximately 10 μm thickness were deposited onto a length of 1.25 mm diameter copper wire (99.9 % purity) from solutions of Zr(IV) or Zr(II) in the $AlCl_3$-EtMeImCl molten salt. The exposed surface area of the copper wire electrode was 0.798 cm^2. The wire was lightly sanded with emery cloth and then washed successively with distilled water and anhydrous ethanol. The copper wire was rotated at 2000 rpm during deposition. The electrodeposits were washed in distilled water and dried under vacuum in the glove box antechamber. The surface morphology of the electrodeposits was examined at NIST with scanning electron microscopy (SEM) by using a JEOL JXA-840 scanning electron microscope. The electrodeposits were also examined by x-ray diffraction (XRD) with a Siemens D-500 diffractometer employing Cu-Kα radiation. The lattice parameters of the deposits were refined using the copper substrate reflections as an internal standard.

Potentiodynamic pitting corrosion measurements were carried out on these alloy samples at room temperature in deaerated, aqueous 0.1 mol L^{-1} solutions of NaCl. The reference electrode for these measurements was a sodium-saturated calomel electrode (SSCE), and the counter electrode was a large surface area platinum wire coil. A known length of the plated Cu wire was exposed to the NaCl solution by using a heat-shrink tubing

---

recommendation or endorsement by NIST.

mask, and the sample was scanned at 0.5 mV s^{-1} by using linear staircase voltammetry with a step-size of 2 mV.

Results and Discussion

Electrochemistry of $ZrCl_4$. – $ZrCl_4$ appeared to be very soluble in the melt. Figure 1 shows typical cyclic staircase voltammograms recorded at a stationary Pt disk electrode in the 66.7 m/o $AlCl_3$-EtMeImCl melt at 353 K before and after the addition of $ZrCl_4$. Before the addition of $ZrCl_4$, the only waves appearing in the former voltammogram are those due to the deposition and stripping of aluminum according to the following well-known reaction

$$4Al_2Cl_7^- + 3e^- \rightleftharpoons Al + 7AlCl_4^- \qquad [1]$$

After the dissolution of $ZrCl_4$, a small, ill-defined reduction wave with a peak potential, E_{pc}, of about 0.92 V was also apparent (see Fig. 1 inset). In addition, the wave ascribed to the reduction reaction in Eq. 1 shows a small negative shift, the oxidation wave due to the stripping of the pure Al deposit from the Pt electrode in pure melt is absent, and new stripping waves are evident at more positive potentials. The latter stripping waves are attributed to the oxidation of one or more electrodeposited Al-Zr alloy phases that are more stable toward oxidation than pure Al. The electrodeposition of Al-Zr alloys from these solutions will be discussed in more detail below.

The voltammetric wave at $E_{pc} \sim 0.92$ V is shown in more detail in Fig. 2. It was difficult to obtain reproducible results for this wave. In many cases, it was only possible to obtain a well-defined wave by polishing the platinum electrode surface before each scan. The difference in the peak potential and half-peak potential, E_{pc}-$E_{pc/2}$, for this wave varied between 0.08 and 0.12 V and did not display any obvious dependence on the scan rate over the range extending from 0.005 to 0.500 V s^{-1}. The smaller values of E_{pc}-$E_{pc/2}$

are reasonably close to the theoretical value of 0.07 V for a one-electron reversible reaction at 353 K, leading us to conclude that the reduction wave in Fig. 2 corresponds to the Zr(IV)/Zr(III) electrode reaction. If the voltammetric scan is reversed immediately after the reduction wave at 0.92 V and scan rates greater than 50 mV s^{-1} are employed, then an associated oxidation wave is observed at $E_{pa} \sim 1.09$ V. Experiments conducted at a fixed scan rate revealed that the voltammetric peak reduction current, i_{pc}, for the wave at 0.92 V did not always display a linear dependence on the $ZrCl_4$ concentration. This behavior was most pronounced at high $ZrCl_4$ concentrations and slow scan rates, and it was traced to the formation of a surface film on the electrode during the reduction of Zr(IV), which led to a decrease in the active area of the electrode and to many of the other anomalous results that were obtained for this voltammetric wave.

The reduction of Zr(IV) was also examined as a function of scan rate at a fixed concentration. Figure 3 shows a plot of the peak reduction current, i_{pc}, versus the square root of the scan rate, $\upsilon^{1/2}$. Each data point in this figure is the average of several measurements. The linearity of this plot indicates that the reduction of Zr(IV) is a diffusion-controlled process. An estimate of the peak current ratio, $i_{pa}/|i_{pc}|$ was obtained by using Nicholson's semi-empirical method.[34] This ratio is less than one at very slow scan rates, but increases to one at faster scan rates (Fig. 3). This latter result suggests that an irreversible homogeneous following chemical step is coupled to the electron transfer reaction.[35] Because $ZrCl_3$, but not $ZrCl_2$, is known to be insoluble in Lewis acidic chloroaluminate melts and in molten $AlCl_3$, this coupled chemical step must be due to the precipitation of $ZrCl_3$ as was found during the reduction of Zr(IV) in Lewis acidic $AlCl_3$-NaCl.[29] Thus, the reduction wave at ca. 0.92 V most likely involves the following sequence of reactions:

$$Zr(IV)_{solv} + e^- \rightleftharpoons Zr(III)_{solv} \quad [2]$$

$$Zr(III)_{solv} + 6AlCl_4^- \rightarrow ZrCl_3(s) + 3Al_2Cl_7^- \quad [3]$$

The latter reaction is the source of the passivating film that forms on the electrode surface at slow scan rates or high Zr(IV) concentrations. We also attempted to investigate the Zr(IV)/Zr(III) reaction by carrying out controlled potential reduction at a large surface area platinum screen electrode at an applied potential of 0.80 V. After the passage of a fraction of the charge necessary to reduce all of the Zr(IV), the electrode became completely passivated by the aforementioned surface film, and the solution became cloudy from a precipitate.

The diffusion coefficient for Zr(IV), $D_{Zr(IV)}$, and the Stokes-Einstein product, $D_{Zr(IV)}\eta/T$, where η is the absolute viscosity of the molten salt, were calculated from the data in Fig. 3. The viscosity data taken from Fannin et al.[36] were used for the latter calculation. The diffusion coefficient for the related Group 4 species, Ti(IV), that was measured in the 60.0 m/o melt at 300 K is given in Table I for comparison. $D_{Ti(IV)}$ can be compared to $D_{Zr(IV)}$ through the Stokes-Einstein product, $D\eta/T$, which considers both the temperature of the measurement and the absolute viscosity of the solvent. $D\eta/T$ is a relative measure of the solvodynamic radius of the diffusing species.[37] Comparison of the calculated Stokes-Einstein products given in Table I shows that despite the seemingly large differences in $D_{Zr(IV)}$ and $D_{Ti(IV)}$, the two Group 4 species have roughly comparable solvodynamic radii. The somewhat smaller value of $D_{Ti(IV)}\eta/T$ may simply reflect the fact that Ti(IV) vaporizes rapidly from the melt as $TiCl_4$.[25] Thus, the diffusion coefficient data reported in the

literature for Ti(IV) may have been measured under conditions that did not take into account the vaporization loss of $TiCl_4$, which would lead to smaller values of $D_{Ti(IV)}$ and $D_{Ti(IV)}\eta/T$.

Overall, these electrochemical results are very similar to those obtained during an investigation of the related titanium system in this same molten salt.[38] In this case, the Ti(IV)/Ti(III) reaction was also found to be complicated by a coupled irreversible following chemical reaction involving precipitation of the trivalent chloride, $TiCl_3$.[38] The insolubility of $TiCl_3$ was also noted during previous investigations involving the electrodeposition of Al-Ti alloys from the Lewis acidic $AlCl_3$-EtMeImCl and $AlCl_3$-NaCl molten salts.[24, 25, 39] A recent investigation of the related vanadium system indicated that VCl_3 was virtually insoluble in the Lewis acidic $AlCl_3$-EtMeImCl melt, whereas the divalent species, VCl_2, was soluble.[26] Thus, the insolubility of the Group 4 and 5 trivalent chlorides appears to be a general trend in Lewis acidic chloroaluminate melts.

Chemical Reduction of $ZrCl_4$. – The voltammogram recorded for the solution containing Zr(IV) shown in Fig. 1 does not exhibit any obvious wave for the reduction of Zr(III) to a lower oxidation state species, even at fast scan rates where the coupled chemical step is unimportant. However, as shown below, compact, chloride-free deposits containing Zr metal can be obtained by the electrochemical reduction of Zr(IV). This indicates that Zr(III), irrespective of its chemical or physical form, must eventually undergo reduction as the potential approaches 0 V versus Al(III)/Al. Therefore, we carried out a series of experiments to determine if it is possible to obtain Zr(II) by the chemical reduction of Zr(IV). There is considerable evidence for the existence of this species. For example, Ruff and Wallstein[40] reported that Zr(II) can be obtained by the chemical reduction of molten $ZrCl_4$ with Al. Larsen et al.[41] obtained the characteristic green crystals of $ZrCl_3$ by the reduction of $ZrCl_4$ dissolved in molten Al_2Cl_6 with Al or Zr metal at 503-583 K. However,

the resulting $ZrCl_3$ is unstable in molten Al_2Cl_6 and slowly disproportionates to an insoluble brown-colored Zr(II) species, $(ZrCl_2)_2AlCl_3$, and $ZrCl_4$. Based on previous work with the related V(II) and Ti(II) species,[25, 26] there is good reason to expect that Zr(II) will be stable and soluble in the acidic $AlCl_3$-EtMeImCl melt.

Figure 4 shows UV-vis spectra of a solution of Zr(IV) in the 66.7 m/o melt before and after this solution was stirred with Al metal at 353.2 K for three days. During the reaction between Zr(IV) and Al, the solution changed from colorless to reddish-brown with no evidence of the formation of the green precipitate of $ZrCl_3$ reported by Larsen et al.[41] in molten Al_2Cl_6 and by Gilbert et al.[29] in acidic $AlCl_3$-NaCl. We ascribe this soluble reddish-brown reduction product to a Zr(II) species; this assignment is supported by the electrochemical experiments described below. When we repeated these experiments in the 60.0 m/o melt containing approximately the same initial concentration of Zr(IV), we obtained a different result. Under the less acidic conditions of this melt, the reduction of Zr(IV) by Al also results in a reddish-brown solution, but the visual density of the color and the intensity of the absorption bands in the spectrum of this solution were greatly diminished compared to the solution resulting from similar experiments in the 66.7 m/o melt. In addition, the reaction vessel contained a considerable quantity of the green crystals of $ZrCl_3$. Likewise, when we repeated these experiments with Zr(IV) in the 66.7 m/o melt by using Zr metal as the reducing agent, the green precipitate of $ZrCl_3$ was obtained in abundance and only a small amount of Zr(II) was obtained. Thus, it would appear from these results that Zr(IV) can only be completely reduced to Zr(II) by using Al metal and employing the very acidic 66.7 m/o melt (Fig. 4).

During the chemical reduction of Zr(IV) with Al in the 66.7 m/o melt described above, the rest potential of a Pt-RDE electrode immersed in the solution shifted to a value

considerably negative of the Zr(IV)/Zr(III) couple. Figure 5 shows a series of voltammograms that were recorded at a Pt-RDE at different rotation rates in two solutions that were prepared in this melt by the chemical reduction of Zr(IV) with Al metal. The concentrations of Zr(IV) used to prepare these two solutions were different, and the voltammograms were initiated from the rest potential of each solution. Each of the voltammograms in Fig. 5 shows two well-defined oxidation waves, and plots of E versus $\log[(i - i_l)/i]$ were linear for both waves. Analysis of the intercepts of these plots gave half-wave potentials, $E_{1/2}$, of 0.80 ± 0.01 and 1.29 ± 0.01 V for the first and second waves, respectively, in the voltammograms recorded in the 5.40 mM solution, and $E_{1/2}$ = 0.66 ± 0.00 and 1.28 ± 0.00 V, respectively, for the oxidation waves acquired in the 19.5 mM solution. Thus, $E_{1/2}$ for the first oxidation wave, but not the second wave in these voltammograms, displays a dependence on the concentration of the electroactive species. Calculations based on the slopes of these plots yielded n = 0.9 ± 0.1 and 1.0 ± 0.2 for the first and second waves, respectively, indicating that both waves correspond to one-electron reactions. Overall, the voltammograms in Fig. 5 are very similar in appearance to those recorded during the oxidation of Ti(II) in this same melt.[25] Taken together, these observations provide good evidence that the species produced during the chemical reduction of Zr(IV) with Al is indeed Zr(II). The maximum concentration of Zr(II) that could be obtained by the Al reduction of Zr(IV) was about 19 mmol L^{-1}.

The inset of Fig. 5 shows that the limiting current densities for the first oxidation waves in Fig. 5 obey the Levich relationship. Diffusion coefficients and Stokes-Einstein products that were calculated from these limiting current density data are collected in Table I along with values for $D_{Ti(II)}$ and $\eta D_{Ti(II)}/T$. Generally, the values of $D_{Zr(II)}$ are in reasonable agreement with those for $D_{Ti(II)}$ in this same molten salt. However, like $D_{Ti(II)}$, $D_{Zr(II)}$ varies

with the concentration of the electroactive solute, becoming smaller as the solute concentration increases. In the case of Ti(II), this phenomenon is attributed to polymerization of the Ti(II) species as $[Ti(AlCl_4)_2]_m$, with m increasing as the Ti(II) concentration is increased.[25, 39, 42, 43] Given the overall similarity of the chemistry of Ti(II) and Zr(II), polymerization of Zr(II) would also be expected. The observed concentration dependence of $E_{1/2}$ for the first Zr(II) oxidation waves, but not the second waves, in Fig. 5 may also be related to such a phenomenon. However, additional experiments beyond the scope of the present investigation are required in order to fully characterize the complicated electrochemistry of Zr(IV) and Zr(II) in the Lewis acidic $AlCl_3$-EtMeImCl melt.

Electrodeposition of Al-Zr alloys. - The electrodeposition of bulk Al-Zr alloys was examined by using dc galvanostatic methods at 353 K in the 66.7 m/o melt containing either Zr(IV) or Zr(II) prepared by the Al reduction of Zr(IV) (vide supra). Because there are no side reactions to compete with the Al-Zr deposition process, the current efficiency is nearly 100 %. The substrate for these deposition experiments was a copper rotating wire electrode. A rotation rate of 2000 rpm was used for these experiments in order to be consistent with previous studies involving the electrodeposition of Al-Ti[25] and Al-V[26] from this same molten salt. The compositions of the Al-Zr alloys resulting from these experiments are shown as a function of current density in Fig. 6. The data in this figure lead to two conclusions. First, the Zr content of the electrodeposited alloys decreases with increasing current density. Second, solutions of Zr(IV) lead to Al-Zr alloys containing greater amounts of Zr than Zr(II) solutions of equal concentration.

The first result is expected because at low reduction current densities and correspondingly less negative potentials, the partial current density for Zr would be a larger fraction of the total current. As the current density is increased, the partial current for the

reduction of the Zr species should reach a limiting value whereas the partial current for the reduction of $Al_2Cl_7^-$, which is present in this melt at a concentration of 3.24 M at 353 K, continues to increase. This behavior is a common feature of overpotential alloy deposition in chloroaluminate melts and was observed during the electrodeposition of Al-Cr[20, 21] Al-Mn,[23, 44] Al-Mo,[45] and Al-Ti.[24, 25, 39, 46] The finding that plating solutions containing Zr(IV) lead to alloys with higher Zr content than plating solutions containing equal concentrations of Zr(II) may be reconciled by considering the diffusion coefficient data in Table I. Because the concentration-dependent diffusion coefficient for Zr(II) is only a small fraction of that for Zr(IV), the observed inefficiency of Zr(II) for plating Al-Zr alloys must be directly related to the mass-transport limitations imposed by the diminutive diffusion coefficient of the latter species.

Characterization of Electrodeposited Al-Zr Alloys. –The surface morphology of Al-Zr deposits of varying composition is shown in Figure 7. The 1.4 a/o Zr, deposit, Fig. 7a, is nodular and the nodules tend to follow the defects, i.e., striations, that were introduced into the drawn wire substrate as the result of its processing. The nodules are typically 5-10 μm in diameter and appear to be single crystals. The 4.9 a/o Zr deposit, Fig. 7b, shows significant grain refinement. The nodules are typically 1 μm in diameter or less. Although the 4.9 a/o Zr deposit was made at a lower current density than the 1.4 a/o Zr deposit, it has a smaller nodule size, suggesting that the grain refinement is driven by the incorporation of Zr into the alloy rather than the deposition overpotential. Similar behavior was recently reported for electrodeposited Al-Ti alloys.[25] The deposit morphology changes significantly with further additions of Zr. Figure 7c shows the surface of a 15.9 a/o Zr deposit having a compact, rounded nodular structure that is generally associated with metallic glasses.

Electrodeposits containing 1.4 to 16.6 a/o Zr were examined by x-ray diffraction. The diffraction patterns for selected deposits are shown in Figure 8. Deposits containing less than 5 a/o Zr have diffraction patterns that can be indexed to a chemically disordered fcc structure very similar to that of pure aluminum, indicating that the Al-Zr alloy is a single phase, supersaturated solid solution. The lack of 100 and 110 superlattice reflections at 21.9° and 31.2°, respectively, indicates that the alloy does not exhibit $L1_2$ ordering. These patterns indicate that the Al grains are randomly oriented and have no preferred crystallographic texture. Two distinct changes in the diffraction patterns with increased Zr composition are observed. The first is a shift in the reflections to lower values of 2θ. This is to be expected as the larger Zr atoms (lattice volume of 23.3 $Å^3$ $atom^{-1}$) substitute for Al (lattice volume of 16.6 $Å^3$ $atom^{-1}$) in the fcc lattice. The second change is the development of a broad reflection centered around a 2θ of about 39°. The deposit containing 9.7 a/o Zr appears to be comprised of an amorphous phase in addition to fcc Al, whereas the deposit containing 16.6 a/o Zr is completely amorphous.

The lattice parameters of the fcc Al phase were refined by using the copper substrate reflections as an internal standard. These parameters are plotted as a function of alloy composition in Fig. 9. In addition, literature values for single-phase solid solutions produced by rapid solidification are plotted for comparison.[2,4] As-quenched alloys containing more that 3.0 a/o Zr were noted to be two-phase.[4] Similar levels of supersaturation have been produced by vapor deposition.[7] It is clear that solid solutions containing up to about 2 a/o Zr follow Vegard's Law; i.e., the lattice volumes of the solid solution are simply linear combinations of the constituent lattice volumes. In the region of 2 to 5 a/o Zr, the lattice volumes are smaller than those predicted by Vegard's Law. It appears that this deviation is real because there is no evidence for any second phase

present in either the rapidly solidified[4] or electrodeposited material in this composition range, e.g., see Fig. 7b. The highest degree of supersaturation was observed in deposits nominally containing 8 to 10 a/o Zr. SEM examination of these deposits indicated that the Zr was not homogeneously distributed throughout the deposit. EDS clearly showed regions containing high levels of Zr with a surface morphology similar to Fig. 7c and regions containing low levels of Zr that had a surface morphology similar to Fig. 7b. In certain areas, a supersaturated fcc phase was seen to nucleate on top of a Zr-rich amorphous layer, suggesting that insufficient Zr was available to maintain deposition of the amorphous phase. Because the Zr is partitioned between the fcc and amorphous phases in these two-phase deposits, the actual amount of Zr retained in solid solution can be estimated from the lattice parameter to be about 6 a/o in these electrodeposits. This level of supersaturation is at least twice that observed in vapor deposited or rapidly quenched alloys reported to date.

Two-phase regions are often observed in electrodeposited aluminum-transition metal alloys when the concentration of the transition metal exceeds the limit of supersaturation in the fcc Al solid solution. The appearance of the second phase, which often has an amorphous structure, generally causes a relaxation in the supersaturation of the solid solution. This has been observed in Al-Cr[20] and Al-Mn[47] alloys electrodeposited from $AlCl_3$-NaCl electrolytes. The two-phase region observed in electrodeposited Al-Zr is clearly different from that that reported in alloys deposited from the high-temperature melt. We have not observed the fine-grained duplex structure that is typically observed in homogeneous two-phase alloys, nor have we observed a relaxation in the supersaturation of Zr in the fcc phase when the amorphous phase is present. This suggests that the two-phase Al-Zr deposits are not intimately co-deposited but consist of

large, discrete regions of single-phase material. The non-uniform distribution of Zr and the resultant inhomogeneous surface morphology revealed by SEM is consistent with this conclusion. The phase distribution appears to follow the composition distribution that appears to be the result of a non-uniform current distribution along the copper wire electrode.

A similar mechanism has also been postulated to explain the two-phase structure observed in Al-Mn alloys electrodeposited under conditions where the Mn^{2+} is reduced near the diffusion-limited rate.[47] It is assumed that the electrode surface can become depleted of Mn^{2+} during deposition of the Mn-rich amorphous phase. At this point, deposition of the amorphous phase can no longer be sustained and a crystalline phase depleted in Mn is deposited. Because only limited amounts of Mn can be incorporated into the fcc structure, the Mn surface concentration recovers to a level that again favors the amorphous structure. This oscillatory behavior in the Mn surface concentration results in a fine-scale duplex structure of the amorphous and slightly supersaturated solid solution phases. Similar results have been observed in Al-Cr alloys electrodeposited from $AlCl_3$-NaCl electrolytes.[20] An fcc-amorphous two-phase region has also been observed in Al-Mn alloys electrodeposited at ambient temperature from $AlCl_3$-EtMeImCl;[48] however, the level of supersaturation in the fcc phase as a function of alloy composition was not reported.

The rounded nodular structure that is often associated with amorphous deposits is not necessarily obtained in all of the amorphous electrodeposits. Figure 10 shows the as-deposited surfaces of three alloys deposited at different current densities. Each contains 15.6 to 16.6 a/o Zr and has an identical amorphous XRD structure. The morphologies are quite different. Deposits formed at low current density (less than 10 mA cm^{-2}) are poorly

nucleated and have a particulate or platelet morphology, Fig. 10a and 10b. In contrast, the amorphous deposit formed at 20 mA cm^{-2} is dense and compact. To the naked eye, it also has a specular appearance. We believe that this may be due to a Zr^{3+} intermediate that may be more prevalent at the lower current densities, i.e., more positive deposition potentials. The limited solubility of Zr^{3+} may lead to its precipitation onto the electrode surface and to disruption of Al-Zr alloy film growth.

Pitting potential measurements of Al-Zr alloys. – The corrosion resistance of the electrodeposited Al-Zr alloys was investigated by recording potentiodynamic anodic polarization curves in N_2-saturated aqueous 0.1 M NaCl. These polarization curves are shown in Fig. 11. As noted for Al-Mn alloys examined under similar conditions,[23] Al-Zr alloys display a stable passive region characterized by a very small potential-independent current followed by a sudden rise in current at the pitting potential as the deposit undergoes electrodissolution. The variation of the Al-Zr pitting potential with alloy composition is shown in Fig. 12. The addition of 8 a/o or more Zr increases the pitting potential of the alloy by about +0.3 V versus pure Al. This increase is close to the value for the $Al_{97}Zr_3$ alloy that was prepared by sputter deposition.[49]

Acknowledgments

This research was supported by the Air Force Office of Scientific Research grant no. F49620-00-1-0123.

References

1. T. B. Massalski, *Binary Alloy Phase Diagrams*, American Society of Metals, Metals Park, OH (1990).

2. L. M. Burov and A. A. Yakunin, *Russ. J. Phys. Chem.*, **42**, 540 (1968).

3. N. I. Varich, L. F. Kolomoytseva, A. N. Varich, and V. V. Maslov, *Fiz. metal. metalloved.*, **27**, 361 (1969).

4. E. Sahin and H. Jones, in *Rapidly Quenched Metals III*, Vol. 138,, The Metals Society (1978).

5. Z. A. Chaudhury and C. Suryanarayana, *Metallography*, **17**, 231 (1984).

6. S. K. Pandey, D. K. Gangopadhyah, and C. Suryanarayana, *Z. Metallkd.*, **77**, 12 (1986).

7. Z. A. Chaudhury and C. Suryanarayana, *Mater. Sci. Eng.*, **67**, 47 (1984).

8. V. I. Dobatkin, V. I. Elagin, V. M. Fedorov, and R. M. Sizova, *Russian Met.*, **2**, 122 (1970).

9. N. Ryum, *Acta Metall.*, **17**, 269 (1969).

10. O. Izumi and D. Oelschlagel, *Scripta Metall.*, **3**, 619 (1969).

11. T. Ohashi and R. Ichikawa, *Met. Trans.*, **3**, 2300 (1972).

12. E. Nes, *Acta Metall.*, **20**, 499 (1972).

13. E. Nes and H. Billdal, *Acta Metall.*, **25**, 1039 (1977).

14. E. Nes and H. Billdal, *Acta Metall.*, **25**, 1031 (1977).

15. G. W. Delamore and R. W. Smith, *Metall. Trans.*, **2**, 1733 (1971).

16. T. Ohashi and R. Ichikawa, *Z. Metallkd.*, **64**, 517 (1973).

17. R. Grimes, M. J. Stowell, and B. M. Watts, *Metals Tech.*, **3**, 154 (1976).

18. B. M. Watts, M. J. Stowell, B. L. Baike, and D. G. E. Owen, *Metal Sci.*, **10**, 198 (1976).

19. B. M. Watts, M. J. Stowell, B. L. Baike, and D. G. E. Owen, *Metal Sci.*, **10**, 189 (1976).

20. T. P. Moffat, *J. Electrochem. Soc.*, **141**, L115 (1994).

21. M. R. Ali, A. Nishikata, and T. Tsuru, *Electrochim. Acta*, **42**, 2347 (1997).

22. G. R. Stafford, *J. Electrochem. Soc.*, **136**, 635 (1989).

23. T. P. Moffat, G. R. Stafford, and D. E. Hall, *J. Electrochem. Soc.*, **140**, 2779 (1993).

24. G. R. Stafford, *J. Electrochem. Soc.*, **141**, 245 (1994).

25. T. Tsuda, C. L. Hussey, G. R. Stafford, and J. E. Bonevich, *J. Electrochem. Soc.*, **150**, C234 (2003).

26. T. Tsuda and C. L. Hussey, *J. Min. and Metall., B*, **39**, 3 (2003).

27. G. R. Stafford and C. L. Hussey, in *Advances in Electrochemical Science and Engineering*, R. C. Alkire and D. M. Kolb, Editors, Vol. 7, p.275, Wiley-VCH Verlag GmbH, Weinheim (2002).

28. M. M. Kawase and Y. Ito, *J. Appl. Electrochem.*, **33**, 785 (2003).

29. B. Gilbert, G. Mamantov, and K. W. Fung, *Inorg. Chem.*, **14**, 1802 (1975).

30. M. Katabua, P. Rolland, G. Mamantov, and L. Hulett, *Inorg. Chem.*, **21**, 3569 (1982).

31. D. Sun and T. Hughbanks, *Inorg. Chem.*, **38**, 992 (1999).

32. R. Bilewicz, K. Wikiel, R. Osteryoung, and J. Osteryoung, *Anal. Chem.*, **61**, 965 (1989).

33. T. B. Scheffler and C. L. Hussey, *Inorg. Chem.*, **23**, 1926 (1984).

34. R. S. Nicholson, *Anal. Chem.*, **37**, 1406 (1965).

35. R. S. Nicholson and I. Shain, *Anal. Chem.*, **36**, 706 (1964).

36. A. A. Fannin, Jr., D. A. Floreani, L. A. King, J. S. Landers, B. J. Piersma, D. J. Stech, R. L. Vaughn, J. S. Wilkes, and L. Williams John, *J. Phys. Chem.*, **88**, 2614 (1984).

37. J. O. M. Bockris and A. K. N. Reddy, *Modern Electrochemistry*, Plenum Press, New York (1998).

38. R. T. Carlin, R. A. Osteryoung, J. S. Wilkes, and J. Rovang, *Inorg. Chem.*, **29**, 3003 (1990).

39. G. R. Stafford and T. P. Moffat, *J. Electrochem. Soc.*, **142**, 3288 (1995).

40. O. Ruff and R. Wallstein, *Z. Anorg. Allg. Chem.*, **128**, 96 (1923).

41. E. M. Larsen, J. W. Moyer, F. Gil-Arnao, and M. J. Camp, *Inorg. Chem.*, **13**, 574 (1974).

42. J. Brynestad, S. von Winbush, H. L. Yakel, and G. P. Smith, *Inorg. Nucl. Chem. Letters*, **6**, 889 (1970).

43. K. W. Fung and G. Mamantov, *J. Electroanal. Chem.*, **35**, 27 (1972).

44. L. W. Austin, M. G. Vucich, and E. J. Smith, *Electrochem. Tech.*, **1**, 267 (1963).

45. T. Tsuda, C. L. Hussey, G. R. Stafford, and J. E. Bonevich, *J. Electrochem. Soc.*,, (2003).

46. T. Takenaka and M. Kawakami, *Int. J. Mater. and Product Tech.*, **2**, 500 (2001).

47. B. Grushko and G. R. Stafford, *Metall. Trans. A*, **20A**, 1351 (1989).

48. P. C. Trulove, J. A. Mitchell, P. L. Hagans, R. T. Carlin, G. R. Stafford, and H. C. De Long, in *Proceedings of the Twelfth International Symposium on Molten Salts*, P. C. Trulove, H. C. De Long, G. R. Stafford, and S. Deki, Editors, PV 99-41, p. 517, The Electrochemical Society Proceedings Series, Pennington, NJ (1999).

49. G. D. Davis, W. C. Moshier, T. L. Fritz, and G. O. Cote, *J. Electrochem. Soc.*, **137**, 422 (1990).

Table. I Summary of electrochemical data for titanium and zirconium solutes in Lewis acidic $AlCl_3$–EtMeImCl.

	Method	Temperature (K)	mol % $AlCl_3$	Concentration (mmol L^{-1})	$10^7 D$ (cm^2 s^{-1})	$10^{11} \eta D/T$ (g cm s^{-2} K^{-1})	Reference
Ti(IV)	NPV	300	60.0	40	8.1	39	38
Zr(IV)	CV	353	66.7	4.85	42	58	This work
Ti(II)	RDE-CV	353	66.7	12.6	2.2	3.1	25
	RDE-CV	353	66.7	25.2	1.2	1.6	25
Zr(II)	RDE-CV	353	66.7	5.40	1.2	1.7	This work
	RDE-CV	353	66.7	19.5	0.64	0.88	This work

NPV: Normal pulse voltammetry; CV: Cyclic voltammetry; RDE-CV: Cyclic voltammetry using a rotating Pt disk elctrode.

Figure Captions

Fig. 1. Cyclic staircase voltammograms recorded at a platinum stationary disk electrode in the 66.7–33.3 m/o $AlCl_3$–EtMeImCl melt: 19.5 mmol L^{-1} $ZrCl_4$ (—); pure melt (- - -). Inset: magnified region of the voltammogram recorded in melt containing $ZrCl_4$. The sweep rate was 10 mV s^{-1}, and the step size was 2 mV.

Fig. 2. Cyclic staircase voltammograms recorded at a platinum stationary disk electrode in the 66.7–33.3 m/o $AlCl_3$–EtMeImCl melt containing 11.6 mmol L^{-1} $ZrCl_4$: first scan (—) and (- - -) fifth scan by continuous voltammetry. The sweep rate was 100 mV s^{-1}, and the step size was 2 mV.

Fig. 3. Peak reduction current density and ratio of the anodic to cathodic peak currents as a function of sweep rate for a series of voltammograms similar to that shown in Fig. 2.

Fig. 4. UV-visible spectra of the 66.7–33.3 m/o $AlCl_3$–EtMeImCl melt containing 5.04 mmol L^{-1} $ZrCl_4$ before (—) and after reduction of the Zr(IV) with Al metal (- - -) and with Zr metal (- - -).

Fig. 5. Staircase voltammograms recorded at a Pt-RDE in the 66.7–33.3 m/o $AlCl_3$–EtMeImCl melt containing (—) 19.5 and (- - -) 5.40 mmol L^{-1} Zr(II). The sweep rate was 10 mV s^{-1}; the rotation rates were 1000, 1250, 1500, 1750, and 2000 rpm; and the step size was 2 mV. (Inset) Relationship between the limiting current densities and the square root of the angular frequency of rotation: (●) 19.5 mmol L^{-1} Zr(II), 0.80 V and (○) 5.40 mmol L^{-1} Zr(II), 0.90 V

Fig. 6. Relationship between the applied current density and Zr content of Al-Zr deposits prepared in the 66.7–33.3 m/o $AlCl_3$–EtMeImCl melt: (●) 19.5 mmol L^{-1} Zr(IV), (○) 19.5 mmol L^{-1} Zr(II), (▲) 4.85 mmol L^{-1} Zr(IV), and (Δ) 4.85 mmol L^{-1} Zr(II). The electrode rotation rate was 2000 rpm.

Fig. 7. Scanning electron micrographs of Al-Zr alloys electrodeposited from the 66.7-33.3 m/o $AlCl_3$-EtMeImCl melt: (a) 1.4 a/o Zr, 20 mA cm^{-2}, 4.85 mmol L^{-1} Zr(IV); (b) 4.9 a/o Zr, 10 mA cm^{-2}, 4.85 mmol L^{-1} Zr(IV); and (c) 15.9 a/o Zr, 20 mA cm^{-2}, 10.2 mmol L^{-1} Zr(IV).

Fig. 8. X-ray diffraction patterns (Cu-Kα) from as-deposited Al-Zr alloys containing: (a) 1.4, (b) 4.9, (c) 9.7, and (d) 16.6 a/o Zr. Copper reflections from the substrate are denoted by ▼ at the top of the figure.

Fig. 9. Lattice parameter for fcc Al as a function of Al-Zr alloy composition: (●) this work, (□) Burov and Yakunin,[2] (○) Sahin and Jones,[4] and (—) Vegard's Law.

Fig. 10. Scanning electron micrographs of Al-Zr alloys electrodeposited from 66.7-33.3 m/o $AlCl_3$-EtMeImCl melt: (a) 15.6 a/o Zr, 5 mA cm^{-2}, 19.5 mmol L^{-1} Zr(IV); (b) 16.6 a/o Zr, 10 mA cm^{-2}, 19.5 mmol L^{-1} Zr(IV); and (c) 15.9 a/o Zr, 20 mA cm^{-2}, 10.2 mmol L^{-1} Zr(IV).

Fig. 11. Anodic polarization curves recorded in deaerated 0.1 mmol L^{-1} aqueous NaCl for Al-Zr alloys electrodeposited from the 66.7–33.3 m/o $AlCl_3$–EtMeImCl melt: (a) Al

(99.999 %), (b) $Al_{97.8}Zr_{2.2}$, (c) $Al_{97.2}Zr_{2.8}$, (d) $Al_{95.5}Zr_{4.5}$, and (e) $Al_{84.3}Zr_{15.7}$. The sweep rate was 0.5 mV s^{-1}, the step size was 2 mV, and the experiments were conducted at room temperature.

Fig. 12. Pitting potentials as a function of composition for the Al-Zr alloys described in Fig. 11. Alloys electrodeposited from solutions containing Zr(II) (●) and Zr(IV) (○).

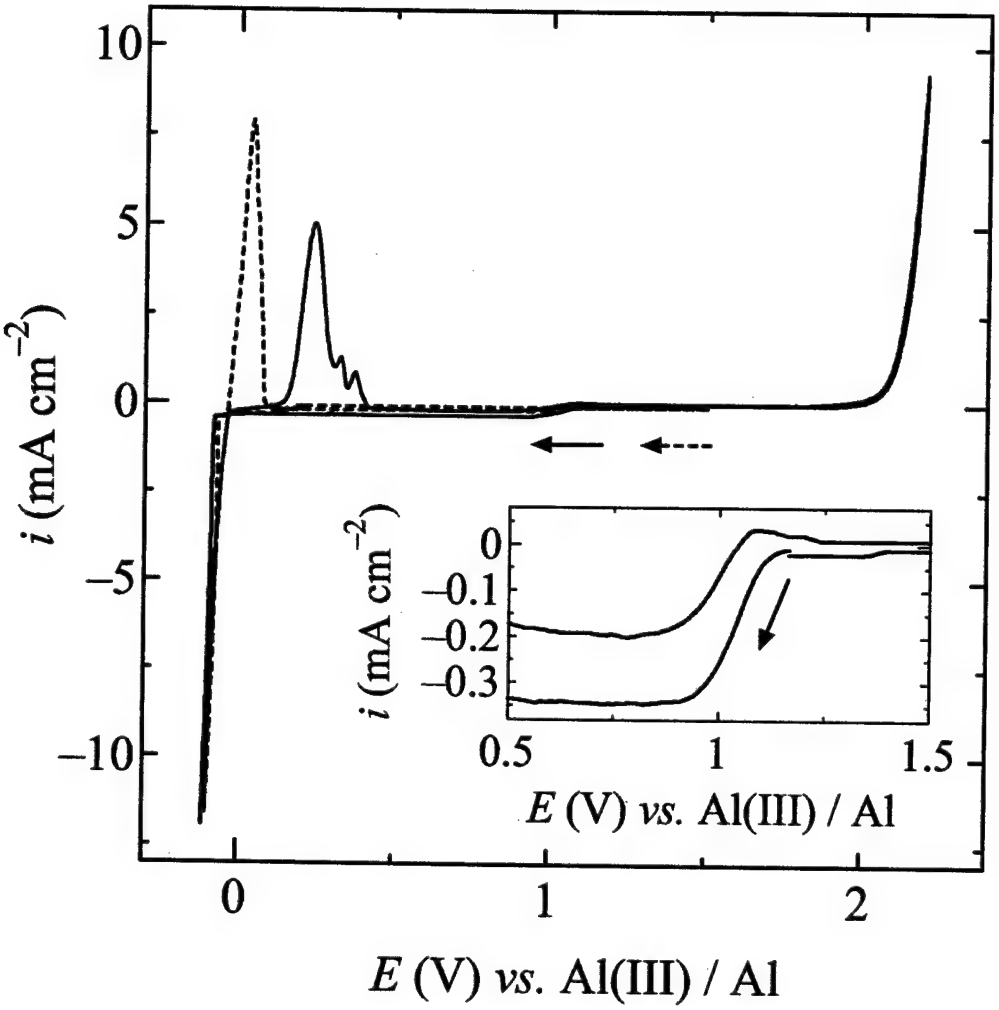
10
5
0
−5
−10
0
1
2
i (mA cm−2)
E (V) vs. Al(III) / Al
0
−0.1
−0.2
−0.3
0.5
1
1.5
i (mA cm−2)
E (V) vs. Al(III) / Al

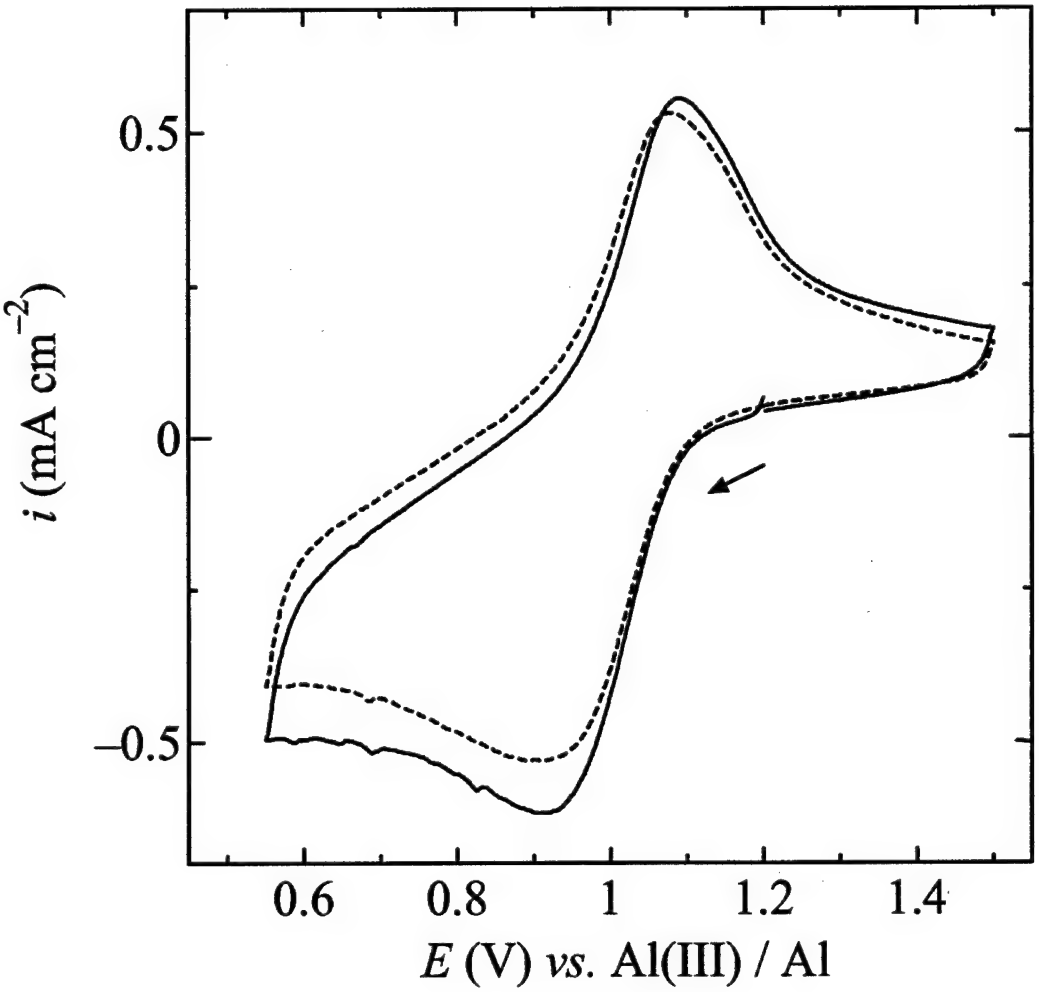
0.5
0
–0.5
i (mA cm^{-2})
0.6
0.8
1
1.2
1.4
E (V) *vs.* Al(III) / Al

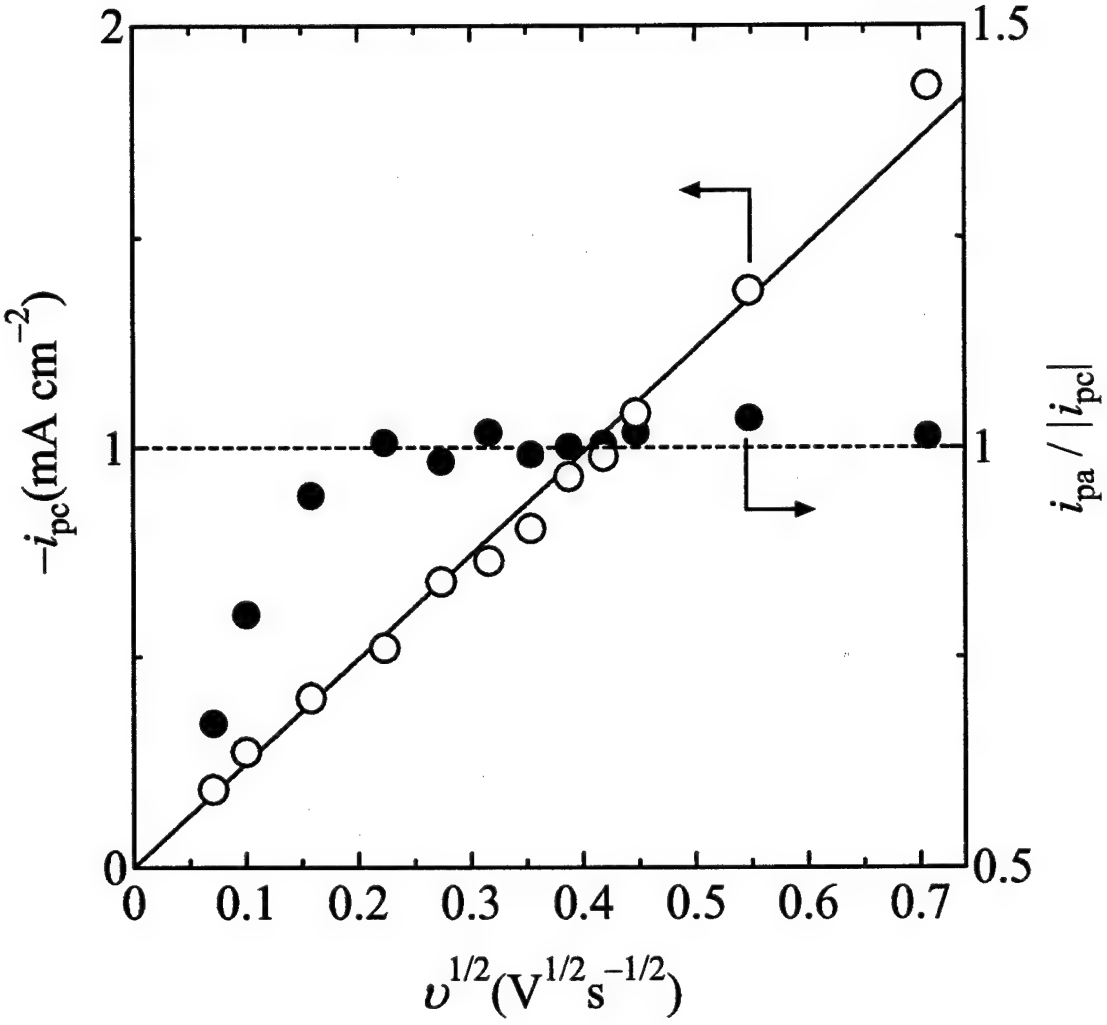
2
1
0
1.5
1
0.5
0
0.1
0.2
0.3
0.4
0.5
0.6
0.7
$-i_{pc}$(mA cm^{-2})
i_{pa} / $|i_{pc}|$
$\upsilon^{1/2}$(V$^{1/2}$s$^{-1/2}$)

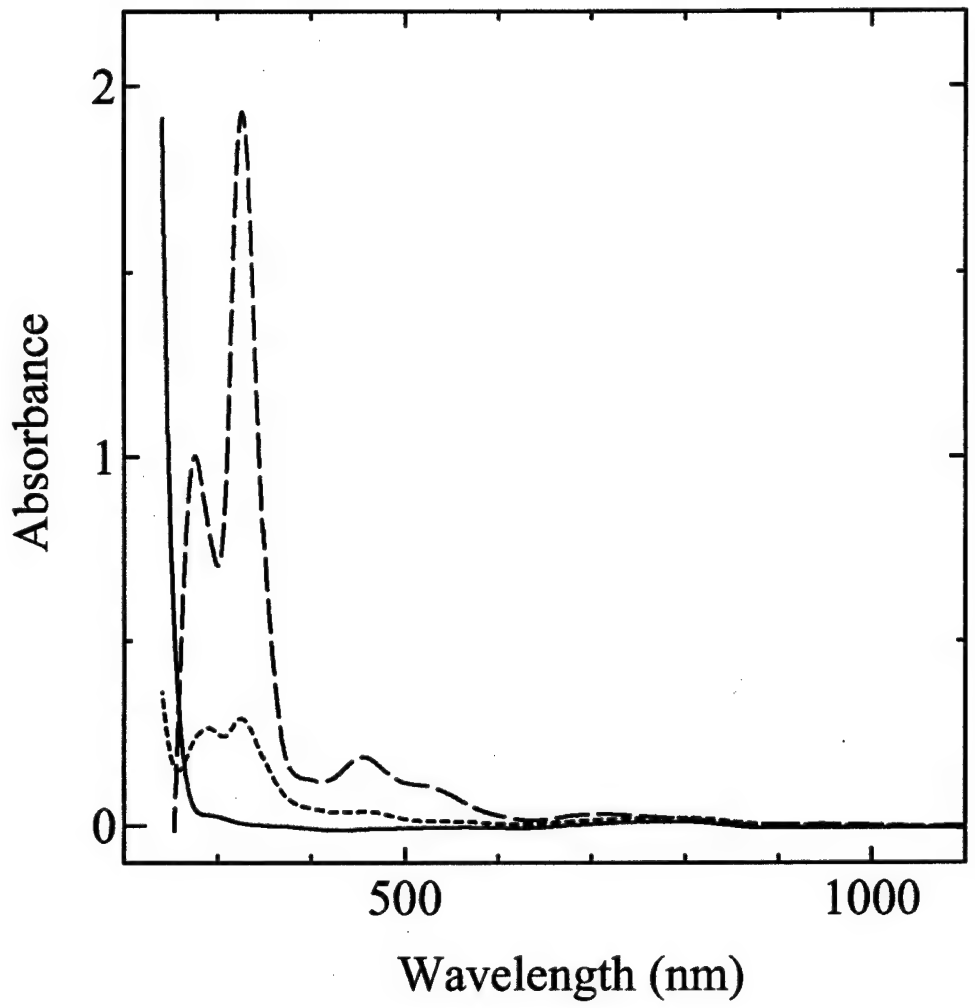
Absorbance
2
1
0
500
1000
Wavelength (nm)

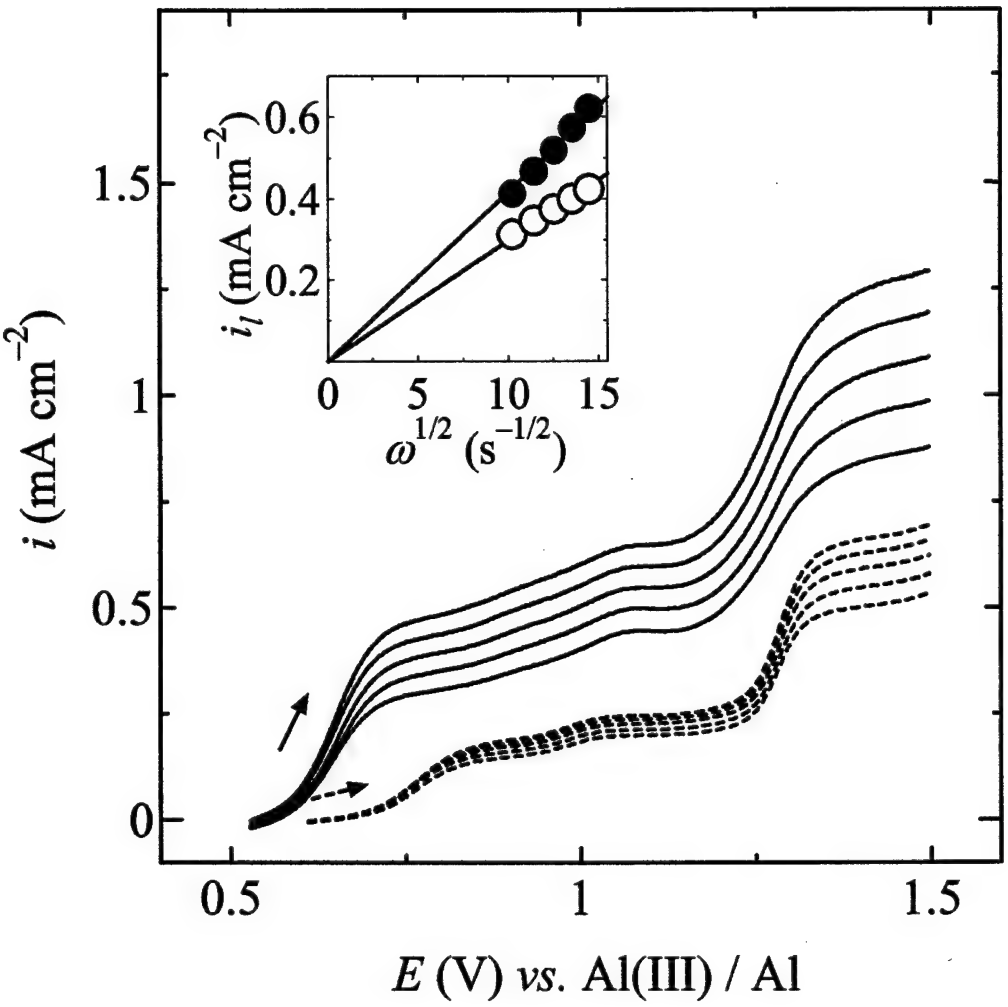
i (mA cm^{-2})
1.5
1
0.5
0
0.5
1
1.5
E (V) *vs.* Al(III) / Al
i_l (mA cm^{-2})
0.6
0.4
0.2
0
5
10
15
$\omega^{1/2}$ (s$^{-1/2}$)

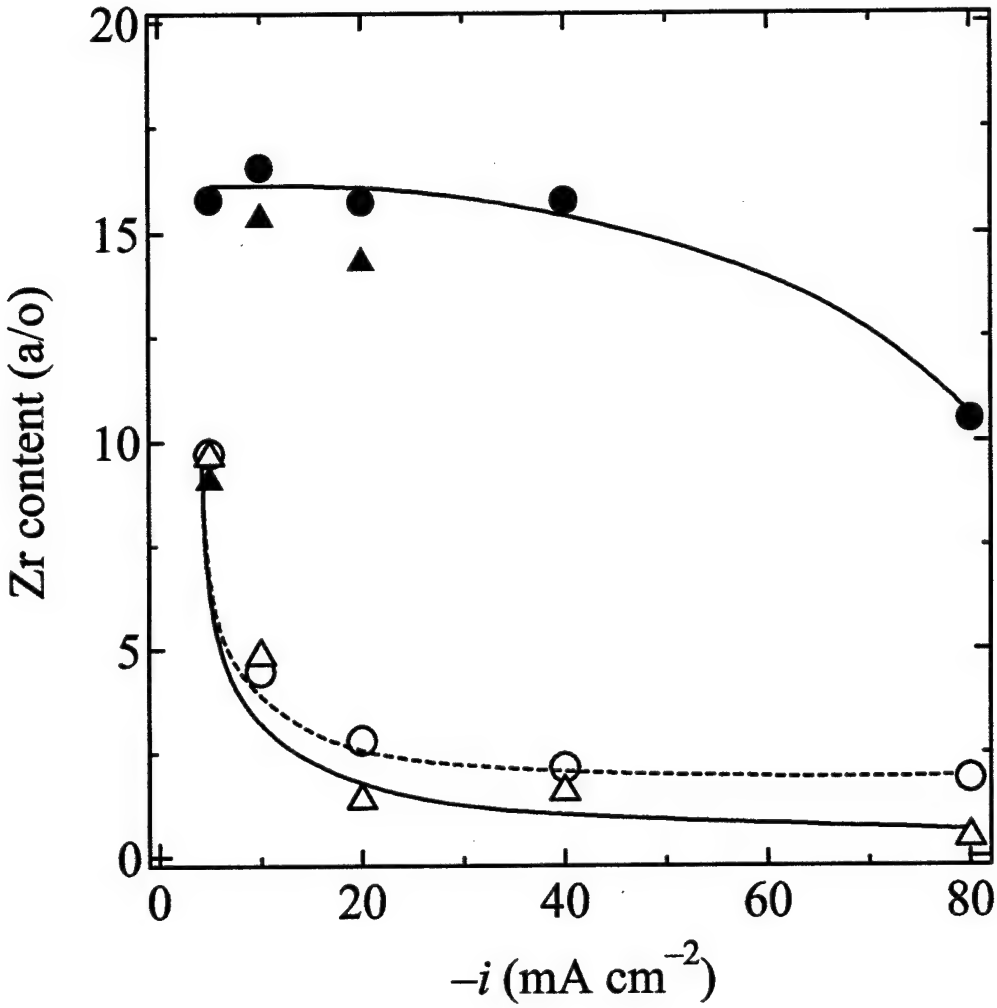
20
15
10
5
0
Zr content (a/o)
0
20
40
60
80
–i (mA cm–2)

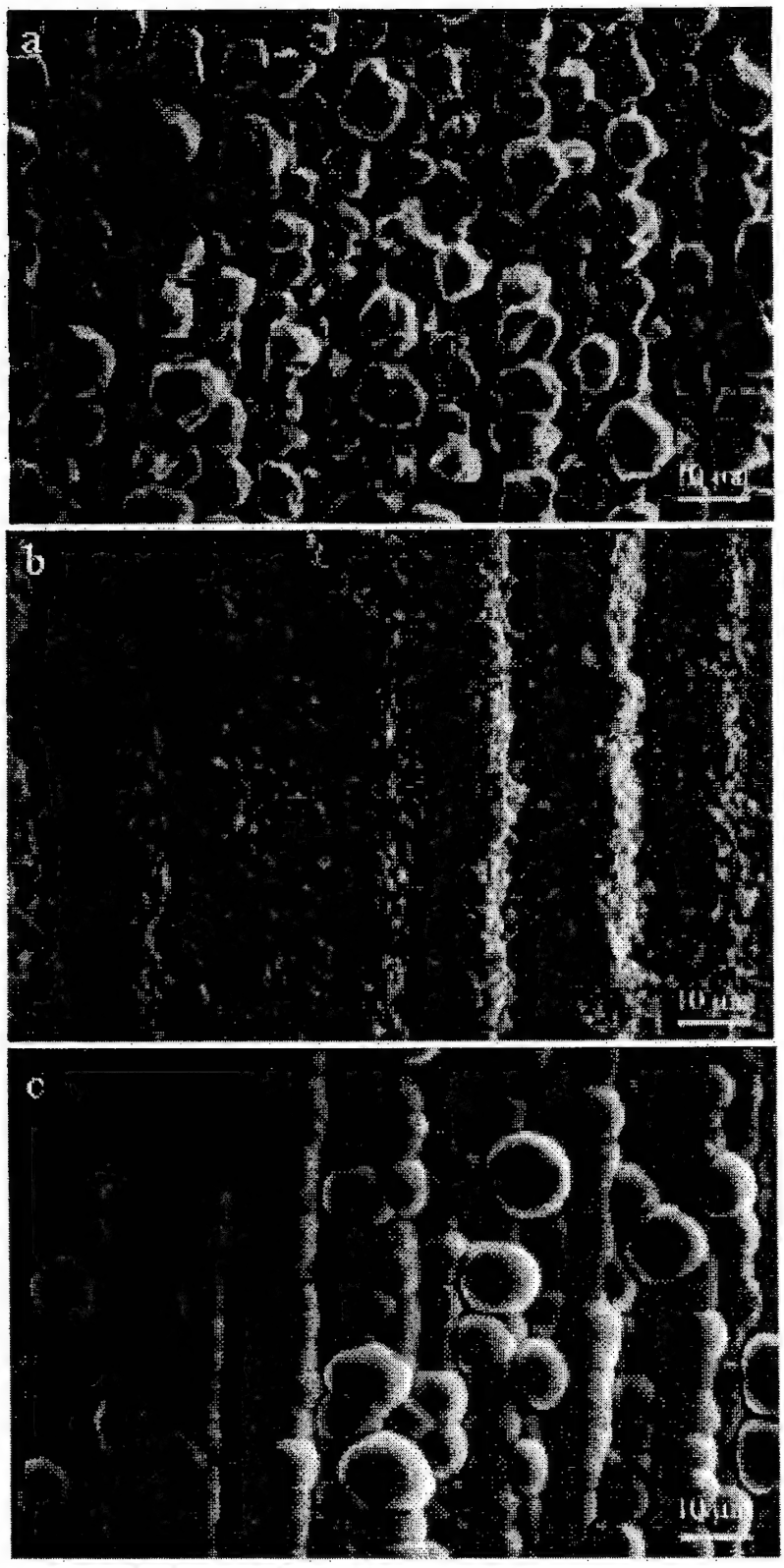
a
b
c

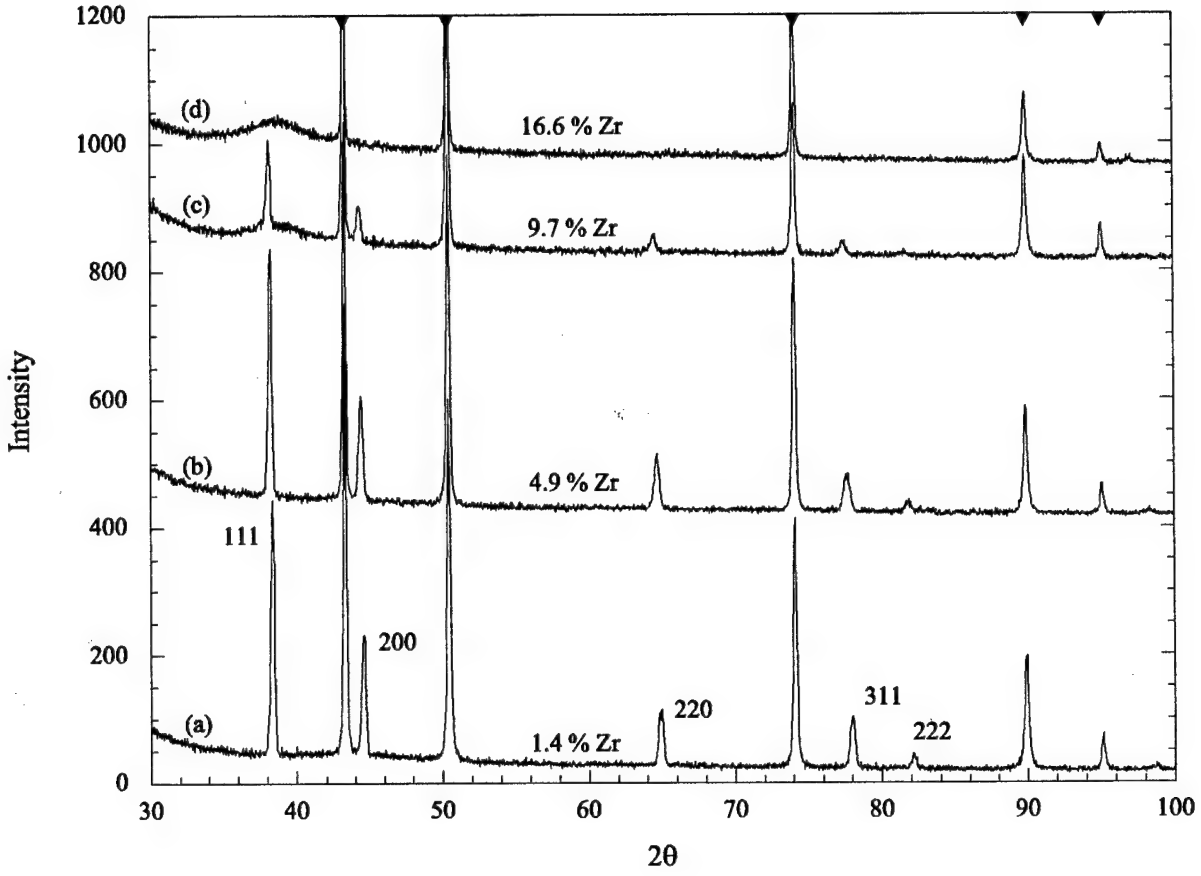
1200
1000
800
600
400
200
0
Intensity
(d)
16.6 % Zr
(c)
9.7 % Zr
(b)
4.9 % Zr
(a)
1.4 % Zr
111
200
220
311
222
30
40
50
60
70
80
90
100
2θ

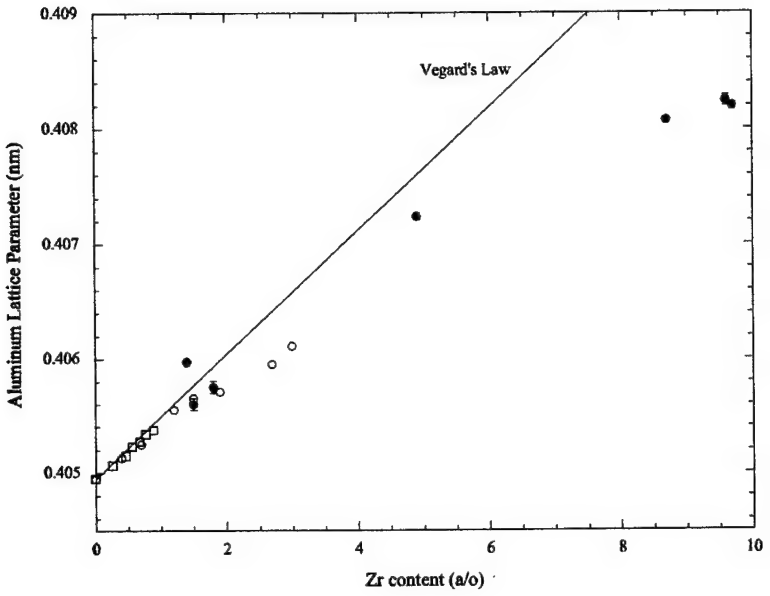
0.409
0.408
0.407
0.406
0.405
Aluminum Lattice Parameter (nm)
Vegard's Law
0
2
4
6
8
10
Zr content (a/o)

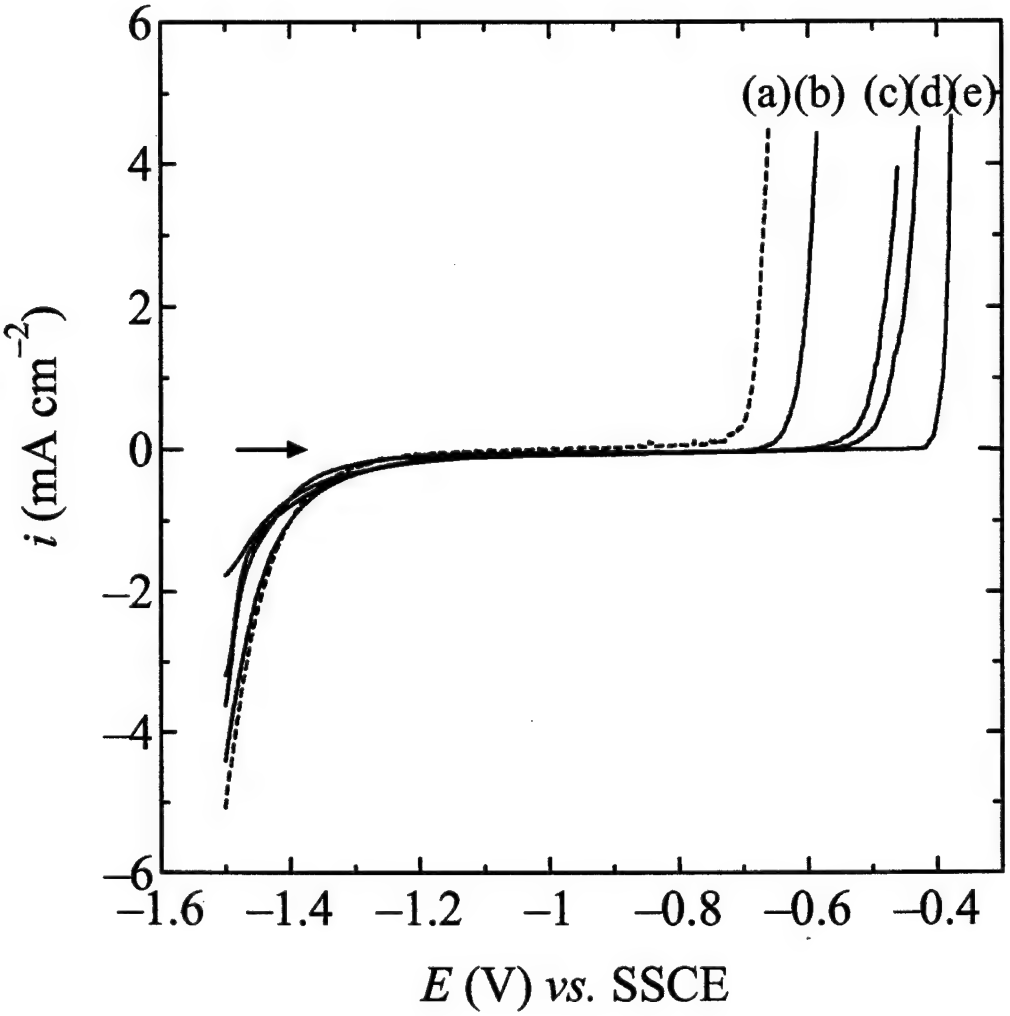
6
4
2
0
–2
–4
–6
–1.6
–1.4
–1.2
–1
–0.8
–0.6
–0.4
(a)(b) (c)(d)(e)
i (mA cm−2)
E (V) vs. SSCE

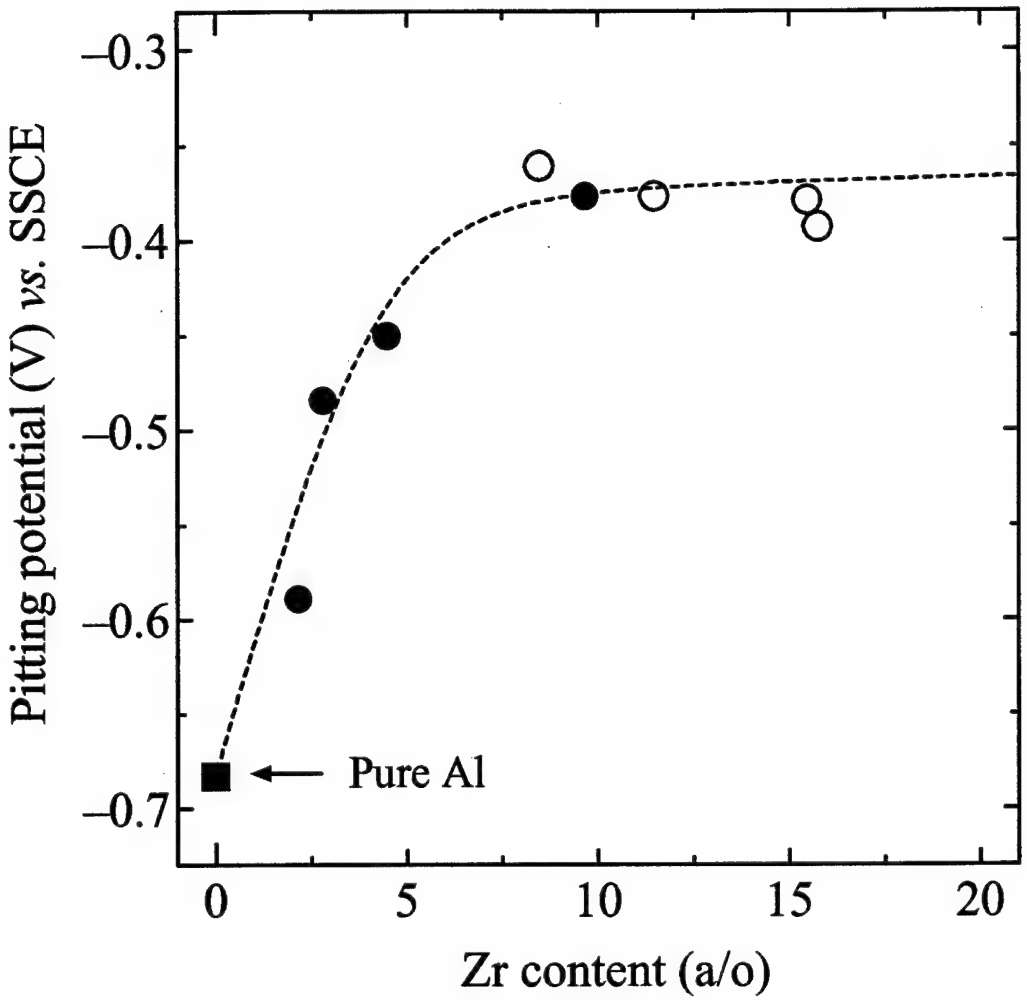
Pitting potential (V) vs. SSCE
–0.3
–0.4
–0.5
–0.6
–0.7
Pure Al
0
5
10
15
20
Zr content (a/o)

APPENDIX II

T. Tsuda, C. L. Hussey, and G. R. Stafford, "Electrodeposition of Al-Mo Alloys from the Lewis Acidic Aluminum Chloride–1-Ethyl-3-methylimidazolium Chloride Molten Salt," *J. Electrochem. Soc.*, in press.

Journal of The Electrochemical Society, **151** (6) 1-0 (2004)
0013-4651/2004/151(6)/1/6/$7.00 © The Electrochemical Society, Inc.

Electrodeposition of Al-Mo Alloys from the Lewis Acidic Aluminum Chloride-1-Ethyl-3-Methylimidazolium Chloride Molten Salt

Tetsuya Tsuda,[a,*] Charles L. Hussey,[a,,z] and Gery R. Stafford[b,*]**

[a]*Department of Chemistry and Biochemistry, The University of Mississippi, University, Mississippi 38677, USA*
[b]*Materials Science and Engineering Laboratory, National Institute of Standards and Technology, Gaithersburg, Maryland 20899, USA*

The electrodeposition of aluminum-molybdenum alloys was examined at copper rotating disk and wire substrates in the Lewis acidic 66.7-33.3 mol % aluminum chloride-1-ethyl-3-methylimidazolium chloride molten salt containing Mo(II) in the form of dissolved $(Mo_6Cl_8)Cl_4$. The molybdenum content of the electrodeposits depended on the electrode rotation rate, Mo(II) concentration, and bath temperature. It was possible to produce nonequilibrium alloys containing up to 11 atom % Mo. These alloy deposits were compact and chloride-free. Al-Mo alloys containing more than 8 atom % Mo exhibited a chloride corrosion pitting potential of approximately +800 mV against pure aluminum. The corrosion resistance of this alloy is superior to that of all the aluminum-transition metal alloys that have been electrodeposited to date from chloroaluminate molten salts.
 [DOI: 10.1149/1.1704611]

Manuscript submitted October 10, 2003; revised manuscript received November 11, 2003.

The resistance of aluminum to chloride-induced pitting corrosion can be enhanced considerably when it is alloyed with transition metals. Although a number of different transition metals have been examined for their efficacy in this role, molybdenum has proven to be one of the most effective additives for imparting corrosion resistance to Al.[1] The maximum solubility of Mo in face-centered cubic (fcc) Al is only 0.07 atom %, and this occurs at the peritectic temperature of 661°C.[2] At room temperature, Mo has negligible solubility in Al.[3] As a consequence, extended solid solutions must be prepared by nonequilibrium alloying methods such as rapid solidification,[4-7] laser-surface melting,[8] mechanical alloying,[9,10] ion implantation,[11-15] and radio frequency (rf)-magnetron sputtering.[1,16-21] These metastable solid solutions are being considered as precursors for precipitation hardenable alloys. Polyesya and Stepina[5] and Logan *et al.*[7] have reported supersaturations of 2.7 and 2.45 atom % Mo, respectively, in rapidly solidified alloys. In the latter case, two metastable crystalline phases were observed along with the solid solution. Enzo *et al.*[10] have observed extended solid solutions following the mechanical alloying of an $Al_{75}Mo_{25}$ mixture of pure elemental powders in a high-energy mixer mill. Lattice parameter measurements were used to estimate a supersaturation of about 6 atom % Mo following 78 h of mechanical alloying.

Isothermal electrodeposition is an attractive method for the preparation of metal or metal alloy coatings because it can lead to thin films with uniform composition and thickness. A number of binary aluminum-transition metal alloys showing improved resistance to chloride-induced pitting corrosion relative to Al have been electrodeposited from plating baths based on Lewis acidic chloroaluminate molten salts. Among these alloys are Al-Cr,[22-24] Al-Mn,[25,26] Al-Ti,[27-30] and Al-V.[31] Industrial applications of chloroaluminate plating baths for coating sheet steel with Al-Mn alloy have been explored.[32-34] Ternary aluminum-transition metal alloys such as Al-Mn-Ce and Al-Mn-Ti have also been electrodeposited from chloroaluminate melts, and both alloys show improved resistance to chloride-pitting corrosion relative to Al. However, there is a paucity of reports describing the electrodeposition of Al-Mo alloys from these melts. In this article, we report the electrodeposition of Al-Mo alloys from the 66.7-33.3 mol % $AlCl_3$-1-ethyl-3-methylimidazolium chloride (EtMeImCl) molten salt[35] containing dissolved $(Mo_6Cl_8)Cl_4$ as a source of Mo(II). The aim of this investigation is to study the effects of the Mo(II) concentration, bath temperature, applied current density, and hydrodynamic transport rate on the composition and chloride-corrosion pitting potential of the electrodeposited Mo-Al alloy films. These alloys may have applications in a saltwater environment.

Experimental

Preparation of the plating bath.—The procedures used for the synthesis of EtMeImCl, the purification of $AlCl_3$ by sublimation, and the preparation and purification of the $AlCl_3$-EtMeImCl molten salt were identical to those described in previous articles.[36,37] Anhydrous molybdenum(II) chloride $[(Mo_6Cl_8)Cl_4]$ of 99.5% purity (Cerac) was used as received and was dissolved in the $AlCl_3$-EtMeImCl molten salt to prepare the plating bath. All experiments except the aqueous corrosion measurements were carried out in a nitrogen gas-filled glove box (VAC Atmospheres NEXUS system) with an O_2 and H_2O content <5 ppm.

Electrochemical and spectroscopic experiments.—Electrochemical experiments were conducted using a three-electrode cell. A Pine Instruments Teflon-sheathed platinum rotating disk electrode (RDE) with a geometrical area of 0.099 cm^2 was used as the working electrode for voltammetry experiments. Coils of 0.10 cm diam aluminum wire (Alfa Aesar, 99.999%) were used for the counter and reference electrodes. These electrodes were immersed in melt with the same composition as the bulk melt but were separated from the bulk melt by a porosity E glass frit (Ace Glass). The aluminum electrodes were cleaned with a mixture of concentrated aqueous H_2SO_4, HNO_3, and H_3PO_4, rinsed with distilled H_2O, and dried under vacuum before use. Alloy samples approximately 10 μm thick were deposited from solutions of $(Mo_6Cl_8)Cl_4$ in the $AlCl_3$-EtMeImCl molten salt onto working electrodes consisting of either a length of 1.25 mm diam copper wire (Cu RWE) or a Teflon-sheathed Cu RDE (geometrical area 0.798 cm^2). Both substrates could be rotated at a fixed rate with a Pine Instruments AFMSRX electrode rotator. At the conclusion of each deposition experiment, the alloy-plated substrate was removed from the glove box and cleaned with distilled water.

Cyclic voltammetry (CV) experiments were conducted by using a Pine Instruments Co. model AFCBP1 bipotentiostat/automatic polarization system controlled with PineChem for Windows software. The electrodeposition of Al-Mo alloys was performed with an EG&G Princeton Applied Research Corp. (PARC) model 173 potentiostat/galvanostat equipped with a model 179 digital coulometer plug-in module. Potentiodynamic pitting measurements were carried out on these alloy samples at room temperature in a 0.1 mol L^{-1} solution of NaCl in distilled H_2O by using an EG&G PARC

* Electrochemical Society Active Member.
** Electrochemical Society Fellow.
z E-mail: chclh@chem1.olemiss.edu

model 263 potentiostat/galvanostat. This potentiostat was controlled with EG&G PARC model 270 software. This solution was thoroughly deaerated with N_2 gas before each experiment. The reference electrode for these measurements was a sodium chloride-saturated calomel electrode (SSCE), and the counter electrode was a large-surface-area platinum wire coil. To carry out these measurements, a known length of the plated Cu wire was exposed to the NaCl solution by using a heat-shrink tubing mask, and the sample was scanned at 0.5 mV s^{-1} by using linear staircase voltammetry.

UV-visible spectroscopic measurements were obtained using a Varian CARY 5 spectrometer. Samples were contained in Wilmad no. 107-7 closed-type quartz cells with a 0.10 cm optical path length.

Characterization of the Al-Mo electrodeposits.—The crystal structure of the Al-Mo electrodeposits was examined with standard X-ray diffraction (XRD) techniques by using a Siemens D-500 X-ray diffractometer at the National Institute of Standards and Technology (NIST). This instrument was operated in the θ-2θ scan mode and employed Cu Kα radiation. The lattice parameters of the fcc Al phase in the alloy deposits were accurately determined by employing the copper substrate reflections as an internal standard. A minimum of five well-resolved reflections was required for lattice parameter refinement. Surface morphology and elemental analysis of the alloy samples were performed with a JEOL JSM-6100 (UM) or JEOL JXA-840 (NIST), or Hitachi S-2600H (Kyoto University) scanning electron microscopes (SEMs). Alloy composition was measured with energy-dispersive X-ray spectroscopy (EDS) on the as-deposited surfaces with pure Al and Mo as standards. The reported composition values are the averages of at least nine measurements made along the length of the copper wire substrate.

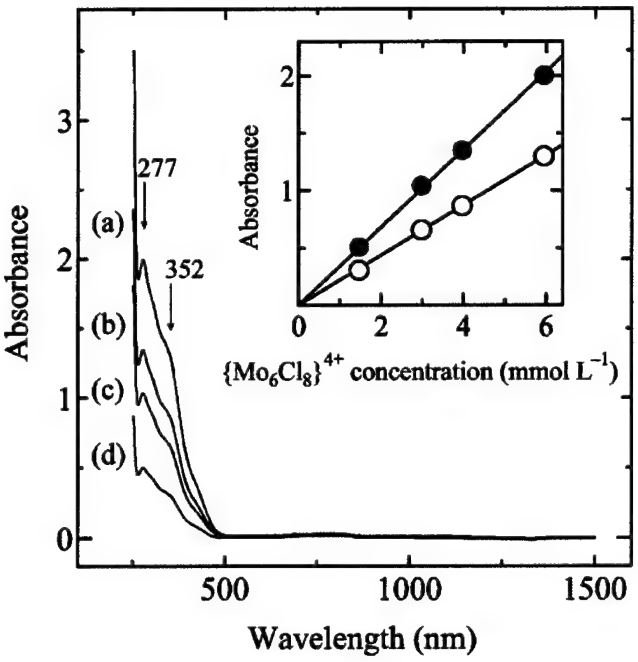

Figure 1. UV-visible spectra of $(Mo_6Cl_8)Cl_4$ dissolved in the 66.7 mol % $AlCl_3$-EtMeImCl melt: (a) 5.94, (b) 3.96, (c) 2.98, and (d) 1.46 mmol L^{-1}. Inset: Beer's Law plots at (●) 276.9 and (○) 352.4 nm. Spectra were recorded at room temperature, and the cell path length was 0.10 cm.

Results and Discussion

Molybdenum(II) chloride, $(Mo_6Cl_8)Cl_4$, is an octahedral hexanuclear metal cluster compound with formal single bonds between the Mo atoms and is normally prepared by the Al reduction of $MoCl_5$ in molten $AlCl_3$-NaCl.[38] The chemistry and electrochemistry of this species has been investigated in the $AlCl_3$-EtMeImCl molten salt.[39] In basic melt, *i.e.*, melt containing less than 50 mol % $AlCl_3$, this species reacts with excess chloride ion to form the hexanuclear chloride complex, $[(Mo_6Cl_8)Cl_6]^{2-}$. This species could be reduced near the negative limit of the melt, but the reduction product is completely unstable, suggesting complete destruction of the cluster. No Mo metal or alloys could be deposited from this composition of the molten salt. $(Mo_6Cl_8)Cl_4$ is soluble in acidic melt, *i.e.*, melt containing more than 50 mol % $AlCl_3$, but no oxidation or reduction waves that can be attributed to this species are apparent. However, it seems likely that the $\{Mo_6Cl_8\}^{4+}$ core structure is preserved in acidic $AlCl_3$-EtMeImCl because the metal-centered luminescence spectrum typically observed at 700 nm[40] for this molybdenum core can still be observed after $(Mo_6Cl_8)Cl_4$ is dissolved in this solvent.[39] [Because the coordination/solvation of dissolved $(Mo_6Cl_8)Cl_4$ is unknown, we refer to the dissolved Mo(II) entity by its core structure, $\{Mo_6Cl_8\}^{4+}$.]

Absorption spectroscopy of $\{Mo_6Cl_8\}^{4+}$.—$(Mo_6Cl_8)Cl_4$ dissolved readily in the 66.7 mol % melt to produce a yellow solution. An electronic absorption spectrum of this solution is shown in Fig. 1. The overall appearance of this spectrum is similar to that observed for this compound in the less acidic 55.5 mol % melt,[39] except that the absorption maximum at 304 nm in this melt is shifted to 277 nm in the 66.7 mol % melt. This shift in wavelength implies that interactions between the solvated $\{Mo_6Cl_8\}^{4+}$ species and the ionic species in the melt change as the melt acidity is altered. Plots of absorbance *vs.* the $\{Mo_6Cl_8\}^{4+}$ concentration for data recorded at 277 and 352 nm are shown in the inset of Fig. 1, and they demonstrate that Beer's law is obeyed at both wavelengths. This result is important because in the absence of any voltammetric waves corresponding to the oxidation or reduction of $\{Mo_6Cl_8\}^{4+}$ in this melt, it is possible to monitor the concentration of dissolved $(Mo_6Cl_8)Cl_4$ by using absorption spectroscopy.

Effect of $(Mo_6Cl_8)Cl_4$ *on the electrodeposition of aluminum.*—The negative potential limit of the Lewis acidic $AlCl_3$-EtMeImCl molten salt arises from the reduction of the coordinately unsaturated $Al_2Cl_7^-$ ion to Al metal according to the following reaction

$$4Al_2Cl_7^- + 3e^- \rightleftharpoons Al + 7AlCl_4^- \qquad [1]$$

On a thermodynamic basis, the deposition and stripping of Al in the 66.7 mol % should take place at potentials very close to 0 V *vs.* a reference electrode consisting of an Al wire immersed in the same melt. In practice, a significant cathodic overpotential is usually required to initiate the electrocrystallization of a three-dimensional bulk Al electrodeposit on a foreign substrate such as Pt. However, electrodissolution of the resulting Al electrodeposit may still occur at potentials very close to 0 V if the deposit is thick enough to exhibit the properties of bulk Al.

Figure 2 shows CVs recorded at Pt stationary and rotating disk electrodes in the 66.7 mol % melt before and after the addition of $(Mo_6Cl_8)Cl_4$. To record these voltammograms, the potential scan was initiated from 1.0 V to a potential sufficiently cathodic to initiate the electrodeposition of Al. The scan was then reversed until it reached the positive limit of the melt at about 2.2 V and was finally returned to the initial potential. This figure shows that a cathodic overpotential of about 100 mV is required to initiate Al deposition on the Pt electrode. However, Al deposition continues on the developing Al deposit as the electrode potential is scanned back to 0 V, producing a classical "nucleation loop." Stripping of the bulk Al electrodeposit begins at 0 V and continues until the aluminum deposit is depleted from the electrode surface. Because the concentration of $Al_2Cl_7^-$ is 3.4 mol L^{-1} in the 66.7 mol % melt at 298.2 K, large currents are encountered if the potential is scanned more than a few hundred millivolts negative of 0 V. The overall current-

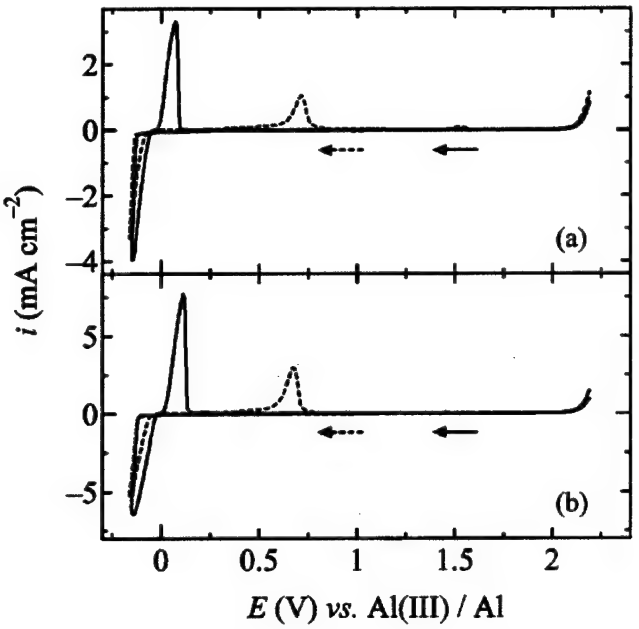

Figure 2. CVs recorded at platinum (a) stationary and (b) rotating disk electrodes in the 66.7 mol % $AlCl_3$-EtMeImCl melt before and after the addition of $(Mo_6Cl_8)Cl_4$. All experiments were conducted at room temperature at a scan rate of 0.01 V s^{-1} and an electrode rotation rate of 2000 rpm: (——) pure melt and (– – –) melt containing 9.42 mmol L^{-1} $(Mo_6Cl_8)Cl_4$.

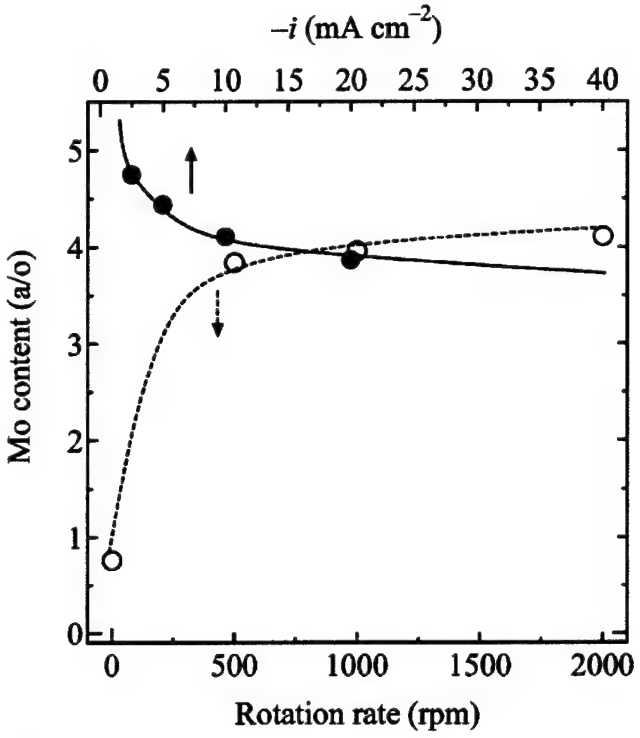

Figure 3. Relationship between the applied current density, electrode rotation rate, and Mo content of bulk Al-Mo alloys electrodeposited from the 66.7 mol % $AlCl_3$-EtMeImCl melt containing 1.78 mmol L^{-1} $(Mo_6Cl_8)Cl_4$ at room temperature: (●) 2000 rpm and (○) −10 mA cm^{-2}.

potential behavior of the Al deposition process is largely unaffected by the addition of $(Mo_6Cl_8)Cl_4$ (Fig. 2). However, the Al stripping waves found in the pure melt are absent, and new waves are present at an anodic peak potential of *ca.* 0.65 V in both the stationary electrode and RDE voltammogams. These new stripping waves are due to the oxidation of electrodeposited Al-Mo alloys. The presence of Mo in these electrodeposits and the lack of reduction waves for $\{Mo_6Cl_8\}^{4+}$ in the voltammograms in Fig. 2 suggest that this Mo(II) reduction reaction takes place simultaneously with the reaction in Eq. 1

$$x\{Mo_6Cl_8\}^{4+} + 8(3 - 2x)Al_2Cl_7^- + 6(3 - x)e^- \rightleftharpoons 6Al_{1-x}Mo_x + 2(21 - 13x)AlCl_4^- \quad [2]$$

Electrodeposition of Al-Mo alloys.—As shown in Fig. 2, the cathodic current for the reaction Eq. 1 rises sharply with small negative changes in potential, making it impractical to investigate the electrodeposition of bulk Al-Mo alloys with any degree of precision using controlled-potential techniques. Therefore, we used controlled-current techniques to prepare alloy samples for detailed compositional and morphological analysis. During previous investigations involving the electrodeposition of Al-Ti alloys on rotating electrode substrates, the alloy composition was found to depend on the electrode rotation rate below a certain threshold value.[30] Because some of the Al-Mo alloy samples were to be electrodeposited on Cu RDE and rotating wire electrode (RWE) substrates, we examined the electrodeposition of bulk Al-Mo alloys on the former by using dc galvanostatic methods at a current density of −10 mA cm^{-2}. The results of this investigation are shown in Fig. 3, and they indicate that the Mo content of these deposits becomes approximately independent of rotation rate above 500 rpm. Therefore, rotation rates exceeding 500 rpm were employed when preparing electrodeposited samples for further analysis.

Figure 3 also shows that the Al-Mo alloy composition depends on the applied current density, with the Mo content of the alloy decreasing as the applied current density is increased. This result is expected because the concentration of the reducible Mo(II) species in the plating solution is much smaller than the concentration of $Al_2Cl_7^-$. Thus, the limiting current density for the electrodeposition of Mo only becomes a significant fraction of the total cathodic current density when the latter is small. That is, the partial current density for $\{Mo_6Cl_8\}^{4+}$ reduction is fixed and small, and an increase in the total cathodic current density simply amplifies the Al partial current density, leading to deposits with less Mo.[41]

The effects of temperature and $(Mo_6Cl_8)Cl_4$ concentration on the Al-Mo alloy composition were also investigated. Figure 4 shows the relationship between the current density and the alloy composition for deposits plated at a fixed temperature from melt solutions containing three different $(Mo_6Cl_8)Cl_4$ concentrations and for deposits plated from solutions with the same $(Mo_6Cl_8)Cl_4$ concentration at two different temperatures. The results from both sets of experiments can be explained by considering the effects of each variable on the limiting current for Mo deposition. For example, increasing the $(Mo_6Cl_8)Cl_4$ concentration increases the limiting current density for $\{Mo_6Cl_8\}^{4+}$ reduction (or the partial current density for Mo deposition). Thus, at a fixed cathodic current density, the Mo partial current density increases as the $(Mo_6Cl_8)Cl_4$ concentration is increased, leading to alloy deposits with a greater Mo content. Increasing the plating bath temperature also seems to increase the partial current for Mo deposition relative to that for Al deposition, leading to electrodeposits with larger amounts of Mo. Thus, increasing the temperature of the plating bath has the same net effect as raising the $(Mo_6Cl_8)Cl_4$ concentration.

SEM/EDS characterization of the Al-Mo alloy deposits.—Figure 5 shows SEM images of some typical bulk Al-Mo alloy samples that were prepared under a variety of deposition conditions on copper substrates with different geometries. The deposition charge used to prepare these samples was sufficient in theory to produce an atomi-

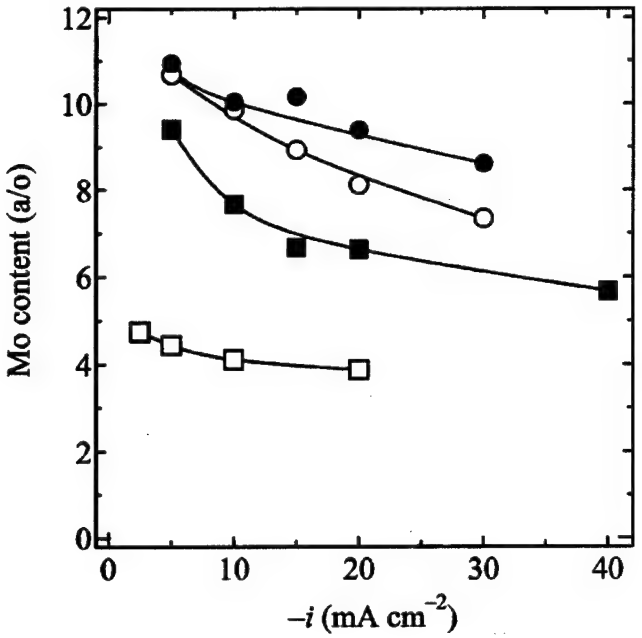

Figure 4. Relationship between the applied current density and Mo content of Al-Mo electrodeposits prepared in the 66.7 $AlCl_3$-EtMeImCl melt at various bath temperatures and $(Mo_6Cl_8)Cl_4$ concentrations: (●) 328 K and 9.42 mmol L^{-1}, (○) 328 K and 5.92 mmol L^{-1}, (■) 328 K and 1.78 mmol L^{-1}, and (□) room temperature and 1.78 mmol L^{-1}.

cally smooth layer of pure Al that was 10 μm thick. The alloy samples depicted in Fig. 5a and b were deposited on the surface of a Cu RDE substrate, whereas those shown in Fig. 5c and d were deposited on a Cu RWE substrate. The samples shown in Fig. 5a, c, and d exhibit a surface morphology consisting mainly of spherical

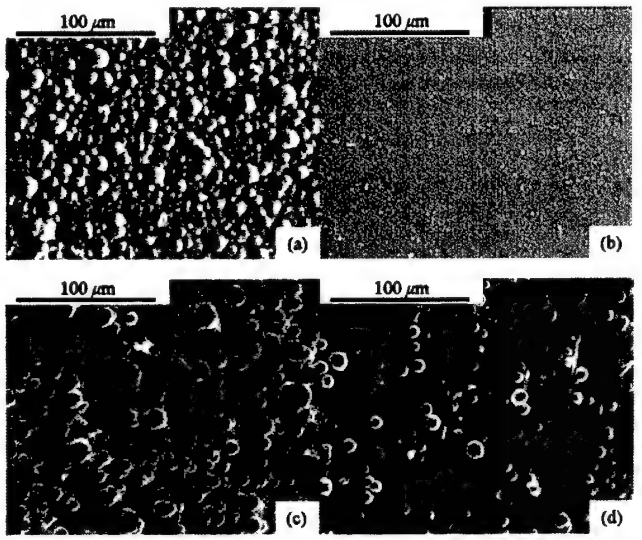

Figure 5. SEM images of bulk Al-Mo alloys electrodeposited from the 66.7 mol % $AlCl_3$-EtMeImCl melt containing $(Mo_6Cl_8)Cl_4$ at 328 K under different conditions: (a) $Al_{90.9}Mo_{9.1}$ on Cu RDE, −5 mA cm^{-2}, 5.92 mmol L^{-1} $(Mo_6Cl_8)Cl_4$; (b) $Al_{91.6}Mo_{8.4}$ on Cu RDE, −40 mA cm^{-2}, 5.92 mmol L^{-1} $(Mo_6Cl_8)Cl_4$; (c) $Al_{90.6}Mo_{9.4}$ on Cu RWE, −20 mA cm^{-2}, 9.42 mmol L^{-1} $(Mo_6Cl_8)Cl_4$; and (d) $Al_{91.4}Mo_{8.6}$ on Cu RWE, −30 mA cm^{-2}, 9.42 mmol L^{-1} $(Mo_6Cl_8)Cl_4$. The electrode rotation rate was 2000 rpm during deposition.

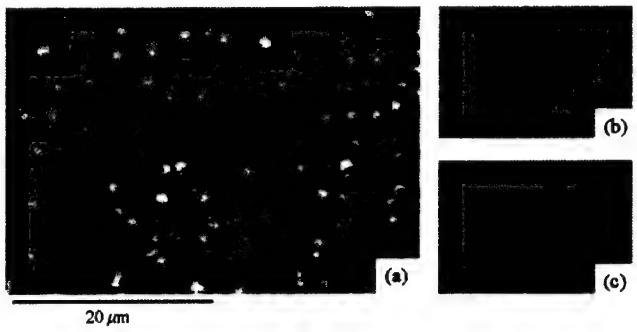

Figure 6. (a) SEM and EDS images of (b) Al and (c) Mo in the $Al_{91.6}Mo_{8.4}$ alloy in Fig. 5b.

nodules that are 5-25 μm diam. These nodules appear to nucleate along the striations of the drawn copper wire substrate in Fig. 5c and d. The deposition conditions used to prepare the sample shown in Fig. 5b resulted in an alloy deposit with a nearly specular surface. The SEM image of the sample shown in Fig. 5b is shown at greater magnification in Fig. 6. Also shown in this figure are EDS maps for the Al and Mo in this electrodeposit. These maps indicate that both elements are distributed more or less evenly over the surface of these deposits. EDS analysis also revealed that all the Al-Mo alloy deposits prepared during this investigation were chloride-free.

XRD analysis of Al-Mo alloy deposits.—Electrodeposits containing 2.6-10.2 atom % Mo were examined by XRD, and the diffraction patterns for selected deposits are shown in Fig. 7. Deposits containing less than 5 atom % Mo have diffraction patterns that can be indexed to an fcc structure very similar to that of pure aluminum, indicating that the Al-Mo alloy is a single phase, supersaturated solid solution. These patterns indicate that the Al grains are randomly oriented and have no preferred crystallographic texture. The primary change in the diffraction patterns with increased Mo composition is the disappearance of the fcc reflections and the development of a broad reflection centered on a 2θ of about 41°, which indicates the presence of an amorphous phase. This broad reflection first appears in deposits containing about 6.5 atom % Mo. The diffraction pattern of the 7.5 atom % Mo deposit shown in Fig. 7b indicates that this is a two-phase deposit, consisting of fcc and amorphous material. As the Mo content of the deposit is increased, the

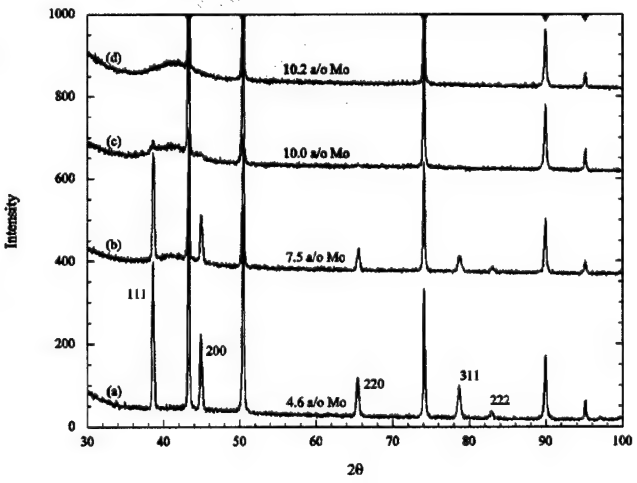

Figure 7. XRD patterns (Cu Kα) from as-deposited Al-Mo alloys: (a) $Al_{95.4}Mo_{4.6}$, (b) $Al_{92.5}Mo_{7.5}$, (c) $Al_{90.0}Mo_{10.0}$, and (d) $Al_{89.8}Mo_{10.2}$. (▼) Copper reflections from the substrate (JCPDS card no. 4-0836, Powder Diffraction File).

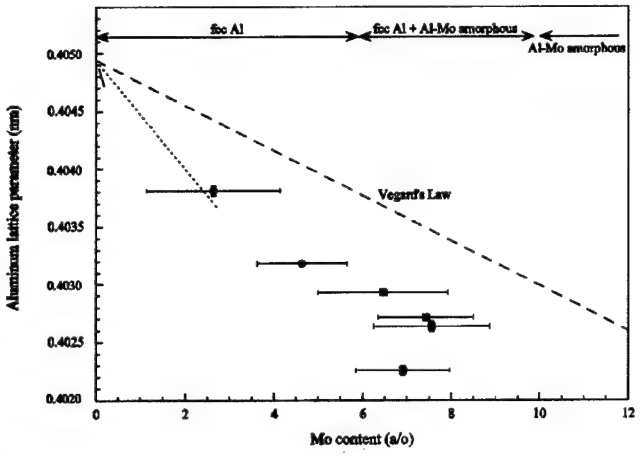

Figure 8. Lattice parameters of fcc Al as a function of alloy composition: (●) this work, single-phase fcc Al; (■) this work, two-phase fcc Al and amorphous Al-Mo; (– – –) Polesya and Stepina;[5] (——) Varich *et al.*;[4] and (—) Vegard's Law.

amount of fcc phase in the alloy decreases whereas that of the amorphous phase increases (Fig. 7c). Deposits containing slightly more than 10 atom % Mo are completely amorphous (Fig. 7d).

The lattice parameters of the fcc Al phase were accurately determined using the copper substrate reflections as an internal standard. The values of the lattice parameters for both single-phase and two-phase deposits are plotted as a function of alloy composition in Fig. 8. The lattice parameter is seen to decrease with increasing Mo content. This is to be expected as the smaller Mo atoms (lattice volume 15.6 $Å^3$ $atom^{-1}$) substitute for Al (lattice volume 16.6 $Å^3$ $atom^{-1}$) in the fcc lattice. In addition to our experimental data, the lattice parameter dependence on composition reported by Varich *et al.*[4] and Polesya and Stepina[5] for rapidly solidified solid solutions is plotted for the pertinent composition ranges using the accepted

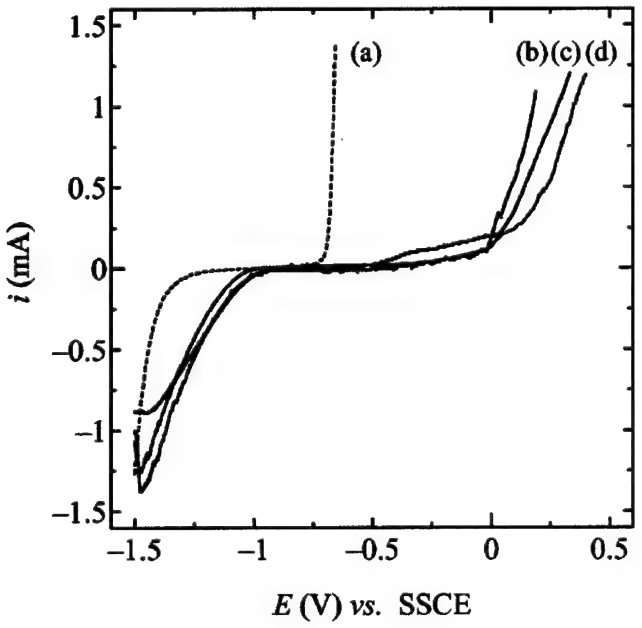

Figure 9. Anodic polarization curves recorded in a N_2-saturated aqueous 0.1 mol L^{-1} NaCl solution for Al and selected Al-Mo alloys electrodeposited from 66.7 mol % $AlCl_3$-EtMeImCl: (a) Al (99.999%), (b) $Al_{92.7}Mo_{7.3}$, (c) $Al_{91.9}Mo_{8.1}$, and (d) $Al_{91.1}Mo_{8.9}$. The scan rate was 0.5 mV s^{-1}.

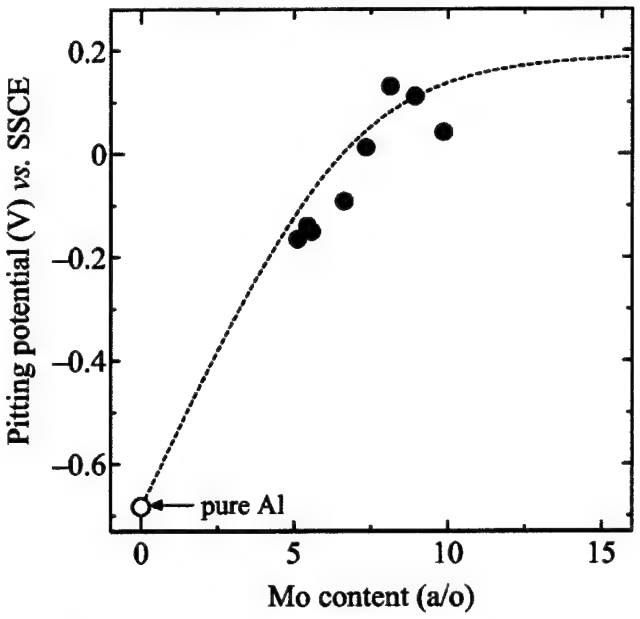

Figure 10. Pitting potentials of electrodeposited Al-Mo alloys.

JCPDS lattice parameter for pure Al of 0.40494 nm (JCPDS card no. 4-0787, Powder Diffraction File). The lattice parameter values predicted by Vegard's Law in which the lattice volume of the solid solution is considered to be a simple linear combination of the constituent lattice volumes is also plotted for comparison. Our lattice parameter dependence on composition is similar to that reported by Polesya *et al.*;[5] however, the level of supersaturation observed in the electrodeposits is significantly higher than that reported for rapidly solidified alloys. This is consistent with observations that the excess free energy possible in electrodeposited alloys is similar to that obtained by vapor deposition and sputtering, which is typically much greater than that possible from solidification from the melt.[42-44]

The level of supersaturation in the two-phase deposits can only be estimated because the Mo content, as measured by EDS, is partitioned between the fcc and amorphous phases. An extrapolation of the Polesya and Stepina[5] data as well as the lattice parameter data from single-phase deposits places the maximum supersaturation at about 6-7 atom % Mo. This level of supersaturation matches that reported in mechanically alloyed materials[10] and is at least twice that observed in rapidly quenched alloys reported to date.[5,7] An estimate of the supersaturation limit has been made by Logan *et al.*,[7] who calculated the free energies of the Al-Mo fcc solid solution and the liquid as a function of composition and temperature. The maximum supersaturation was then estimated from the intersection of the free energy-composition curves, which represented the point where the compositionally invariant transformation of the liquid to the solid solution might become thermodynamically possible, assuming no other phases were nucleated. This treatment yielded a maximum solubility of 6.5 atom % Mo at 10 K and 4.5 atom % Mo at room temperature.[7]

In addition to the level of supersaturation obtained in the fcc phase, it is interesting to note that the supersaturation is maintained when the amorphous phase is codeposited. Similar behavior was also noted for Al-Zr alloys electrodeposited at ambient temperature from $AlCl_3$-EtMeImCl.[45] Aluminum alloys electrodeposited from higher temperature $AlCl_3$-NaCl melts show very different behavior in that the appearance of the amorphous phase results in a relaxation in the supersaturation of the solid solution to levels closer to equilibrium values.[22,46]

Pitting potential measurements.—The pitting potentials of electrodeposited Al-Mo alloys were determined by carrying out poten-

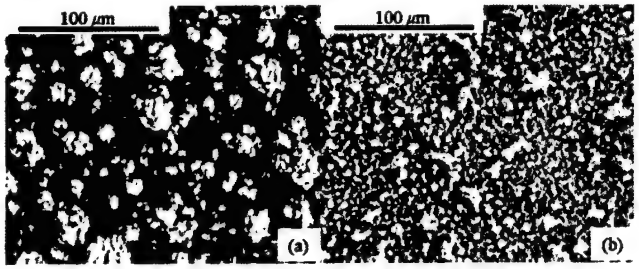

Figure 11. SEM images of the $Al_{94.4}Mo_{5.6}$ alloy (a) before and (b) after anodic polarization in a deaerated aqueous 0.1 mol L^{-1} NaCl solution.

tiodynamic anodic polarization experiments in deaerated aqueous NaCl. These experiments were conducted with alloy samples that were deposited on copper wire substrates. Some examples of the resulting potentiodynamic current-potential curves are shown in Fig. 9. As noted for some other electrodeposited stainless aluminum alloys, *e.g.*, Al-Mn,[26] Al-Ti,[30] Al-V,[31] and Al-Zr,[45] the Al-Mo alloys are spontaneously passive at the rest potential of the solution. During anodic polarization, they display a stable passive region characterized by a very small potential-independent current followed by a sudden rise in current at the pitting potential. The variation of the pitting potential with alloy composition is shown in Fig. 10. The addition of ~10 atom % Mo increases the pitting potential of the alloy by about +0.800 mV. This increase in the pitting potential is comparable to that found for Al-Mo alloys prepared by sputter deposition.[1,17] These materials are the most corrosion-resistant aluminum-transition metal alloys that have been deposited from chloroaluminate molten salts to date.

Figure 11 shows SEM images of the surface of the $Al_{94.4}Mo_{5.6}$ alloy before and after this sample was subjected to pitting potential measurements. The surface morphology of the alloy deposit undergoes considerable modification during anodic polarization in that the dense aggregate of surface nodules disappears and the surface becomes relatively flat. In addition, EDS analysis revealed an increase in the Mo surface concentration, indicating that Al was the primary element lost during oxidation. Because the oxidation was carried out in aqueous solution, surface oxygen was also detected.

Acknowledgment

The authors express their appreciation to Professor Yasuhiko Ito, Dr. Toshiyuki Nohira, and Dr. Takahisa Iida of Kyoto University for their kind assistance. The research was supported by the Air Force Office of Scientific Research, grant no. F49620-00-1-0123.

The University of Mississippi assisted in meeting the publication costs of this article.

References

1. G. S. Frankel, M. A. Russak, C. V. Jahnes, M. Mirzamaani, and V. A. Brusic, *J. Electrochem. Soc.*, **136**, 1243 (1989).
2. L. F. Mondolfo, *Aluminum Alloys: Structure and Properties*, Butterworth and Co., London (1976).
3. T. B. Massalski, *Binary Alloy Phase Diagrams*, American Society of Metals, Metals Park, OH (1990).
4. N. I. Varich, L. M. Burov, K. Y. Kolesnichenko, and A. P. Maksimenko, *Fiz. Met. Metalloved.*, **15**, 292 (1963).
5. A. F. Polesya and A. I. Stepina, *Fiz. Met. Metalloved.*, **27**, 885 (1969).
6. C. P. Chang and M. H. Loretto, *Met. Sci. Eng.*, **98**, 185 (1988).
7. E. A. Logan, J. N. Pratt, and M. H. Loretto, *Mater. Sci. Technol.*, **5**, 123 (1989).
8. Y. Y. Qiu, A. Almedia, and R. Vilar, *J. Mater. Sci.*, **33**, 2639 (1998).
9. M. V. Zdujic, K. F. Kobayashi, and P. H. Shingu, *J. Mater. Sci.*, **26**, 5502 (1991).
10. S. Enzo, R. Frattini, P. Canton, M. Monagheddu, and F. Delogu, *J. Appl. Phys.*, **87**, 2753 (2000).
11. A. H. Al-Saffar, V. Ashworth, A. K. O. Bairamov, D. J. Chivers, W. A. Grant, and R. P. M. Procter, *Corros. Sci.*, **20**, 127 (1980).
12. M. V. Zeller and J. A. Kargol, *Appl. Phys. Lett.*, **18**, 63 (1984).
13. P. M. Natishan, E. McCafferty, and G. K. Hubler, *J. Electrochem. Soc.*, **133**, 1061 (1986).
14. E. McCafferty, G. K. Hubler, P. M. Natishan, P. G. Moore, R. A. Kant, and B. D. Sartwell, *Mater. Sci. Eng.*, **86**, 1 (1987).
15. P. M. Natishan, E. McCafferty, and G. K. Hubler, *J. Electrochem. Soc.*, **135**, 321 (1988).
16. W. C. Moshier, G. D. Davis, J. S. Ahearn, and H. F. Hough, *J. Electrochem. Soc.*, **133**, 1063 (1986).
17. W. C. Moshier, G. D. Davis, J. S. Ahearn, and H. F. Hough, *J. Electrochem. Soc.*, **134**, 2677 (1987).
18. W. C. Moshier, G. D. Davis, and G. O. Cote, *J. Electrochem. Soc.*, **136**, 356 (1989).
19. G. D. Davis, W. C. Moshier, T. L. Fritz, and G. O. Cote, *J. Electrochem. Soc.*, **137**, 422 (1990).
20. G. S. Frankel, R. C. Newman, C. V. Jahnes, and M. A. Russak, *J. Electrochem. Soc.*, **140**, 2192 (1993).
21. H. Mitsui, H. Habazaki, E. Akiyama, A. Kawashima, K. Asami, K. Hashimoto, and S. Mrowec, *Mater. Trans., JIM*, **37**, 379 (1996).
22. T. P. Moffat, *J. Electrochem. Soc.*, **141**, L115 (1994).
23. M. R. Ali, A. Nishikata, and T. Tsuru, *Electrochim. Acta*, **42**, 2347 (1997).
24. M. Matsunaga, T. Kitazaki, K. Hosokawa, S. Hirano, and M. Yoshida, in *Molten Salts*, C. L. Hussey, D. S. Newman, G. Mamantov, and Y. Ito, Editors, PV 94-13, p. 422, The Electrochemical Society Proceedings Series, Pennington, NJ (1994).
25. G. R. Stafford, *J. Electrochem. Soc.*, **136**, 635 (1989).
26. T. P. Moffat, G. R. Stafford, and D. E. Hall, *J. Electrochem. Soc.*, **140**, 2779 (1993).
27. G. M. Janowski and G. R. Stafford, *Metall. Trans. A*, **23A**, 2715 (1992).
28. G. R. Stafford, *J. Electrochem. Soc.*, **141**, 245 (1994).
29. T. Takenaka and M. Kawakami, *Int. J. Mater. Prod. Technol.*, **2**, 500 (2001).
30. T. Tsuda, C. L. Hussey, G. R. Stafford, and J. E. Bonevich, *J. Electrochem. Soc.*, **150**, C234 (2003).
31. T. Tsuda and C. L. Hussey, *J. Min. Metall., B*, **39**, 3 (2003).
32. J. Uchida, Y. Yamamoto, and H. Seto, Jpn. Pat. JP 06 65,780 (1994).
33. A. Shibuya, J. Uchida, Y. Yamamoto, H. Seto, and T. Tsuda, *Mater. Sci. Forum*, **73-75**, 577 (1991).
34. J. Uchida, T. Hirayama, M. Abe, H. Seto, Y. Yamamoto, T. Tsuda, and A. Shibuya, in *Recent Advances in Coated Steels Used for Automobiles*, K. Yamakawa and H. Fujikawa, Editors, p. 145, Elsevier Science B.V. and The Society of Materials Science, Japan-Amsterdam (1996).
35. J. S. Wilkes, J. A. Levisky, and R. A. Wilson, *Inorg. Chem.*, **21**, 1263 (1982).
36. B. J. Tierney, W. R. Pitner, J. A. Mitchell, C. L. Hussey, and G. R. Stafford, *J. Electrochem. Soc.*, **145**, 3110 (1998).
37. X. H. Xu and C. L. Hussey, *J. Electrochem. Soc.*, **140**, 1226 (1993).
38. W. C. Dorman and R. E. McCarley, *Inorg. Chem.*, **13**, 491 (1974).
39. P. A. Barnard, I. W. Sun, and C. L. Hussey, *Inorg. Chem.*, **29**, 3670 (1990).
40. A. W. Maverick and H. B. Gray, *J. Am. Chem. Soc.*, **103**, 1298 (1981).
41. G. R. Stafford and C. L. Hussey, in *Advances in Electrochemical Science and Engineering*, R. C. Alkire and D. M. Kolb, Editors, Vol. 7, p. 275, Wiley-VCH Verlag GmbH, Weinheim (2002).
42. J. C. Baker and J. W. Cahn, *Thermodynamics of Solidification*, American Society of Metals, Metals Park, OH (1971).
43. A. K. Sinha, B. C. Giessen, and D. E. Polk, in *Treatise on Solid State Chemistry*, N. B. Hannay, Editor, Plenum Press, New York (1976).
44. D. E. Polk and B. C. Giessen, *Metallic Glasses*, American Society of Metals, Metals Park, OH (1978).
45. T. Tsuda, C. L. Hussey, G. R. Stafford, and O. Kongstein, *J. Electrochem. Soc., Submitted* , (2004).
46. B. Grushko and G. R. Stafford, *Metall. Trans. A*, **20A**, 1351 (1989).

APPENDIX III

T. Tsuda, C. L. Hussey, and G. R. Stafford, "Electrodeposition of Aluminum-Hafnium Alloy from the Lewis Acidic Aluminum Chloride–1-Ethyl-3-methylimidazolium Chloride Molten Salt," (Draft manuscript for submission to *Electrochimica Acta*)

Electrodeposition of Aluminum-Hafnium Alloy from the Lewis Acidic Aluminum Chloride–1-Ethyl-3-methylimidazolium Chloride Molten Salt

Tetsuya Tsuda[a], Charles L. Hussey[a,]*, and Gery R. Stafford[b]

[a]*Department of Chemistry and Biochemistry, The University of Mississippi, P.O. Box 1848, University, Mississippi 38677, USA*

[b]*Materials Science and Engineering Laboratory, National Institutes of Standards and Technology, Gaithersburg, Maryland 20899, USA*

ABSTRACT

The electrochemistry of Hf(IV) and the electrodeposition of Al-Hf alloy was examined in the Lewis acidic 66.7–33.3 mole percent (m/o) aluminum chloride–1-ethyl-3-methylimidazolium chloride ($AlCl_3$–EtMeImCl) molten salt containing $HfCl_4$. When cyclic staircase voltammetry was carried out at a platinum electrode in this melt containing $HfCl_4$, the deposition and stripping waves for Al shifted to negative and positive potentials, respectively, suggesting that the aluminum stripping is more difficult due to the formation of Al-Hf alloy. The Hf content of the Al-Hf deposits depended on the $HfCl_4$ concentration in the melt and the applied current density. Al-Hf alloy samples containing ~ 11 atomic percent (a/o) Hf were obtained on the surface of a Cu rotating wire electrode. The alloy surface was covered with dense crystals, the alloy was completely chloride free, and the morphology did not depend on the Hf content of the samples, but on the applied current density. The pitting potential of the Al-Hf alloys was approximately +0.30 V against pure aluminum when the Hf content was above 10 a/o.

Keywords: chloroaluminate melts, 1-ethyl-3methylimidazolium chloride, room-temperature molten salt, Al-Hf alloy, pitting potential.

* Corresponding author; E-mail: chclh@chem1.olemiss.edu

INTRODUCTION

A great number of corrosion-resistant aluminum-transition metal alloys [1], *e.g.*, Al-Cr [2-7], Al-Mn [8-11], Al-Mo [12], Al-Ti [13-17], Al-Zr [18], and Al-V [19], have been electrodeposited from Lewis acidic chloroaluminate molten salts because this method readily produces Al alloy coatings of uniform thickness with reproducible composition and structure. The molten salts used to deposit these alloys consist of aluminum chloride ($AlCl_3$) and alkali chlorides, such as sodium chloride (NaCl) and/or potassium chloride (KCl), or quaternary ammonium chloride salts, such as 1-(1-butyl)pyridinium chloride (BuPyCl) or 1-ethyl-3-methylimidazolium chloride (EtMeImCl). However, inorganic Lewis acidic chloroaluminate melts exhibit high vapor pressure due to the escape of $AlCl_3$ and are not appropriate for use in electroplating baths. Although the electrochemistry of hafnium has been investigated in the Lewis acidic $AlCl_3$–NaCl melt [20], no effort has been made to electrodeposit Al-Hf alloys from the low temperature systems like $AlCl_3$-EtMeImCl. In this article, we report the electrodeposition of Al-Hf alloy on Cu substrates from the Lewis acidic $AlCl_3$–EtMeImCl molten salt, and the electrochemistry of Hf(IV) in this melt as it pertains to the electrodeposition of these alloys.

EXPERIMENTAL[a]

The procedures used for the synthesis of EtMeImCl, the purification of $AlCl_3$ by sublimation, and the preparation and purification of the $AlCl_3$–EtMeImCl molten salt were identical to those described in previous articles [21, 22]. Anhydrous hafnium (IV) chloride (Cerac, 99 %) was used as received.

All experiments were conducted using a three-electrode cell. A Pine Instruments Teflon sheathed platinum rotating disk electrode (geometrical area = 0.099 cm^2) was used for the working electrode, and coils of 0.10 cm diameter aluminum wire (Alfa Aesar, 99.999 %) were used for the counter and reference electrodes. These electrodes were immersed in the melt of the same composition as the bulk melt, but were separated from the bulk melt by a porosity E glass frit (Ace Glass). The aluminum electrodes were cleaned with a mixture of concentrated H_2SO_4, HNO_3, and H_3PO_4, rinsed with distilled H_2O, and dried under vacuum before use. All experiments were carried out in a nitrogen gas-filled glove box (VAC Atmospheres NEXUS system) with O_2 and H_2O < 5 ppm. Alloy samples of approximately 10 μm thickness were deposited from the 66.7–33.3 m/o $AlCl_3$-EtMeImCl melt containing $HfCl_4$ onto a length of 1.25 mm diameter copper wire (geometrical area = 0.798 cm^2). The copper wire was rotated at 2000 rpm during the electrodeposition experiments. The resulting electrodeposits were washed in distilled water and dried under vacuum.

Cyclic staircase voltammetry experiments were conducted by using an EG&G Model 273 potentiostat/galvanostat. Electrodeposition of Al-Hf alloy was performed with an EG&G PARC Model 173 potentiostat/galvanostat equipped with a Model 179

[a] Certain trade names are mentioned for experimental information only; in no case does it imply a recommendation or endorsement by NIST.

digital coulometer plug in module. All electrochemical experiments were carried out at 353 K unless noted.

Potentiodynamic pitting measurements were carried out on these alloy samples at room temperature in a 0.1 mol L^{-1} solution of NaCl in distilled H_2O. This solution was deaerated with nitrogen gas for more than 6 hours before each experiment. The reference electrode for these measurements was a sodium-saturated calomel electrode (SSCE), and the counter electrode was a large surface area platinum wire coil. A know length of the plated Cu wire was exposed to the NaCl solution by using a heat-shrink tubing mask, and the sample was scanned at 0.5 mV s^{-1} by using linear staircase voltammetry. Electronic resistance compensation was employed during all staircase voltammetry experiments. The step size used for staircase voltammetry, 2 mV, was small enough to permit the analysis of the resulting voltammograms with the conventional theories developed for linear scan voltammetry [23].

UV-visible spectra of dissolved hafnium ions were obtained by using a Varian CARY 5 spectrometer employing a Wilmad No. 107-7 closed type quartz cells. The path length of these cells was 0.10 cm.

The surface morphology and elemental analysis of alloy samples were investigated with a JEOL JSM-6100 scanning electron microscope (SEM) equipped with a Link energy dispersive X-ray (EDX) spectrometer at the University of Mississippi SEM/EDX facility located in the Department of Mechanical Engineering or with a JEOL JXA-840 field-emission scanning electron microscope at the National Institute of Standards and Technology. The electrodeposits were also examined by X-ray diffraction (XRD) by using a Siemens D-500 diffractometer with Cu-Kα radiation.

RESULTS AND DISCUSSION

Electrochemistry of $HfCl_4$. – Figure 1 shows typical cyclic staircase voltammograms recorded at a stationary Pt disk electrode in a 66.7 m/o $AlCl_3$-EtMeImCl melt containing $HfCl_4$. In pure melt, oxidation and reduction waves appear because of the deposition and stripping of aluminum according to the following well-known reaction:

$$4Al_2Cl_7^- + 3e^- \rightleftharpoons Al + 7AlCl_4^- \qquad (1)$$

After dissolution of the $HfCl_4$, the wave ascribed to the reduction reaction in Eq.(1) shows small negative shift. The stripping wave of the pure Al deposit from the Pt electrode is absent, and a new stripping wave is evident at slightly more positive potential. The positive shift of the stripping wave suggests the dissolution of an aluminum that is more difficult to oxidize than the pure melt. The bulk electrodeposition of the Al-Hf alloy will be discussed in detail below.

In this voltammetric experiment, we found out that a small and an ill-defined reduction wave appears at +0.95 V (Fig. 1, inset), but it was difficult to obtain reproducible results for this wave without polishing the platinum electrode surface before each scan. As shown in Fig. 2, another reduction wave appears with the original wave at faster scan rates. We have attempted to explain the reaction theoretically by the use of cyclic staircase voltammetry at different scan rates. The peak potential-half peak potential separation for this wave, $E_{pc/2}$-E_{pc}, is given in Table I. At a scan rate of 0.025 V s^{-1}, the slowest scan rate employed, this separation was 0.094 V. However, this value is considerably larger than the theoretical value of 0.070 V for a one-electron reversible

reaction at 353 K. It implies that this electrode reaction is quasireversible. Figure 3 shows a plot of the peak reduction current, i_{pc}, versus the square root of the scan rate, $v^{1/2}$. This plot shows a good linear relationship at slow scan rates. However, the deviation from the linear relationship increases with the scan rate, suggesting the presence of weak adsorption of the reactant [25]. The peak current ratio, $i_{pa}/|i_{pc}|$, for this wave was calculated by using Nicholson's semi-empirical method [25]. This ratio is less than one at very slow scan rates, but increases to 1.4 at faster scan rates, again indicating the presence of weak adsorption of the reactant. In addition, the waveform is not in agreement with that derived from theoretical calculations, but is very similar to that seen for a reduction reaction with a coupled irreversible chemical step [26]; i.e., the peak ratio is less than one at very slow scan rates and increases to one at faster scan rates. Weak adsorption of the reactant causes this ratio to increase to more than one. The new wave appearing at faster scan rates may also affect the result that the peak ratio does not converge to one. Figure 4 shows voltammograms recorded over different scan ranges at 0.50 V s^{-1}. The reduction waves A and C correspond with oxidation waves E and D, respectively. However, we could not see an oxidation wave for B at faster scan rates. This wave must arise from the reduction of a precipitated hafnium chloride species on the Pt electrode, which is produced by an irreversible following chemical reaction. In fact, similar results have been reported for some other Group 4 elements, Ti and Zr, in this molten salt system [16, 18, 27, 28]. Taken together, the reduction reaction at *ca.* 0.95 V most likely involves the following sequence of reactions:

$$Hf(IV)_{solv} + e^- \rightleftharpoons Hf(III)_{solv} \quad \text{(quasireversible reaction)} \qquad (2)$$

$$Hf(III)_{solv} + 6AlCl_4^- \rightarrow HfCl_3(s) + 3Al_2Cl_7^- \text{ (irreversible chemical reaction)} \quad (3)$$

The reaction in Eq. 3 is the source of the passivating film that forms on the electrode surface.

The diffusion coefficient for Hf(IV), $D_{Hf(IV)}$, and the Stokes-Einstein product, $D_{Hf(IV)}\eta/T$, where η is the absolute viscosity of the molten salt, were calculated from the linear relationship in Fig. 3, assuming that the reaction behaved reversibly at slow scan rates. The viscosity data taken from Fannin et al. [29] were used for the latter calculation. The diffusion coefficient is given in Table I along with the data for some related Group 4 species, Ti(IV) and Zr(IV). $D_{Ti(IV)}$ and $D_{Zr(IV)}$ can be compared to $D_{Hf(IV)}$ through the Stokes-Einstein product, $D\eta/T$, which considers both the temperature of the measurement and the absolute viscosity of the solvent. $D\eta/T$ is a relative measure of the solvodynamic radius of the diffusing species [30]. The somewhat smaller value of $D_{Ti(IV)}\eta/T$ may simply reflect the fact that Ti(IV) vaporizes rapidly from the melt as $TiCl_4$ [28]. Thus, the diffusion coefficient data reported in the literature for Ti(IV) may have been measured under conditions that did not take into account the vaporization loss of $TiCl_4$, which would lead to smaller values of $D_{Ti(IV)}$ and $D_{Ti(IV)}\eta/T$. The diffusion coefficient of Hf(IV) is smaller than that of Zr(IV) because Hf(IV) has larger ion-radius than Zr(IV).

Chemical reduction of Hf(IV). – Figure 5 shows UV-vis spectra of a colorless solution of Hf(IV) in the 66.7 m/o melt along with the data the related Group 4 elements. The absorption maximum of tetravalent cations shifts to lower wavelength with an increase in the atomic radius of the species, suggesting that greater energy is required for the electron transitions as the volume of the cation increases. It must be noted that spectra cannot be recorded below 250 nm due to interference from absorption by the organic cation of the melt.

In previous investigations, we produced Ti(II) and Zr(II) in the 66.7 m/o melt by reducing the higher oxidation state species with Al wire. Therefore we carried out a series of experiments to determine if it is possible to obtain Hf(II) by the chemical reduction of Hf(IV). The reduction of Hf(IV) with Al produced an orange solution with no visible precipitate. However, we could not see any absorption peaks for this solution (Fig. 5f). During previous investigations $TiCl_3$ and $ZrCl_4$ solutions in this melt, we noticed that the rest potential of the Pt working electrode shifts to negative values after the chemical reduction of these species to Ti(II) and Zr(II), respectively [16, 18]. In order to be certain that we were generating Hf(II) during the reduction of Hf(IV) with Al, we conducted similar electrochemical experiments with this solution. However, in the case of Hf(IV), the potential did not change appreciably, and we concluded that it was difficult to produce large amount of Hf(II). This is consistent with the observation that species with the highest oxidation number become more stable with increasing atomic number [31].

Electrodeposition of Al-Hf alloys. –The electrodeposition of bulk Al-Hf alloys was examined by using dc galvanostatic methods at 353 K in the 66.7 m/o melt containing $HfCl_4$. The substrate for these deposition experiments was a copper rotating wire electrode. Based on previous investigations, a rotation rate of 2000 rpm, was employed for all experiments [6, 12, 18]. The compositions of the Al-Hf alloy resulting from the experiment are shown as a function of current density in Fig. 6 together with the data obtained from similar experiments carried out with Zr(IV) solutions in this same melt. The Hf content of the electrodeposited alloys decreases with increasing of the current density, but this is not the case if the applied current density is less than 5 mA cm^{-2}. Usually, as the current density is increased, the partial current for the reduction of the transition metal cation alloying with Al reaches a limiting value, whereas the partial current for the reduction of $Al_2Cl_7^-$, which is

present in this melt at a concentration of 3.24 M at 353 K, continues to increase. This behavior is a common feature of overpotential alloy deposition in chloroaluminate melts containing divalent transition metal cations [1, 12, 16, 18]. However, in solutions containing either Hf(IV) or Zr(IV), this behavior is obviously different from that observed with solutions of containing divalent cations. We deduce from this observation that the irreversible chemical reaction given in Eq. 3, i.e., the precipitation of insoluble $HfCl_3$ or $ZrCl_3$ on the electrode, is related to this anomalous behavior.

Characterization of electrodeposited Al-Hf alloys. – The surface morphology of selected Al-Hf deposits is shown in Fig. 7. The surface morphology is dependent on the applied current density, but is independent of the Hf content in the samples. At low current density (Fig 7a and 7c), the alloys have a very smooth surface. However, the grain size becomes larger as the applied current density increases (Fig 7b and 7d).

Pitting potential measurements of Al-Hf alloys. – The corrosion resistance of the Al-Hf alloys was investigated by recording potentiodynamic anodic polarization curves in N_2-saturated aqueous 0.1 M NaCl. These polarization curves are shown in Fig. 8. As noted for Al-Ti and Al-Zr alloys examined under similar conditions [16,18], Al-Hf alloys display a stable passive region characterized by a very small potential-independent current followed by a sudden rise in current at the pitting potential. The variation of the Al-Hf pitting potential with alloy composition is shown in Fig. 9. Included are the values for Al-Ti and Al-Zr alloys produced in the 66.7 m/o melt. The addition of Hf in amounts exceeding 10 a/o increases the pitting potential of the alloy by *ca.* +0.3 V. This increase is close to the value found for Al-Zr alloy electrodeposited under the same conditions [18].

Acknowledgment

This research was supported by the Air Force Office of Scientific Research grant no. F49620-00-1-0123.

References

[1]. G.R. Stafford and C.L. Hussey, in Advances in Electrochemical Science and Engineering, R.C. Alkire and D.M. Kolb, Editors, Vol. 7, p.275, Wiley-VCH Verlag GmbH, Weinheim (2002).

[2]. T.P. Moffat, J. Electrochem. Soc. 141 (1994) L115.

[3]. M. Matsunaga, T. Kitazaki, K. Hosokawa, S. Hirano, and M. Yoshida, in Ninth International Symposium on Molten Salts, C. L. Hussey, D. S. Newman, G. Mamantov, and Y. Ito, Eds., PV 94-13, p. 422, The Electrochemical Society, (1994).

[4]. H.C. De Long and P.C. Trulove, in Tenth International Symposium on Molten Salts, R.T. Carlin, S. Deki, M. Matsunaga, D.S. Newman, J.R. Selman, and G.R. Stafford, Eds., PV 96-7, p. 276, The Electrochemical Society, (1996).

[5]. M.R. Ali, A. Nishikata, and T. Tsuru, Electrochim. Acta 42 (1997) 2347.

[6]. M. Matsunaga, M. Morimitsu, M. Nagano, and T. Tsuda, Molten Salt Forum 5-6 (1998) 601.

[7]. D.E. Clinton, P.C. Trulove, P.L. Hagans, and H.C. DeLong, Molten Salt Forum 5-6 (1998) 593.

[8]. G.R. Stafford, J. Electrochem. Soc. 136 (1989) 635.

[9]. T.P. Moffat, G.R. Stafford, and D.E. Hall, J. Electrochem. Soc. 140 (1993) 2779.

[10]. H.C. De Long, J.A. Mitchell, and P.C. Trulove, High Temp. Material Processes 2 (1998) 507.

[11]. P.C. Trulove, J.A. Mitchell, P.L. Hagans, R.T. Carlin, G.R. Stafford, and H.C. De Long, in Twelfth International Symposium on Molten Salts, P.C. Trulove, H.C. De Long, G.R. Stafford, and S. Deki, Eds., PV 99-41, p. 517, The Electrochemical Society, (2000).

[12]. T. Tsuda, C.L. Hussey, and G.R. Stafford, J. Electrochem. Soc., in printing.

[13]. G.R. Stafford, J. Electrochem. Soc. 141 (1994) 245.

[14]. G.R. Stafford and T.P. Moffat, J. Electrochem. Soc. 142 (1995) 3288.

[15]. T. Takenaka and M. Kawakami, Int. J. Mater. and Product Tech. 2, 500 (2001).

[16]. T. Tsuda, C.L. Hussey, G.R. Stafford, and J.E. Bonevich, J. Electrochem. Soc. 150 (2003) C234.

[17]. G.R. Stafford, T. Tsuda and C.L. Hussey, J. Min. and Metall., B 39 (2003) 23.

[18]. T. Tsuda, C.L. Hussey, G.R. Stafford, and O. Kongstein, J. Electrochem. Soc. in printing.

[19]. T. Tsuda and C.L. Hussey, J. Min. and Metall., B 39 (2003) 3.

[20]. M. Katabua, P. Rolland, G. Mamantov, and L. Hulett, Inorg. Chem. 21 (1982) 3569.

[21]. X.H. Xu and C.L. Hussey, J. Electrochem. Soc. 140 (1993) 1226.

[22]. B.J. Tierney, W.R. Pitner, J.A. Mitchell, C.L. Hussey, and G.R. Stafford, J. Electrochem. Soc. 145 (1998) 3110.

[23]. R. Bilewicz, K. Wikiel, R. Osteryoung, and J. Osteryoung, Anal. Chem. 61 (1989) 965.

[24]. A.J. Bard, L.R. Faulkner, Electrochemical Methods: Fundamentals and Applications, John Wiley & Sons, New York, 2001.

[25]. R.S. Nicholson, Anal. Chem. 37 (1965) 1406.

[26]. R.S. Nicholson and I. Shain, Anal. Chem. 36 (1964) 706.

[27]. B. Gilbert, G. Mamantov, and K.W. Fung, Inorg. Chem. 14 (1975) 1802.

[28]. R.T. Carlin, R.A. Osteryoung, J.S. Wilkes, and J. Rovang, Inorg. Chem. 29 (1990) 3003.

[29]. A.A. Fannin, Jr., D.A. Floreani, L.A. King, J.S. Landers, B.J. Piersma, D.J. Stech, R.L. Vaughn, J.S. Wilkes, and L.W. John, J. Phys. Chem. 88 (1984) 2614.

[30]. J.O.M. Bockris and A.K.N. Reddy, Modern Electrochemistry, Plenum Press, New York (1998).

[31]. D.E. Shriver, P.W. Atkins, and C.H. Langford, in Inorganic Chemistry, W.H. Freeman and Company, New York, (1990) p. 255.

Table I. Summary of voltammetric data for the reduction of 4.6 mM Hf(IV) at a Pt stationary disk electrode at 353.2 K

v	$-10^{-3}\, i_{pc} v^{-1/2}$	$i_{pa} / \lvert i_{pc} \rvert$	E_{pc}	$E_{pc/2}-E_{pc}$
(V s^{-1})	(A cm^{-2} $V^{-1/2}$ $s^{1/2}$)		(V)	(V)
0.005	1.67	0.59	0.953	0.099
0.010	1.53	0.65	0.966	0.100
0.025	1.62	0.67	0.970	0.094
0.050	1.66	0.79	0.967	0.098
0.075	1.62	0.89	0.965	0.095
0.100	1.69	0.90	0.946	0.114
0.150	1.62	1.03	0.919	0.141
0.200	1.63	1.15	0.928	0.134
0.300	1.69	1.26	0.959	0.104
0.500	1.78	1.32	0.955	0.097
0.750	1.85	1.36	0.932	0.107
1.000	2.01	1.37	0.925	0.107
1.500	2.08	1.39	0.879	0.129

Table II. Summary of voltammetric data for the reduction of tetravalent cations of Group 4 elements in the Lewis acidic $AlCl_3$-EtMeImCl melt at a Pt electrode.

	mol % $AlCl_3$	Method	Concentration (mmol L^{-1})	10^6 D (cm^2 s^{-1})	10^{10} $\eta D/T$ (g cm s^{-2} K^{-1})	Reference
Ti(IV)	60.0	NPV	40	0.81	3.9	[28]
Zr(IV)	66.7	CV	4.9	4.2	5.8	[18]
Hf(IV)			4.6	1.8	2.4	This work

NPV: Normal pulse voltammetry; CV: Cyclic voltammetry.

Table III. Summary of absorption spectral data for Group IV species in the 66.7–33.3 m/o $AlCl_3$–EtMeImCl melt at 298 K.

Anion	Concentration (mmol L^{-1})	λ_{max} (nm)	Reference
Ti(IV)	2.2	~ 250, 287	[16]
Zr(IV)	5.0	~ 250	[18]
Hf(IV)	7.5	~ 250	This work
Ti(III)	4.9	–	[16]
Ti(II)	4.1	340, 407,[a] 433	[16]
Zr(II)	5.0	276, 327, 455	[18]
Hf(II)	4.8	–	This work

[a] Shoulder

Table IV. Summary of aluminum-Group IV alloys produced in the 66.7–33.3 m/o $AlCl_3$–EtMeImCl melt.

	Maximum content in alloy (a/o)	Amorphous structure	Transition metal content in alloys		Reference
			Increase of M(II) or M(IV) concentration	Increase of current density	
Ti	19	×	↑	↓	[16]
Zr	17	10 ~ 17	↑	↓*	[18]
Hf	11	×	↑	↓*	This work

×: no amorphous structure; *: over -10 mA cm^{-2}

Figure Captions

Figure 1. Cyclic staircase voltammograms recorded at a platinum stationary disk electrode in the 66.7–33.3 m/o $AlCl_3$–EtMeImCl molten salt: (- - -) pure melt; (——) after the addition of 4.6 mmol L^{-1} $HfCl_4$. The temperature was 353.2 K; the sweep rate was 10 mV s^{-1}; and the step size was 2 mV.

Figure 2. Cyclic staircase voltammograms recorded at a platinum stationary disk electrode in the 66.7–33.3 m/o $AlCl_3$–EtMeImCl molten salt containing 4.6 mmol L^{-1} $HfCl_4$. The scan rates were: 0.05 V s^{-1} (——) and 0.50 V s^{-1} (- - -). The temperature was 353.2 K, and the step size was 2 mV.

Figure 3. The cathodic peak current, i_{pc}, and ratio of anodic to cathodic peak currents, $i_{pa}/|i_{pc}|$, as a function of sweep rate constructed from the data in Table I.

Figure 4. Cyclic staircase voltammograms recorded at a platinum stationary disk electrode in the 66.7–33.3 m/o $AlCl_3$–EtMeImCl molten salt containing 4.6 mmol L^{-1} $HfCl_4$. The scan rate was 0.50 V s^{-1}; the temperature was 353.2 K; and the step size was 2 mV.

Figure 5. UV-visible spectra recorded at room temperature in the 66.7–33.3 m/o $AlCl_3$–EtMeImCl molten salt: (a) 2.2 mmol L^{-1} $TiCl_4$, (b) 5.0 mmol L^{-1} $ZrCl_4$, (c) 7.5 mmol L^{-1} $HfCl_4$, (d) 8.2 mmol L^{-1} $TiCl_2$, (e) after reduction of 5.0 mmol L^{-1} $ZrCl_4$ by using Al metal at 353 K for three days, and (f) after reduction of 8.6 mmol L^{-1} $HfCl_4$ by using Al metal at 353 K for three days. The cell path length was 0.10 cm.

Figure 6. Relationship between the applied current density (mA cm^{-2}) and Hf content (a/o) of the deposits prepared in the 66.7–33.3 m/o $AlCl_3$–EtMeImCl molten salt containing $ZrCl_4$ or $HfCl_4$: (●) 19.5 mmol L^{-1} $ZrCl_4$ [18]; (○) 4.9 mmol L^{-1} $ZrCl_4$ [18]; (▲) 27.9 mmol L^{-1} $HfCl_4$; (Δ) 4.5 mmol L^{-1} $HfCl_4$. The electrode rotation rate was 2000 rpm; the temperature was 353.2 K.

Figure 7. SEM images of the Al-Hf alloy samples prepared in the 66.7–33.3 m/o $AlCl_3$–EtMeImCl molten salt: (a) 4.5 mmol L^{-1} $HfCl_4$, -5 mA cm^{-2}, $Al_{93.2}Hf_{6.8}$; (b) 4.5 mmol L^{-1} $HfCl_4$, -40 mA cm^{-2}, $Al_{93.8}Hf_{6.2}$; (c) 27.9 mmol L^{-1} $HfCl_4$, -5 mA cm^{-2}, $Al_{91.6}Hf_{8.4}$; (d) 27.9 mmol L^{-1} $HfCl_4$, -40 mA cm^{-2}, $Al_{90.3}Hf_{9.7}$. The electrode rotation rate was 2000 r.p.m.; the temperature was 353.2 K.

Figure 8. Anodic polarization curves recorded in deaerated, aqueous 0.1 M-NaCl for Al-Hf alloys obtained in the 66.7–33.3 m/o $AlCl_3$–EtMeImCl molten salt containing $HfCl_4$: (a) Al (99.999 %); (b) $Al_{93.7}Hf_{6.3}$; (c) $Al_{92.1}Hf_{7.9}$; (d) $Al_{91.0}Hf_{9.0}$; and (e) $Al_{89.7}Hf_{10.3}$. The temperature was 353.2 K; the sweep rate was 0.5 mV s^{-1}; and the step size was 2 mV.

Figure 9. Pitting potentials as a function of alloy composition for the Al-Group 4 alloys electrodeposited from chloroaluminate melts. (Δ)Al-Ti [16]; (▲) Al-Zr [18]; and (●) Al-Hf.

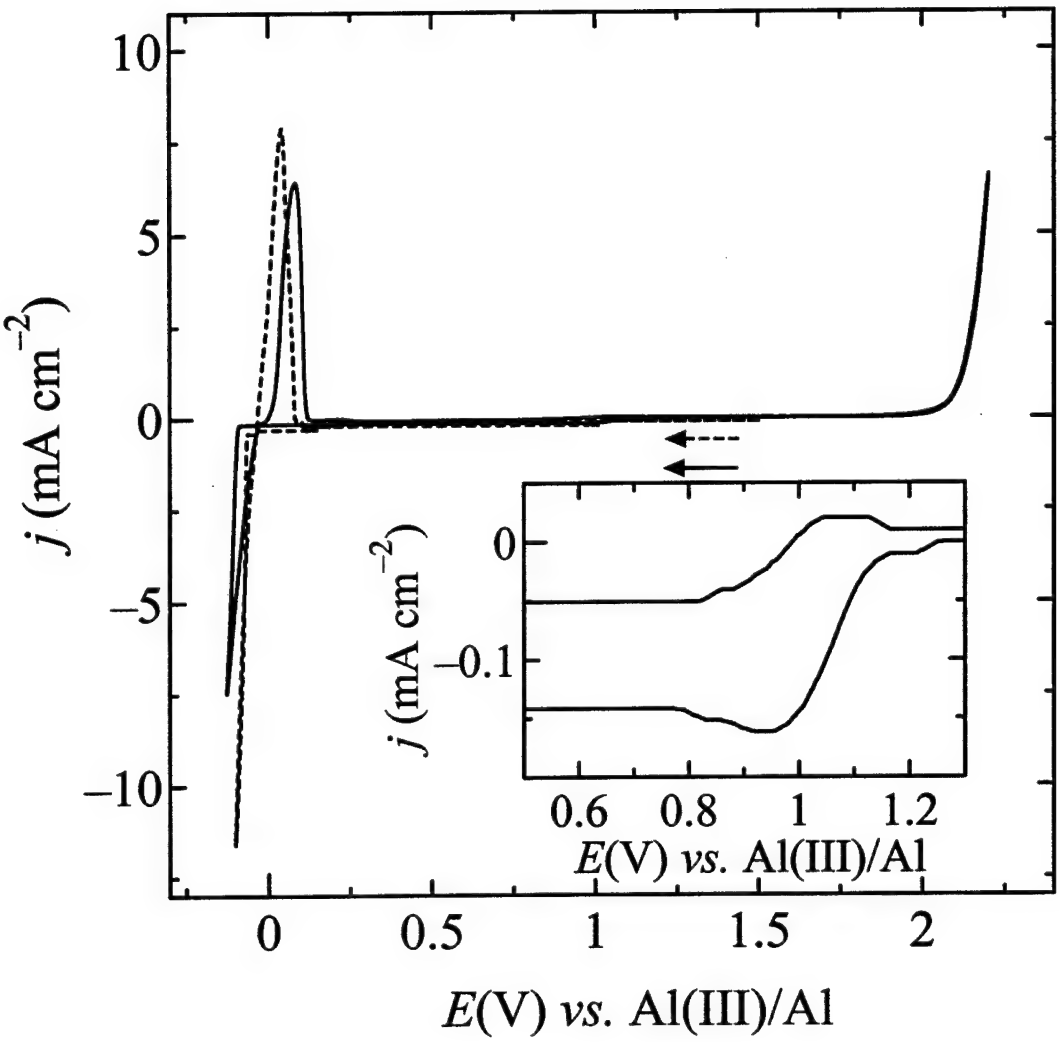
10
5
0
−5
−10
j (mA cm−2)
0
0.5
1
1.5
2
E(V) vs. Al(III)/Al
0
−0.1
j (mA cm−2)
0.6
0.8
1
1.2
E(V) vs. Al(III)/Al

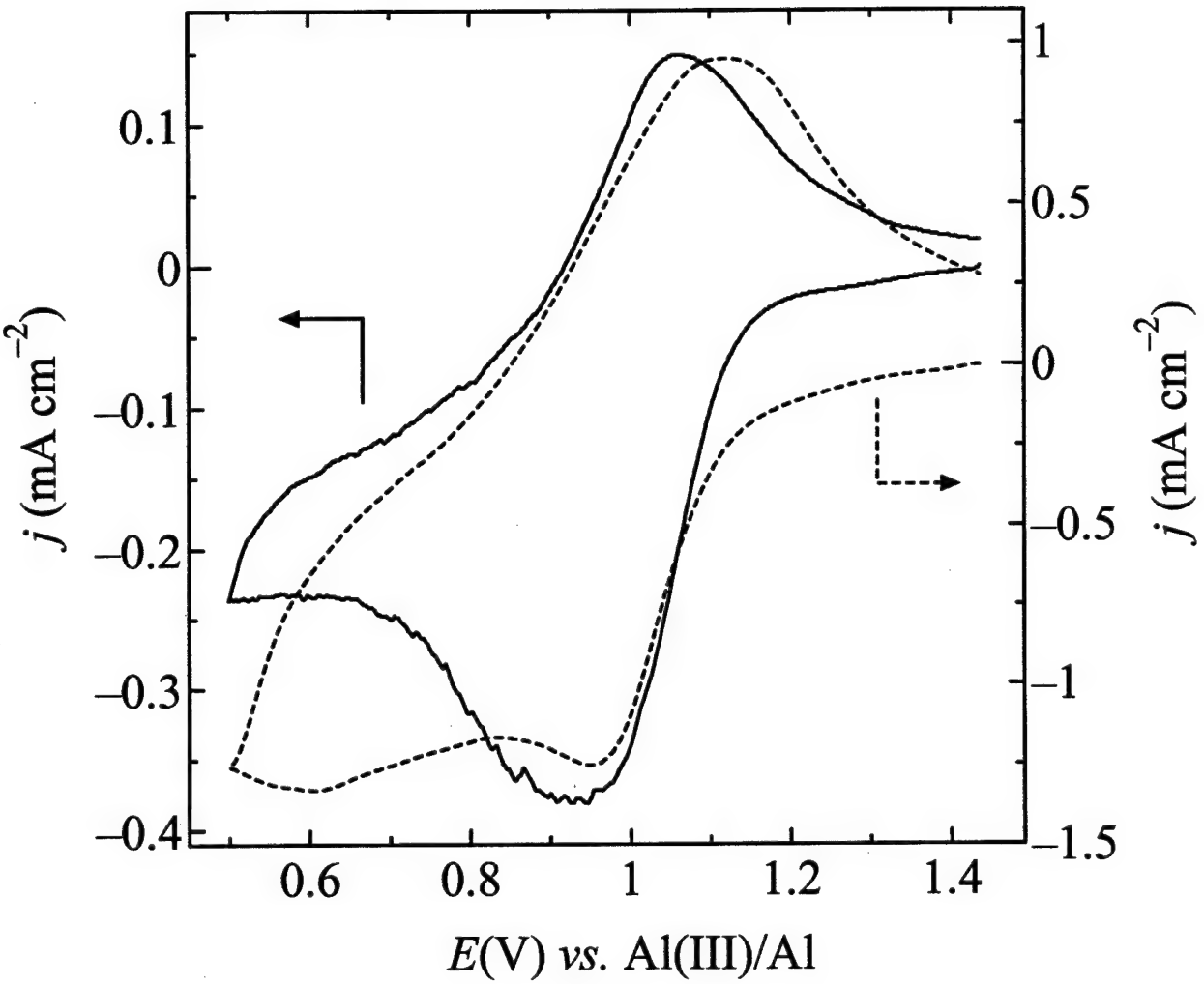
0.1
0
–0.1
–0.2
–0.3
–0.4
1
0.5
0
–0.5
–1
–1.5
0.6
0.8
1
1.2
1.4
j (mA cm–2)
j (mA cm–2)
E(V) vs. Al(III)/Al

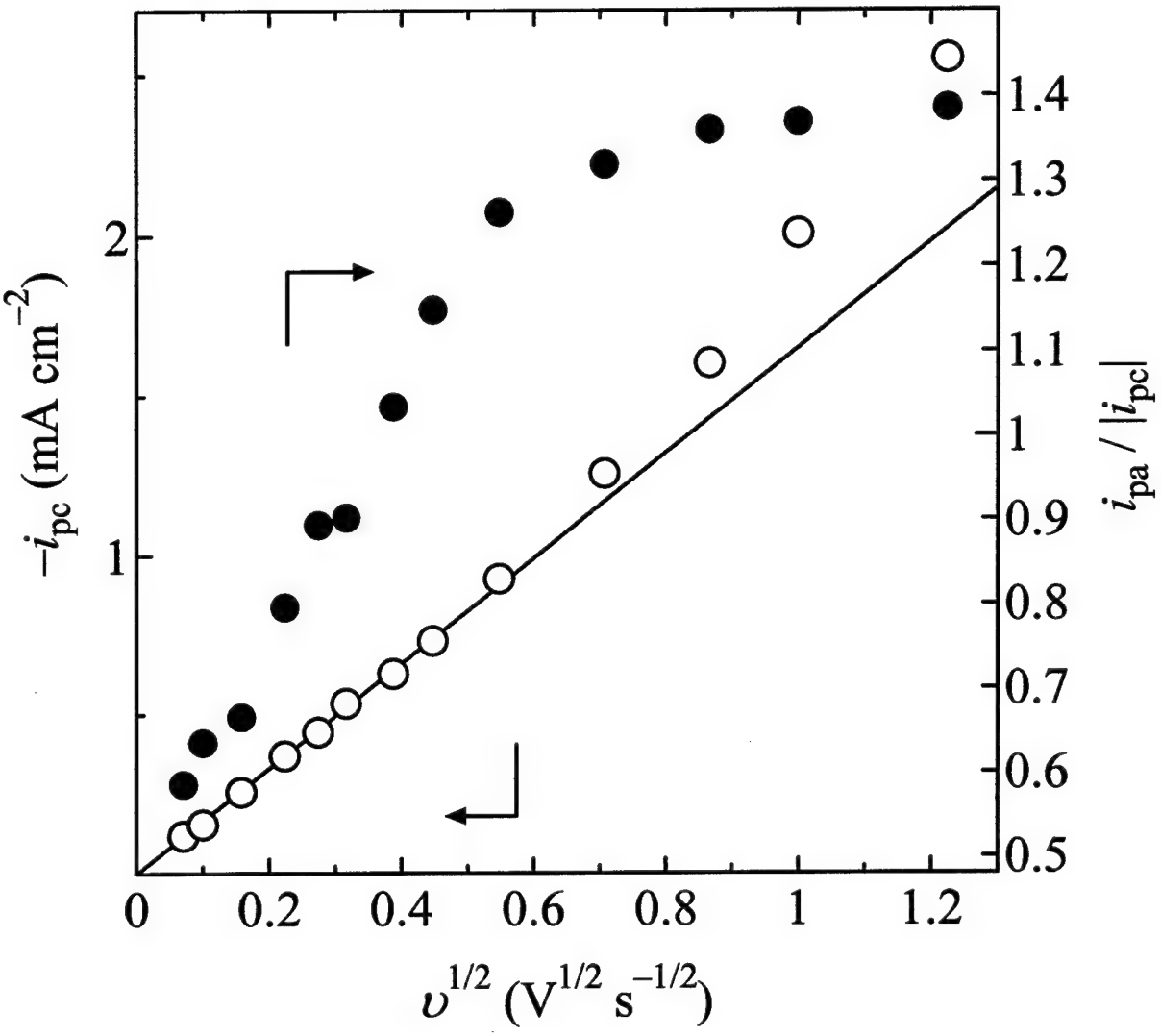
$-i_{pc}$ (mA cm^{-2})
i_{pa} / $|i_{pc}|$
$\upsilon^{1/2}$ (V$^{1/2}$ s$^{-1/2}$)
0
0.2
0.4
0.6
0.8
1
1.2
1
2
0.5
0.6
0.7
0.8
0.9
1
1.1
1.2
1.3
1.4

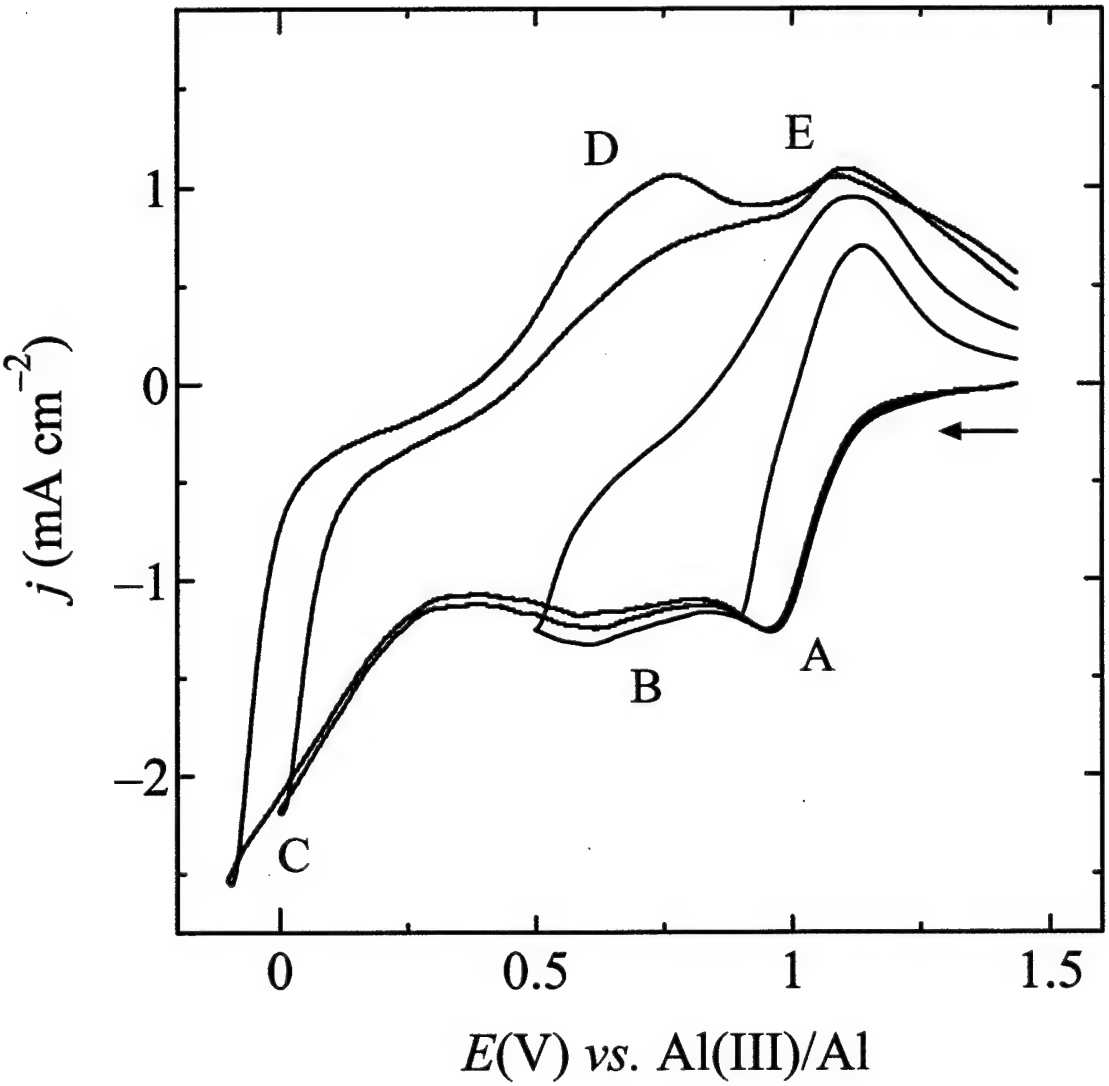
D
E
A
B
C
1
0
−1
−2
0
0.5
1
1.5
j (mA cm^{-2})
E(V) *vs.* Al(III)/Al

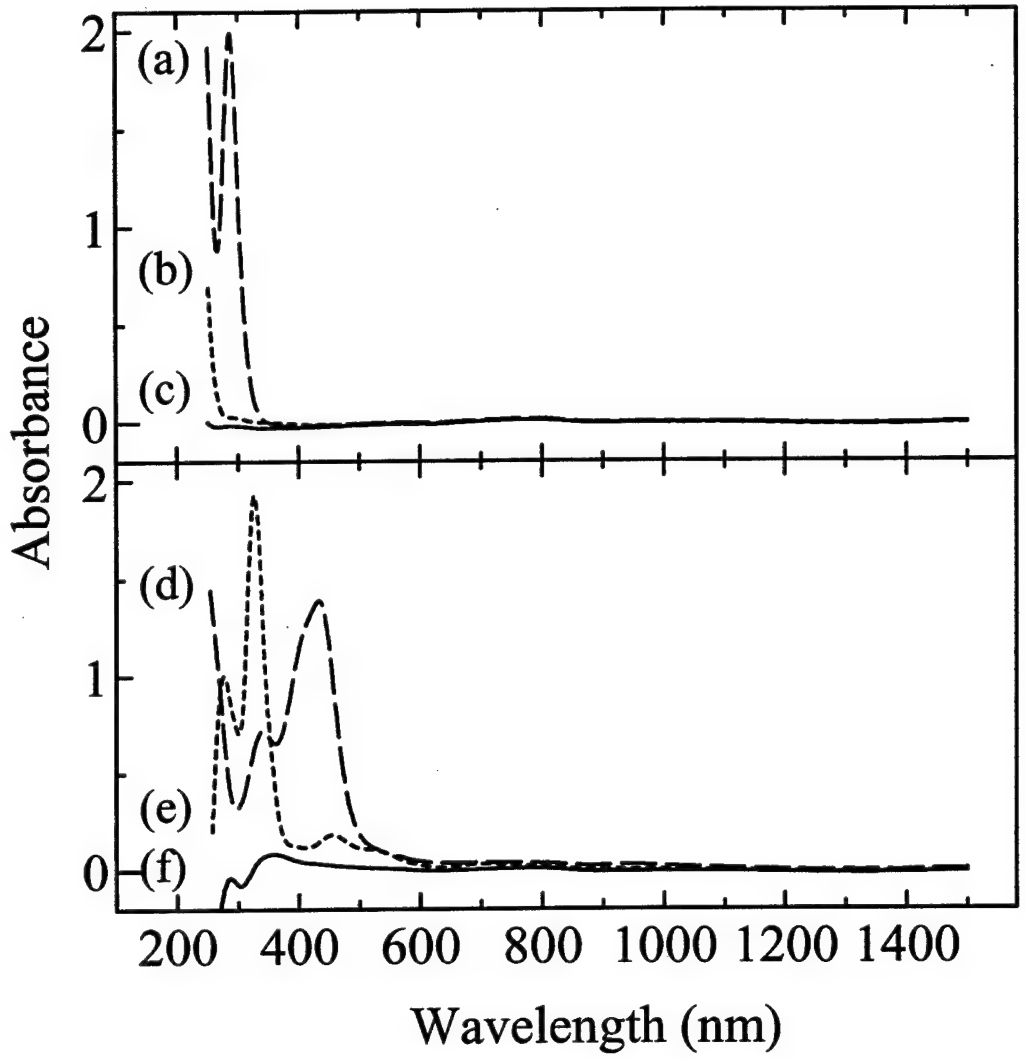
Absorbance
2
1
0
(a)
(b)
(c)
2
1
0
(d)
(e)
(f)
200
400
600
800
1000
1200
1400
Wavelength (nm)

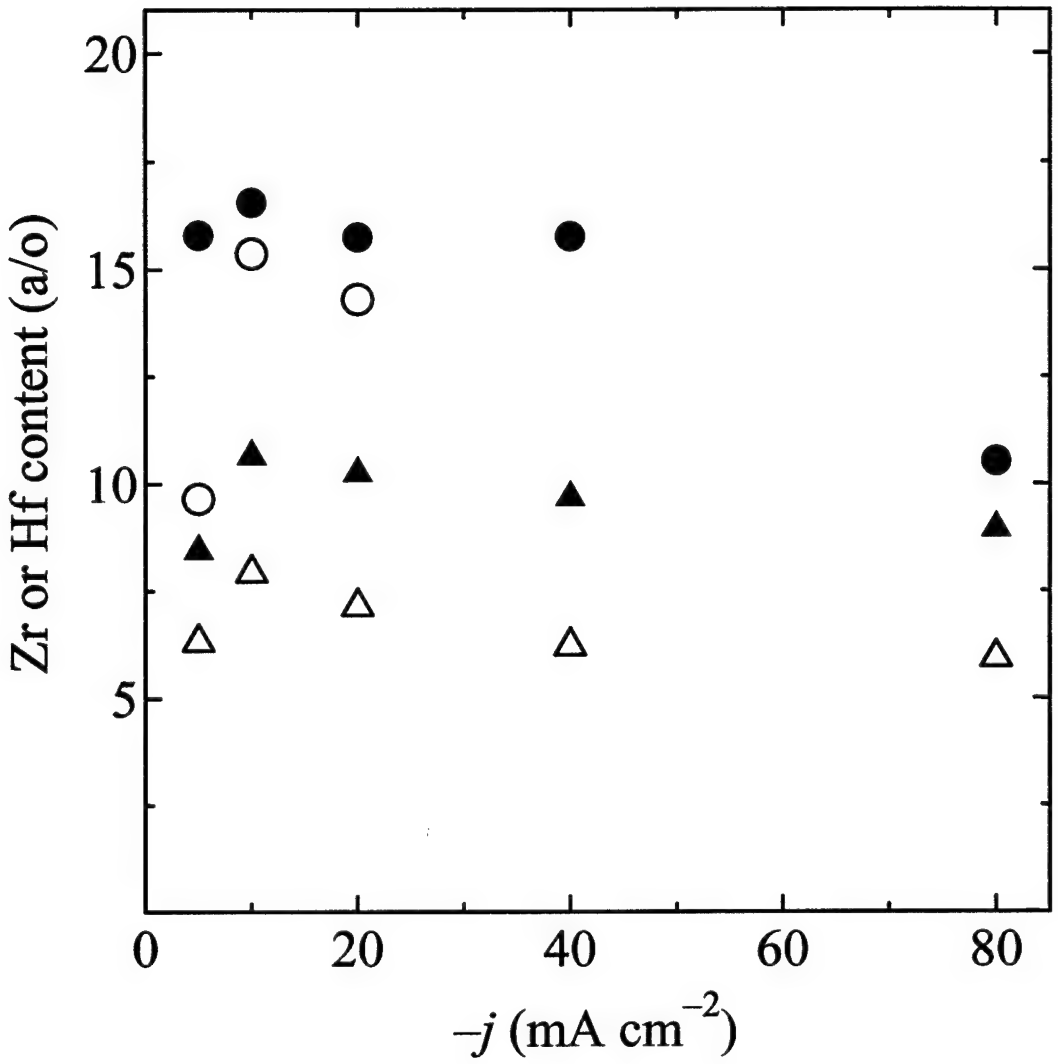
20
15
10
5
0
20
40
60
80
Zr or Hf content (a/o)
–j (mA cm–2)

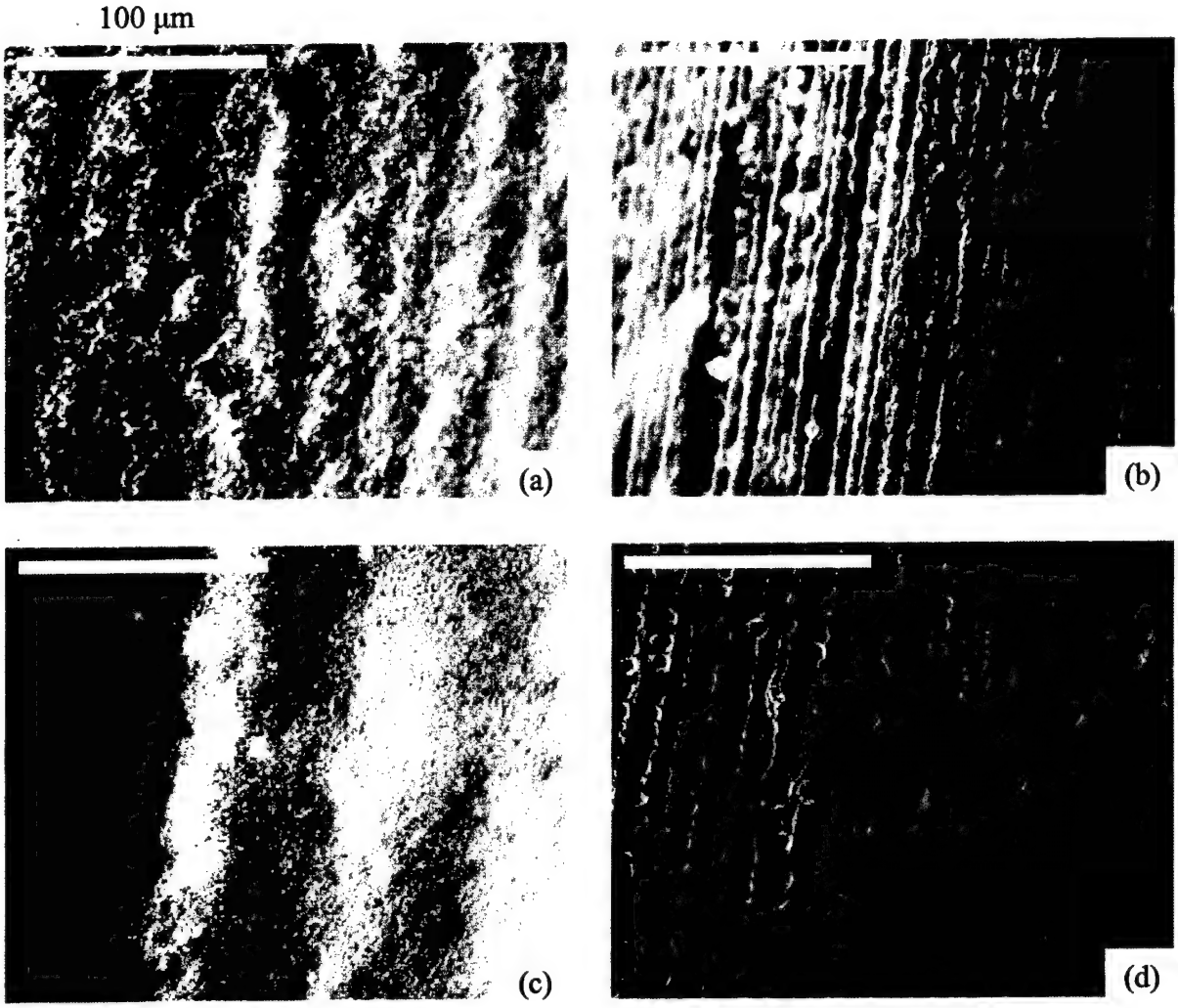
100 µm
(a)
(b)
(c)
(d)

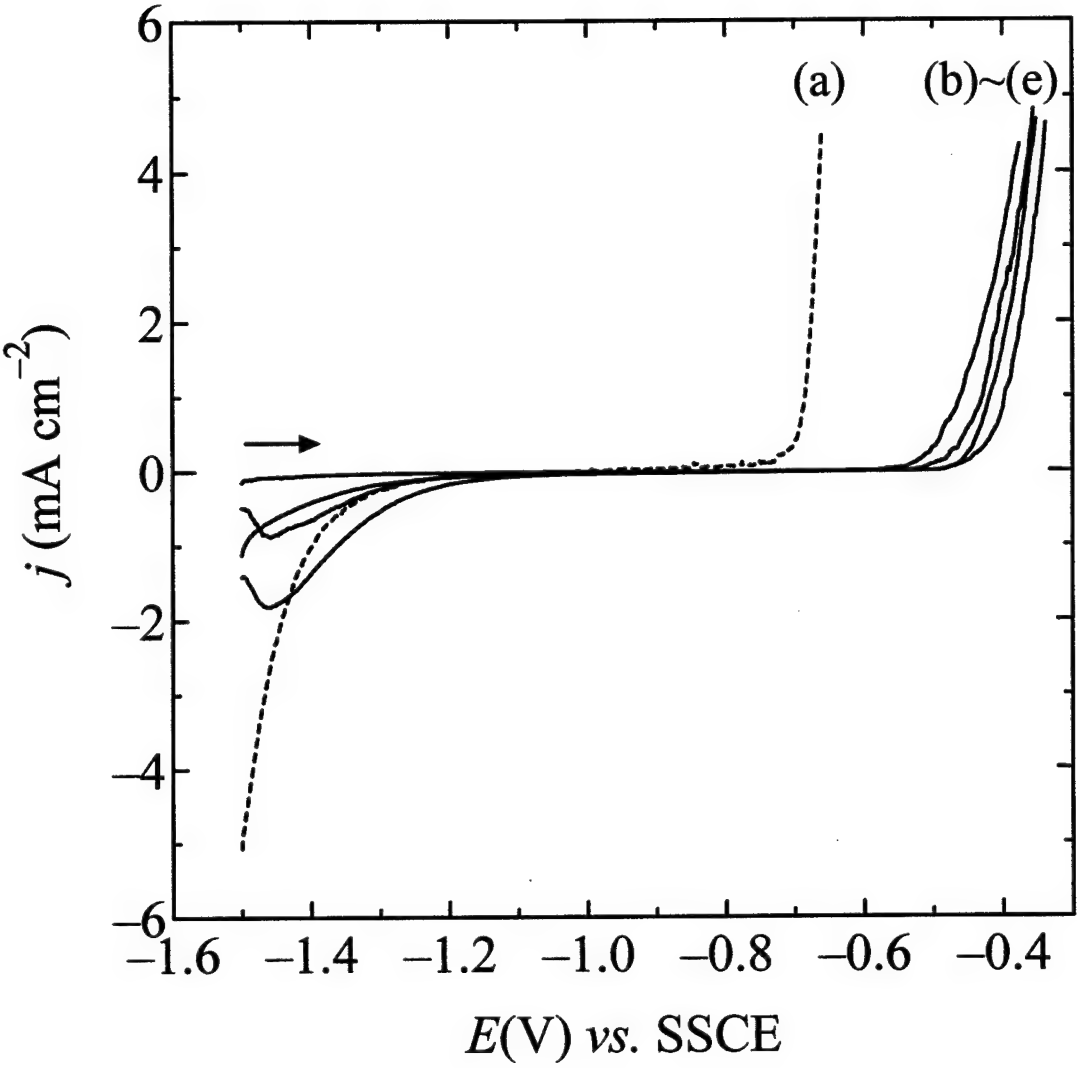
6
4
2
0
−2
−4
−6
−1.6
−1.4
−1.2
−1.0
−0.8
−0.6
−0.4
(a)
(b)~(e)
j (mA cm−2)
E(V) vs. SSCE

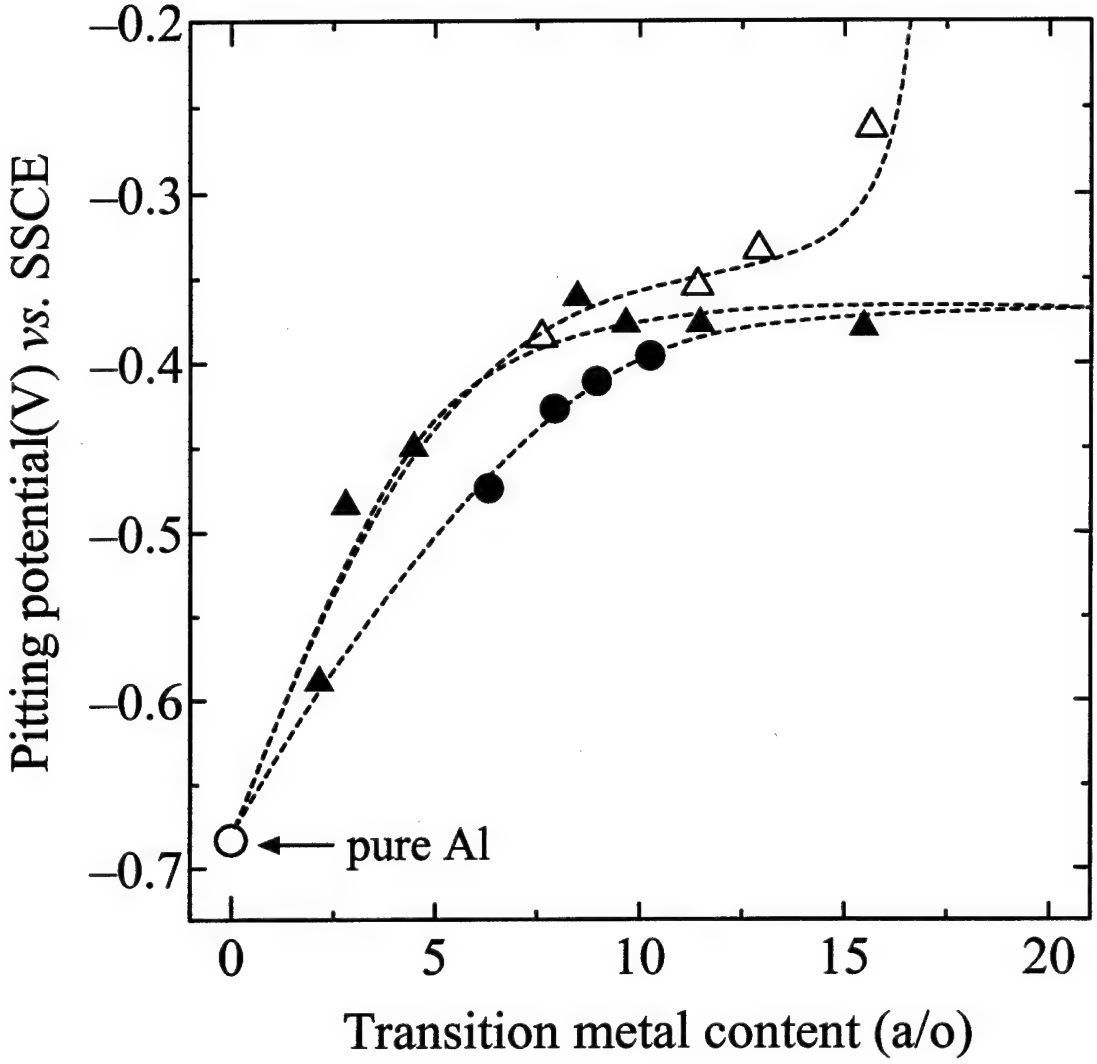
–0.2
–0.3
–0.4
–0.5
–0.6
–0.7
Pitting potential(V) vs. SSCE
pure Al
0
5
10
15
20
Transition metal content (a/o)

APPENDIX IV

T. Tsuda, W. E. Cleland, C. L. Hussey, and G. R. Stafford, "Electrochemistry of Tungsten Species and Electrodeposition of Al-W alloy in the Lewis Acidic Aluminum Chloride–1-Ethyl-3-methylimidazolium Chloride Melt," (Draft manuscript for submission to *J. Electrochem. Soc.*)

Electrochemistry of Tungsten Species and Electrodeposition of Al-W alloy in the Lewis Acidic Aluminum Chloride–1-Ethyl-3-methylimidazolium Chloride Melt

Tetsuya Tsuda,[a,*] Walter E. Cleland, Jr.,[a] Charles L. Hussey,[a,,z] and Gery R. Stafford[b,*]**

[a]*Department of Chemistry and Biochemistry, The University of Mississippi, P.O. Box 1848, University, Mississippi 38677, USA*

[b]*Materials Science and Engineering Laboratory, National Institutes of Standards and Technology, Gaithersburg, Maryland 20899, USA*

The electrochemistry and spectrochemistry of tungsten solutes were examined in the Lewis acidic 66.7–33.3 mole percent (m/o) aluminum chloride–1-ethyl-3-methylimidazolium chloride ($AlCl_3$–EtMeImCl) molten salt. UV-visible spectroscopic data for a solution of WCl_6 changed slowly over several hours at 353 K, leading to the conclusion that the W(VI) monomer, $W(AlCl_4^-)_6$, was transformed to dimeric species, possibly $W_2(AlCl_4^-)_{10}$. The W(VI)/W(V) and W(V)/W(IV) electrode reactions are reversible one-electron charge transfer processes. In solutions of WCl_4, the electrode reaction for W(IV)/W(III) involves a following irreversible chemical step in which W(III) precipitates as WCl_3(s). The electroplating of Al-W alloys proceeded most efficiently from melt containing $K_3W_2Cl_9$, and it was possible to obtain alloy samples containing about 14 atomic percent (a/o) tungsten. The pitting potential of these alloys was approximately 1150 mV positive of that for pure aluminum. This is the most corrosion-resistant alloy that we have electrodeposited from chloroaluminate melts.

* Electrochemical Society Active Member
** Electrochemical Society Fellow
[z] E-mail: chclh@chem1.olemiss.edu

INTRODUCTION

The electrodeposition of a number of non-equilibrium aluminum alloys[1] has been achieved in the Lewis acidic compositions of the room-temperature chloroaluminate molten salt, $AlCl_3$–1-ethyl-3-methylimidazolium chloride (EtMeImCl). These alloys include Al-Ti,[2,3] Al-V,[4] Al-Cr,[5-8] Al-Mg,[9] Al-Mn,[10,11] Al-Mo,[12] Al-Zr,[13] and Al-Hf.[14] (Lewis acidic chloroaluminate contain a molar excess of $AlCl_3$ over the organic chloride salt, i.e., the mole fraction of the former, x_{Al}, is greater than 0.500. Electrodeposition is a powerful and efficient method for preparing these alloys because this approach can easily make non-equilibrium alloy coatings of uniform composition and structure.

Non-equilibrium aluminum-transition metal alloys are of interest because of their outstanding resistance to chloride-induced pitting corrosion. Among the alloys in this class that have been investigated in the past, sputter-deposited Al-W alloys show excellent resistance to chloride-induced pitting corrosion.[15-19] In fact, if the W content of the alloys exceeds 10 atomic percent (a/o), the passive region is extended to more than 2600 mV positive of pure Al.[15] Furthermore, low W content Al alloys (< 10 a/o W) are also expected to be an important component for liquid crystal display (LCD) devices[20] and cellular phones.[21] However, there is no report of the electrodeposition of Al-W alloys in chloroaluminate melts or other non-aqueous solvents, and previous investigations of tungsten solutes in chloroaluminate melts[22-25] indicated that the electrochemistry of tungsten is very complicated in these ionic solvents. In this article, we report an electrochemical investigation of tungsten in the Lewis acidic 66.7–33.3 m/o $AlCl_3$–EtMeImCl melt s as it pertains to the electrodeposition of the Al-W alloys.

EXPERIMENTAL

The procedures used for the synthesis of EtMeImCl, the purification of $AlCl_3$ by sublimation, and the preparation and purification of the $AlCl_3$–EtMeImCl ionic liquid were identical to those described in previous articles.[26,27] Anhydrous tungsten (IV) chloride of 97 % purity (Aldrich) and anhydrous tungsten (VI) chloride of 99 % purity (Alfa Aesar) were used as received. The preparation of $K_3W_2Cl_9$ has been described in a previous article [22]

All the experiments were conducted using a three-electrode cell. A Pine Instruments Teflon-sheathed platinum rotating disk electrode (geometrical area = 0.099 cm^2) was used for the working electrode. A coil of 0.10 cm diameter aluminum wire (Alfa Aesar, 99.999 %) was used for the counter and reference electrodes. These electrodes were immersed in melt with the same composition as the bulk melt, but were separated from the bulk melt by a porosity E glass frit (Ace Glass). The aluminum electrodes were cleaned with a mixture of concentrated H_2SO_4, HNO_3, and H_3PO_4, rinsed with distilled H_2O, and dried under vacuum before use. All experiments were carried out in a nitrogen gas-filled glove box (VAC Atmospheres NEXUS system) with O_2 and H_2O < 5 p.p.m. Alloy samples of approximately 10 μm thickness were deposited from solutions of different tungsten ionic species in the 66.7–33.3 m/o $AlCl_3$–EtMeImCl ionic liquid onto a length of 1.25 mm diameter copper wire (geometrical area = 0.798 cm^2). The electrodeposits that were obtained were washed in distilled water and dried in vacuo.

Voltammetry experiments were conducted by using an EG&G Model 273 potentiostat/galvanostat. Electrodeposition of Al-W alloy were performed with an EG&G PARC Model 173 potentiostat/galvanostat equipped with a Model 179 digital coulometer

plug-in module. Potentiodynamic pitting-potential measurements were carried out on these alloy samples at room temperature in a 0.1 mol L^{-1} solution of NaCl in distilled H_2O. This solution was deaerated with nitrogen gas for more than 6 hours before each experiment. The reference electrode for these measurements was a sodium-saturated calomel electrode (SSCE), and the counter electrode was a large surface area platinum wire coil. A known length of the plated Cu wire was exposed to the NaCl solution by using a heat-shrink tubing mask, and the sample was scanned at 0.5 mV s^{-1} by using linear staircase voltammetry. Electronic resistance compensation was employed during all staircase voltammetry experiments. The step size used for these experiments was 2 mV.

The UV-visible spectra of dissolved tungsten ions were obtained by using a Varian CARY 5 spectrometer employing a Wilmad No. 107-7 closed type quartz cells. The path length of these cells was 0.10 cm.

The surface morphology and elemental analysis of alloy samples were investigated with a JEOL JSM-6100 scanning electron microscope equipped with a Link energy dispersive X-ray (EDX) spectrometer at the University of Mississippi SEM/EDX facility located in the Department of Mechanical Engineering or with a JEOL JXA-840 field-emission scanning electron microscope at the National Institute of Standards and Technology (NIST). The electrodeposits were also examined by X-ray diffraction (XRD) by using a Siemens D-500 diffractometer with Cu-Kα radiation at NIST.

RESULTS AND DISCUSSION

Electrochemistry of W(VI). – Tungsten (VI) chloride, WCl_6, dissolved readily in a Lewis acidic 66.7–33.3 m/o $AlCl_3$–EtMeImCl melt to produce a red solution. Cyclic staircase voltammograms recorded at a Pt disk electrode in melt containing 9.0 mmol L^{-1} WCl_6 are shown in Fig. 1(a). This voltammograms is fairly similar to those recorded in the Lewis acidic 63–37 m/o $AlCl_3$–NaCl melt by Mamantov *et al.*[23] We first investigated the electrochemical reaction corresponding to wave A. Here, voltammetric data obtained at 0.10 V s^{-1} is given in Table I along with data from the 63 m/o $AlCl_3$–NaCl melt.[23] The value for E_{pc} shows good agreement with the reported data, considering the differences in bath temperature. The number of electrons involved in the reaction was approximately one. An anodic potential sweep from the rest potential did not reveal any oxidation waves except that attributed to oxidation of the melt (Fig. 1a, dashed line).[1] Thus, the reaction corresponding to wave A must correspond to the reversible, one-electron charge transfer reaction:

$$W(VI) + e^- \leftrightarrow W(V) \qquad (1)$$

However, the W(VI) reduction wave disappeared completely, and the rest potential shifted to negative values within hours of the addition of WCl_6 (compare Fig. 1a and b), and the solution changed from a red color to orange. A similar phenomenon has been reported in Lewis basic 44.4–55.6 m/o $AlCl_3$–EtMeImCl melt containing WCl_6,[22] but the cause of this behavior reason has not been elucidated. We investigated this phenomenon by using UV-visible spectroscopy (Fig. 2 and Table II) and found that the spectrum of the solution of

WCl_6 obtained after stirring for several hours at 353.2 K is definitely different from the solution soon after the addition of WCl_6. However, the solution of WCl_6 was stable for several days and the spectrum was unchanged if the melt is kept at room temperature. In addition, it is well known that tungsten (V) chloride readily forms a dimeric species, W_2Cl_{10}, consisting of two WCl_6 octahedra sharing an edge.[28] Considering these results, the changes in the voltammograms and UV-vis spectra may be due to the structural transformation from a monomeric to a dimeric species:

$$2\ W(AlCl_4^-)_6 \rightarrow W_2(AlCl_4^-)_{10} + 2\ AlCl_4^-\ [> 300\ K] \qquad (2)$$

After the rest potential reached a steady-state value of about *ca.* 1.50 V *vs.* Al(III)/Al, wave B in Fig. 1b was analyzed by using pulse voltammetry.[29] Figure 3 shows normal pulse voltammograms at various pulse widths. The inset of this figure shows plots of $\ln[(i_l - i)/i]$ *vs.* E constructed from this voltammetric data, where i_l is the limiting current density and i is the current density corresponding to the ascending portion of the wave. The number of electrons involved in the reaction, n, and the half wave potential, $E_{1/2}$, was estimated from the plots in the inset and are given in Table III. The resulting values of n were close to 1, and $E_{1/2}$ ranged from 1.37 to 1.40 V, depending on the pulse width that was employed. The limiting current density ratio of wave B to C, i_C / i_B, increased with increasing pulse width. This implies that the reaction corresponding to wave C is not simple process, but involves coupled homogeneous chemistry. Waves B and C were also investigated by using differential pulse voltammetry,.[29] and the results are shown in Fig. 4. The waves in this figure that correspond to B in Fig. 3 are narrow and symmetrical with a width at half-height, $W_{1/2}$, in the range expected for a one-electron reversible reaction at the temperature of the

experiment (Table 4) in good agreement with the normal pulse voltammetry results. However, the waves corresponding to C in Fig. 3 are small and asymmetric, suggesting that the reaction corresponding to wave C is complicated. Thus, the reaction corresponding to wave B is the reversible one-electron shown below:

$$W(V) + e^- \leftrightarrow W(IV) \qquad (3)$$

In order to investigate this process further, experiments were conducted by dissolving WCl_4 in the 66.7 m/o melt.

Electrochemistry of W(IV). – Tungsten (IV) chloride, WCl_4, was found to be slightly soluble in the 66.7 m/o melt. The solubility was estimated by using UV-vis spectroscopy and found to be less than 3.0 mmol L^{-1} at 353 K (Fig. 2d). A cathodic staircase voltammogram recorded in the WCl_4-saturated melt revealed only a singe small reduction wave at *ca.* 1.0 V *vs.* Al(III)/Al (Fig. 1c). This wave was examined as a function of scan rate; Fig. 5 shows that the reduction potential is nearly the same as the potential of wave C in Figs. 1(a) and (b). After the sweeping through this reduction wave, the Pt electrode became covered with a gray-colored film. Therefore, it was necessary to wipe the electrode surface after every measurement to obtain accurate electrochemical data. The voltammetric data from Fig. 5 are given in tabular form as a function of scan rate in Table V. The cathodic peak current function, $i_{pc}\nu^{-1/2}$, converged to a constant value, 2.1±0.1 x 10^{-3} A cm^2 $V^{-1/2}$ $s^{1/2}$, when the sweep rate exceeds 0.075 V s^{-1}. The peak current ratio, $i_{pa}/|i_{pc}|$, which was estimated by using Nicholson's semi-empirical method,[30] is less than one at slow scan rates, but increases toward one as the scan rate is increased (Table V and Fig. 5). Thus, the electrode reaction involves a reduction reaction with a coupled irreversible chemical step.[31]

At 0.025 V s^{-1}, the peak potential-half peak potential separation for this wave, $E_{pc/2}$-E_{pc}, approaches the 0.067 V value expected for a one-electron reversible electrode reaction at 353.2 K. However, $E_{pc/2}$-E_{pc} increased slightly as the sweep rate increases, suggesting that the electron transfer reaction may not be completely reversible. Similar reactions are often reported in the 66.7 m/o acidic melt containing the transition metal chlorides.[2,4,13] We concluded that wave C in Fig. 5 arises from the one-electron quasi-reversible reduction of W(IV) to W(III) followed by precipitation of WCl_3(s) onto the electrode:

$$W(IV) + e^- \leftrightarrow W(III) \quad (4)$$

$$W(III) \rightarrow WCl_3(s) \quad (5)$$

The diffusion coefficient for W(IV), $D_{W(IV)}$, and the Stokes-Einstein product, $D_{W(IV)}\eta/T$, where η is the absolute viscosity of the molten salt, were calculated from the data in Fig. 5. The viscosity data taken from Fannin et al.[32] were used for this calculation. The former was found to be 7.3×10^{-6} cm^2 s^{-1} at 353.2 K, and the latter was estimated to be 10×10^{-11} g cm s^{-2} K^{-1}.

Chemical reduction of W(VI). – In order to produce W(II), we attempted to reduce W(VI) by using Al metal in the 66.7 m/o melt containing WCl_6 at 353 K. However, several hours after the addition of Al, the melt became dark due to the formation of a black precipitate. This precipitate may be WCl_4 because the solubility of WCl_4 was quite low in the melt and the color was identical our commercial sample of WCl_4, but the UV-visible spectrum of the solution prepared from the Al reduction of a melt containing a low

concentration of WCl_6 concentration melt differed from the spectrum prepared by dissolving WCl_4 (Fig. 2e).

Electrochemistry of $W_2Cl_9^{3-}$. – Figure 6b shows cyclic staircase voltammograms recorded at a Pt electrode in the melt containing 3.2 mmol L^{-1} $K_3W_2Cl_9$. After the dissolution of this compound, the potential for Al deposition shifts to slightly more negative values (*ca.* 20 mV) and the wave for Al oxidation shifts to more positive potentials. Such behavior is often observed when aluminum is alloys with transition metals.[1,2,5-14]

The oxidation of $W_2Cl_9^{3-}$ was examined by the use of cyclic staircase voltammetry at different scan rates (Fig. 7). The voltammetric data are collected in Table VI as a function of the scan rate. The anodic peak current function, $i_{pa}v^{-1/2}$, shows approaches a constant value of 0.8±0.1 x 10^{-3} A cm^2 $V^{-1/2}$ $s^{1/2}$ if the scan rate exceeds 0.01 V s^{-1}. The peak current ratio, $|i_{pc}|/i_{pa}$, which was estimated by the aforementioned methods,[30] is less than one at slow scan rates, but increases toward 1 as the scan rate increases (Table VI and Fig. 7(inset)). This indicates that the electrode reaction involves a reduction reaction with a coupled irreversible chemical step.[31] The peak potential-half peak potential separation for this wave, E_{pa}-$E_{pa/2}$, is close to the 0.067 V expected for a one-electron reversible electrode reaction at 353.2 K. It suggests that the oxidation of $W_2Cl_9^{3-}$ proceeds by E_rC_{ir} mechanism as found in the Lewis basic 44.4-55.6 m/o melt.[22] However, we could not identify the chemical step in this mechanism. The diffusion coefficient for $W_2Cl_9^{3-}$, D_{W2Cl9}^{3-}, and the Stokes-Einstein product, $D_{W2Cl9}^{3-}\eta/T$, estimated from Fig. 7 was 9.8×10^{-7} cm^2 s^{-1} at 353.2 K and 1.4×10^{-11} g cm s^{-2} K^{-1}, respectively.

The oxidation of $W_2Cl_9^{3-}$ was also examined by the use of a Pt rotating disk electrode (Pt-RDE) in the same solution (Fig. 8). Each limiting current was sampled at 1.50 V. The electrochemical data estimated from plots of $\ln[i / (i_d - i)]$ *vs.* E(V) is given in Table

VII. The inset of Figure 8 shows a Levich plot, *i.e.*, a plot of the limiting current density, i_l, versus the square root of the electrode rotation rate, $\omega^{1/2}$, that was constructed from the data in Figure 8 and Table VII. The slope of this plot was used with the Levich equation to calculate the diffusion coefficient, D_{W2Cl9}^{3-}, and the Stokes-Einstein product, $D_{W2Cl9}^{3-}\eta/T$. The aforementioned viscosity data was employed for the calculation.[32] These electrochemical data are summarized in Table VIII along with that reported in the 44.4 m/o melt. The diffusion coefficient for $W_2Cl_9^{3-}$ in the 66.7 m/o melt is considerably larger than the reported data for the 44.4 m/o melt, but taking into account differences in the temperature and corresponding differences in the viscosity of the molten salts, *i.e.*, by using the Stokes-Einstein product for comparison, the diffusion coefficient reported herein is very similar to that measured in the 44.4 m/o melt.

In order to estimate the standard heterogeneous rate constant, k^0, and the transfer constant, α, for the $W_2Cl_9^{2-}$/ $W_2Cl_9^{3-}$ electrode reaction, we constructed Koutecký-Levich plots of i^{-1} *vs.* $\omega^{-1/2}$, from the data in Fig. 8. As shown in Fig. 9, these plots are linear and exhibit potential-dependent intercepts. From the intercepts at $\omega^{-1/2}=0$ and following equation,[29] the potential dependent heterogeneous rate constants, $k_f(E)$, were estimated.

$$1/i = 1/i_k + 1/(0.620nFAC_0^*D^{2/3}\nu^{-1/6}\omega^{1/2}) \quad (6)$$

$$i_k = nFAk_f(E)C_0^* \quad (7)$$

k^0 and α can be determined with equation (8) and the intercept and the slope for the plot of ln $k_f(E)$ vs. E-E^0:

$$\ln k_f(E) = \ln k^0 + \alpha n F(E-E^{0'})/RT \quad (8)$$

$$E^{0'} = E_{1/2} + RT/(nF)\ln[(D_R/D_O)^{2/3}] \quad (9)$$

Usually the formal potential, $E^{0'}$, is estimated by the use of equation (9).[29] However, the diffusion coefficient for the $W_2Cl_9^{2-}$ is not known. Therefore, we assumed that the diffusion coefficient for this species is equal to that for $W_2Cl_9^{3-}$ and that $E^{0'} = E_{1/2}$. The average value of $E_{1/2}$ given in Table VII was used estimate k^0 and α from the plot shown in the inset of Fig. 9 and are given in Table VIII.

As expected, the UV spectrum of the $K_3W_2Cl_9$ differed from that for the other tungsten cations (Fig. 2 and Table II). The overall appearance of this spectrum is similar to that observed for this compound in the basic 44.4 m/o melt.[22] The shift in wavelength implies that interactions between the $W_2Cl_9^{3-}$ species and the ionic species in the melt change as the melt acidity is altered. The solubility of this species was estimated to be 3.3 mmol L^{-1} at 298 K and 8.0 mmol L^{-1} at 353 K by using cyclic staircase voltammetry and UV-vis spectroscopy. However, we employed low concentrations of $K_3W_2Cl_9$ during the preparation of Al-W alloys described below because alloys containing large amount of W do not adhere well to the Cu substrate.

Electrodeposition and characterization of Al-W alloys. – The electrodeposition of bulk Al-W alloys was examined by using dc galvanostatic methods at a current density of -5 ~ -80 mA cm^{-2}. The substrate for these experiments was a copper-wire rotating electrode. In keeping with previous investigations, we used an electrode rotation rate of 2000 rpm.[2,12] As shown in Fig. 10, the W content of bulk Al-W alloys prepared in a 9.0 mmol L^{-1} WCl_6 solution and a 3.2 mmol L^{-1} $K_3W_2Cl_9$ solution increases as the applied current density

decreases. Just for reference, we also show the W content of the alloys obtained from the solution containing W(II) (unknown concentration). These results are a well known feature of overpotential aluminum alloy deposition from the Lewis acidic chloroaluminate ionic liquids.[1] This behavior results from a decrease in the ratio of the partial currents for transition metal reduction compared to Al reduction with increasing cathodic current density. This occurs because the transition metal is being reduced at the mass-transport limited rate, whereas the current for Al deposition increases as this current is increased. In fact, we could prepare Al-W alloys in the $K_3W_2Cl_9$-saturated melt at 353 K having higher W content, but the alloys were too fragile to characterize.

Figure 11 shows SEM images of the Al-W alloys prepared from the solution containing 3.2 mmol L^{-1} $K_3W_2Cl_9$. When the W content is low, the surface morphology of these alloys was similar to that of some other transition metal aluminum alloys.[2,4,12-14] The surface of the Al-W alloy became covered with powdery crystals appeared as the W content was increased.

Pitting potential measurements. - Potentiodynamic anodic polarization curves recorded in deaerated aqueous NaCl for Al-W alloys electrodeposited on copper wire rotating electrodes are shown in Fig. 12. As noted in previous reports,[2,4,12-14] alloys with a low W content alloy (Fig.12b) displayed a stable passive region characterized by a very small potential-independent current followed by a sudden rise in current at the pitting potential. However, the anodic polarization curves become complicated with increase of the W content. Such behavior implies that the samples have several crystal structures in the alloy because changes in the crystal structure of the Al-W alloys is known to affect the pitting potential.[17] The variation of the pitting potential with alloy composition is shown in Fig. 13 along with the data for Al-Mo alloys discussed in a previous article

from this laboratory. prepared in previous investigationsby the electrodeposition.[12] The pitting potential of the Al-W alloys was shifted approximately 1150 mV against pure aluminum when the W content was *ca.* 14 a/o. At low W content (~ 5 a/o), the result was essentially identical to the data for sputter-deposited Al alloys reported by Frankel et al.,[18] but the value for alloys with a high W content was greatly inferior to that for sputter-deposited Al-W alloys.[15,16,19]

Acknowledgment

This research was supported by the Air Force Office of Scientific Research, Grant No. F49620-00-1-0123.

References

1. G. R. Stafford and C. L. Hussey, "Electrodeposition of Transition Metal-Aluminum Alloys from Chloroaluminate Molten Salts," in *Advances in Electrochemical Science and Engineering*, R. C. Alkire and D. M. Kolb, Editors, Vol. 6, P.275, Wiley-VCH Verlag GmbH, Weinheim, (2002).
2. T. Tsuda, C. L. Hussey, G. R. Stafford, and J. E. Bonevich, *J. Electrochem. Soc.*, **150**, C234 (2003).
3. T. Takenaka and M. Kawakami, *Int. J. Mater. and Product Tech.*, **2**, 500 (2001).
4. T. Tsuda and C. L. Hussey, *J. Min. and Metall., B*, **39**, 3 (2003).
5. M. Matsunaga, T. Kitazaki, K. Hosokawa, S. Hirano, and M. Yoshida, in *Ninth International Symposium on Molten Salts*, C. L. Hussey, D. S. Newman, G. Mamantov, and Y. Ito, Eds., PV 94-13, p. 422, The Electrochemical Society, (1994).
6. M. Matsunaga, M. Morimitsu, M. Nagano, and T. Tsuda, *Molten Salt Forum*, **5-6**, 601 (1998).
7. H. C. De Long and P. C. Trulove, in *Tenth International Symposium on Molten Salts*, R. T. Carlin, S. Deki, M. Matsunaga, D. S. Newman, J. R. Selman, and G. R. Stafford, Eds., PV 96-7, p. 276, The Electrochemical Society, (1996).
8. D. E. Clinton, P. C. Trulove, P. L. Hagans, and H. C. De Long, *Molten Salt Forum*, **5-6**, 593 (1998).
9. M. Morimitsu, N. Tanaka, and M. Matsunaga, *Chem. Lett.*, 1028 (2000).
10. H. C. De Long, J. A. Mitchell, and P. C. Trulove, *High Temp. Material Processes*, **2**, 507 (1998).

11. P. C. Trulove, J. A. Mitchell, P. L. Hagans, R. T. Carlin, G. R. Stafford, and H. C. De Long, in *Twelfth International Symposium on Molten Salts*, P. C. Trulove, H. C. De Long, G. R. Stafford, and S. Deki, Eds., PV 99-41, p. 517, The Electrochemical Society, (2000).

12. T. Tsuda, C. L. Hussey, and G. R. Stafford, *J. Electrochem. Soc.*, in press.

13. T. Tsuda, C. L. Hussey, G. R. Stafford, and O. Kongstein, *J. Electrochem. Soc.*, in press.

14. T. Tsuda, C. L. Hussey, and G. R. Stafford, *Electrochim. Acta*, to be submitted.

15. B. A. Shaw, T. L. Fritz, G. D. Davis, and W. C. Moshier, *J. Electrochem. Soc.*, **137**, 1317 (1990).

16. B. A. Shaw, G. D. Davis, T. L. Fritz, B. J. Rees, and W. C. Moshier, *J. Electrochem. Soc.*, **138**, 3288 (1991).

17. G. D. Davis, B. A. Shaw, B. J. Rees, and M. Ferry, *J. Electrochem. Soc.*, **140**, 951 (1993).

18. G. S. Frankel, R. C. Newman, C. V. Jahnes, and M. A. Russak, *J. Electrochem. Soc.*, **140**, 2192 (1993).

19. M. Metikoš-Huković, N. Radić, Z. Grubač, and A. Tonejcv, *Electrochim. Acta*, **47**, 2387 (2002).

20. K. Kobayashi, H. Ochi, T. Hara, and T. Fujita, *Jpn. Kokai Tokkyo Koho (Japanese Patent)*, JP2000187233 (2000).

21. N. Kimura, M. Nakano, and K. Sato, *Jpn. J. Appl. Phys.*, **37**, 1017 (1998).

22. T. B. Scheffler and C. L. Hussey, *Inorg. Chem.*, **23**, 1926 (1984).

23. J.-P. Schoebrechts, P. A. Flowers, G. W. Hance, and G. Mamantov, *J. Electrochem. Soc.*, **135**, 3057 (1988).

24. I.-Wen Sun, A. G. Edwards, and G. Mamantov, *J. Electrochem. Soc.*, **140**, 2733 (1993).

25. G. Mamantov, G.-S. Chen, H. Xiao, Y. Yang, and E. Hondrogiannis, *J. Electrochem. Soc.*, **142**, 1758 (1995).

26. B. J. Tierney, W. R. Pitner, J. A. Mitchell, C. L. Hussey, and G. R. Stafford, *J. Electrochem. Soc.*, **145**, 3110 (1998).

27. X. H. Xu and C. L. Hussey, *J. Electrochem. Soc.*, **140**, 1226 (1993).

28. F. A. Cotton and C. E. Rice, Acta Cryst., B, **B34**, 2833 (1978).

29. A. J. Bard, L. R. Faulkner, Electrochemical Methods: Fundamentals and Applications, John Wiley & Sons, New York, 2001.

30. R. S. Nicholson, *Anal. Chem.*, **37**, 1406 (1965).

31. R. S. Nicholson, I. Shain, *Anal. Chem.*, **36**, 706 (1964).

32. A. A. Fannin, Jr., D. A. Floreani, L. A. King, J. S. Landers, B. J. Piersma, D. J. Stech, R. L. Vaughn, J. S. Wilkes, and L. Williams John, *J. Phys. Chem.*, **88**, 2614 (1984).

33. W. C. Dorman and R. E. McCarley, *Inorg. Chem.*, **13**, 491 (1974).

Table I. Cyclic voltammetric data for WCl_6 in the 66.7 m/o melt.

Solvent	v ($V\ s^{-1}$)	E_{pc} (V)	E_{pc}-E_{pa} (V)	Temp. (K)	n	Reference
63 m/o $AlCl_3$–NaCl*	0.02	1.615	0.090	448	0.99[a]	23
	0.05	1.620	0.090	448	0.99[a]	23
	0.10	1.620	0.090	448	0.99[a]	23
66.7 m/o $AlCl_3$–EtMeImCl	0.10	1.634	0.068	353	1.02[b]	This work

*Working electrode: glassy carbon.
Theoretical value of E_{pc}-E_{pa} at 448 K: 0.089 V[a]; at 353 K: 0.070 V.[b]

Table II. Absorption spectroscopic data for tungsten ionic species

Solute	Solvent	λ, nm (ε, mol^{-1} L cm^{-1})	Reference
WCl_6	Vapor	225, 275,[a] 330, 375,[a] 430	23
WCl_6	$AlCl_3$–$NaCl_{sat}$	288, 338	24
$KWCl_6$		288, 338	24
WCl_6	44.4 m/o $AlCl_3$–EtMeImCl	275,[a] 299 (~1.5×10^4), 347 (~8×10^3), 390[a]	22
$KWCl_6$		275,[a] 298 (~1.3×10^4), 350 (~7×10^3), 390[a]	22
K_2WCl_6		287 (7.7×10^3), 308,[a] 350[a]	22
$K_3W_2Cl_9$		460 (4.0×10^3), 626 (~70), 764 (~35)	22
WCl_6	66.7 m/o $AlCl_3$–EtMeImCl	~250, 270,[a] 359 (3.6×10^3), 460[a]	This work
W(V)		256 (5.6×10^3), 279,[a] 334 (1.8×10^4), 376[a]	This work
WCl_4		~250, 284 (8.6×10^2), 353 (6.4×10^2)	This work
W(II)*		~250, 289	This work
$K_3W_2Cl_9$		269 (8.5×10^3), 345 (4.6×10^3), 571 (6.8×10^2)	This work

[a]Shoulder

* 66.7 m/o $AlCl_3$–EtMeImCl melt containing W(VI) stirred with pure Al at 353 K for three days.

Table III. Normal pulse voltammetric data for the redaction of 9.0 mmol L^{-1} W(V) at a stationary Pt electrode in the 66.7 m/o melt..

Pulse width (ms)	Limiting current density (mA cm^{-2})		n	$E_{1/2}$ (V)
	Wave B	Wave C (i_C / i_B)	Wave B	Wave B
25	2.797	2.686 (0.96)	0.91	1.395
50	4.280	5.686 (1.33)	0.99	1.384
100	4.324	6.745 (1.56)	1.08	1.371

Table IV. Differential pulse voltammetric data for the reduction of 9.0 mmol L^{-1} W(V) at a stationary Pt electrode in the 66.7 m/o melt.

	Wave B			Wave C		
Pulse width (ms)	25	50	100	25	50	100
E_p (V)	1.419	1.428	1.440	0.945	0.955	0.966
$i_{p/2}$ (mA cm^{-2})	0.192	0.370	0.460	0.094	0.188	0.260
$W_{1/2}$ (V)	0.100	0.093	0.092	0.214	0.206	0.190
n[a]	1.07	1.15	1.16	0.50	0.52	0.56

[a]Values for number of electrons (n) were determined using the equation: $W_{1/2} = 3.52\ RT / nF$.[29]
Pulse height: 25 mV.

Table V. Voltammetric data for the reduction of 3.0 mmol L^{-1} W(IV) at a stationary Pt electrode in the 66.7 m/o melt at 353 K.

v	$10^{-3}\, i_{pc} v^{-1/2}$	$i_{pa} / \lvert i_{pc} \rvert$	E_{pc}	$E_{pc/2}$-E_{pc}
(V s^{-1})	(A cm^{-2} $V^{-1/2}$ $s^{1/2}$)		(V)	(V)
0.005	2.78	0.60	0.962	0.090
0.010	2.37	0.73	0.973	0.084
0.025	2.25	0.83	0.982	0.075
0.050	2.27	0.83	0.962	0.085
0.075	2.04	0.82	0.939	0.091
0.100	2.05	0.83	0.921	0.102
0.125	2.10	0.84	0.916	0.105
0.150	2.23	0.83	0.900	0.108
0.200	2.14	0.83	0.885	0.111
0.300	2.00	0.85	0.859	0.124
0.500	2.07	0.89	0.816	0.143
0.750	2.11	0.93	0.754	0.180
1.000	1.96	0.96	0.699	0.215

Table VI. Voltammetric data for the reduction of 3.2 mmol L^{-1} $W_2Cl_9^{3-}$ at a stationary Pt electrode in the 66.7 m/o melt at 353.2 K.

v ($V\ s^{-1}$)	$10^{-3}\ i_{pa}v^{-1/2}$ ($A\ cm^{-2}\ V^{-1/2}\ s^{1/2}$)	$\lvert i_{pc}\rvert / i_{pa}$	E_{pa} (V)	E_{pa}-$E_{pa/2}$ (V)
0.005	1.00	0.65	1.443	0.057
0.010	0.91	0.84	1.442	0.057
0.025	0.89	1.03	1.442	0.056
0.050	0.85	1.11	1.447	0.059
0.100	0.83	1.15	1.457	0.065
0.150	0.83	1.17	1.459	0.067
0.200	0.81	1.18	1.466	0.070
0.250	0.81	1.17	1.472	0.072
0.300	0.79	1.19	1.478	0.075

Table VII. Voltammetric data for the reduction of 3.2 mmol L^{-1} $W_2Cl_9^{3-}$ at a Pt-RDE in the 66.7 m/o melt at 353.2 K.

ω (rpm)	i_l (mA cm^{-2})	$E_{1/2}$ (V)	d^a	n
1000	0.317	1.411	0.024	1.25
1250	0.353	1.411	0.024	1.25
1500	0.387	1.412	0.025	1.20
1750	0.413	1.412	0.025	1.20
2000	0.442	1.412	0.025	1.20

[a]The theoretical value for n =1 is 0.030.

Table VIII. Diffusion coefficients for tungsten ionic species in $AlCl_3$–EtMeImCl molten salts.

Solute	Solvent	Temperature (K)	Method	$10^7 D$ ($cm^2\ s^{-1}$)	$10^{11}\ \eta D/T$ (g cm s^{-2} K^{-1})	α	$10^3 k^0$ (cm s^{-1})	References
$KWCl_6$	44.4 m/o $AlCl_3$–EtMeImCl	313 K	CV	2.8 ± 0.2	2.0 ± 0.1	-	-	22
K_2WCl_6				2.2 ± 0.1	1.5 ± 0.1	-	-	22
$K_3W_2Cl_9$				1.5 ± 0.1	1.1 ± 0.1	-	-	22
WCl_4	66.7 m/o $AlCl_3$–EtMeImCl	353 K		73	10	-	-	This work
$K_3W_2Cl_9$				9.8	1.4	-	-	This work
			RDE-CV	8.7	1.2	0.505	5.25	This work

CV: Cyclic voltammetry; RDE-CV: Cyclic voltammetry using a rotating Pt disk electrode.

Figure Captions

Figure 1. Cyclic staircase voltammograms recorded at a platinum disk electrode in the 66.7–33.3 m/o $AlCl_3$–EtMeImCl melt: (a) immediately after the dissolution of 9.0 mmol L^{-1} WCl_6; (b) several hours after the dissolution in (a); (c) containing 3.0 mmol L^{-1} WCl_4; (----) pure melt. The temperature was 353 K, and the sweep rate was 0.10 V s^{-1}.

Figure 2. UV-visible spectra of the 66.7–33.3 m/o $AlCl_3$–EtMeImCl melt: (a) containing 3.1 mmol L^{-1} WCl_6; (b) several hours after the dissolution of 0.5 mmol L^{-1} WCl_6; (c) containing 1.2 mmol L^{-1} $K_3W_2Cl_9$; (d) containing 3.1 mmol L^{-1} WCl_4; (e) after reduction of the melt containing 1.4 mmol L^{-1} WCl_6 by using Al wire at 353 K for three days. The cell path length was 0.10 cm.

Figure 3. Normal pulse voltammograms recorded at a platinum disk electrode in the 66.7–33.3 m/o $AlCl_3$–EtMeImCl melt containing 9.0 mmol L^{-1} W(V). The pulse width was (a) 25 ms; (b) 50 ms; (c) 100 ms. The temperature was 353 K, and the sweep rate was 4 mV s^{-1}. (inset) Plots of ln $[(i_l - i) / I]$ vs. E(V) constructed from the data in Fig. 3 and Table III.

Figure 4. Differential pulse voltammograms recorded at a platinum disk electrode in the 66.7–33.3 m/o $AlCl_3$–EtMeImCl melt containing 9.0 mmol L^{-1} W(V). The pulse widths were (a) 25 ms; (b) 50 ms; (c) 100 ms. The temperature was 353 K; and the sweep rates were 4 mV s^{-1}. The pulse height was 25 mV.

Figure 5. Cyclic staircase voltammograms recorded at a platinum disk electrode in the 66.7–33.3 m/o $AlCl_3$–EtMeImCl melt containing 3.0 mmol L^{-1} WCl_4. The temperature was 353 K and the sweep rates are shown in Table V. (inset) Peak reduction current density and the ratio of the anodic to cathodic peak currents as a function of sweep rate for the series of voltammograms shown in Fig. 5.

Figure 6. Cyclic staircase voltammograms recorded at a platinum disk electrode in the 66.7–33.3 m/o $AlCl_3$–EtMeImCl melt: (a) Al wire + 9.0 mmol L^{-1} WCl_6 at 353 K for three days; (b) 3.2 mmol L^{-1} $K_3W_2Cl_9$ melt; (- - - -) pure melt. The temperature was 353 K, and the sweep rates were 0.10 V s^{-1}.

Figure 7. Cyclic staircase voltammograms recorded at a platinum disk electrode in the 66.7–33.3 m/o $AlCl_3$–EtMeImCl melt containing 3.2 mmol L^{-1} $K_3W_2Cl_9$ melt. The temperature was 353 K and the sweep rates are given in Table VI. (inset) Peak reduction current density and ratio of the cathodic to anodic peak currents as a function of sweep rate for te series of voltammograms shown in Fig. 7.

Figure 8. Cyclic staircase voltammograms recorded at a Pt-RDE in the 66.7–33.3 m/o $AlCl_3$–EtMeImCl melt containing 3.2 mmol L^{-1} $K_3W_2Cl_9$. The temperature was 353 K,a nd the sweep rates were 0.01 V s^{-1}. The angular rotation frequencies are (from bottom up) 105, 131, 157, 183, and 209 rad s^{-1} [1000, 1250, 1500, 1750, and 2000 rpm.]. (Inset) relationship between the limiting current densities at 1.50 V and the square root of the angular rotation frequency, $\omega^{1/2}$.

Figure 9. Plots of inverse of the current, i^{-1}, *vs.* the inverse of the square root of the angular rotation frequencies, $\omega^{-1/2}$, at selected potentials in Fig. 7. The potentials are (from top down) 1.40, 1.41, 1.42, 1.43, 1.44, 1.45, 1.46, 1.47, 1.48, 1.49, and 1.50 V. (Inset) Relationship between E-$E^{0'}$ and $\ln k_f$(E).

Figure 10. Relationship between the applied current density (mA cm^{-2}) and W content (a/o) of the deposits prepared in the 66.7–33.3 m/o $AlCl_3$–EtMeImCl melt: (▲) 9.0 mmol L^{-1} WCl_6; (●) W(II) produced from 9.0 mmol L^{-1} WCl_6 and Al metal at 353.2 K; (○) 3.2 mmol L^{-1} $K_3W_2Cl_9$. The rotation rate was 2000 rpm; and the temperature was 353.2 K.

Figure 11. SEM images of the Al-W alloy samples prepared in the 66.7–33.3 m/o $AlCl_3$–EtMeImCl melt containing 3.2 mmol L^{-1} $K_3W_2Cl_9$ at different applied current densities: (a) -20 mA cm^{-2}, $Al_{97.7}W_{2.3}$; (b) -10 mA cm^{-2}, $Al_{92.7}W_{7.3}$; (c) -5 mA cm^{-2}, $Al_{86.0}W_{14.0}$. The rotation rates were 2000 rpm; and the temperatures were 353.2 K.

Figure 12. Anodic polarization curves recorded in a deaerated aqueous 0.1 M-NaCl for Al-W alloys obtained in the 66.7–33.3 m/o $AlCl_3$–EtMeImCl melt: (a) Al (99.999 %); (b) $Al_{97.7}W_{2.3}$; (c) $Al_{95.0}W_{5.0}$; and (d) $Al_{86.0}W_{14.0}$. The temperatures were 353.2 K, and the sweep rates were 0.5 mV s^{-1}. The step size was 2 mV.

Figure 13. Pitting potentials as a function of alloy composition for electrodeposited Al-W alloys (●) and Al-Mo alloys (▲).[12] (a) Al (99.999 %); (b) $Al_{97.7}W_{2.3}$; (c) $Al_{95.0}W_{5.0}$; (d) $Al_{86.0}W_{14.0}$.

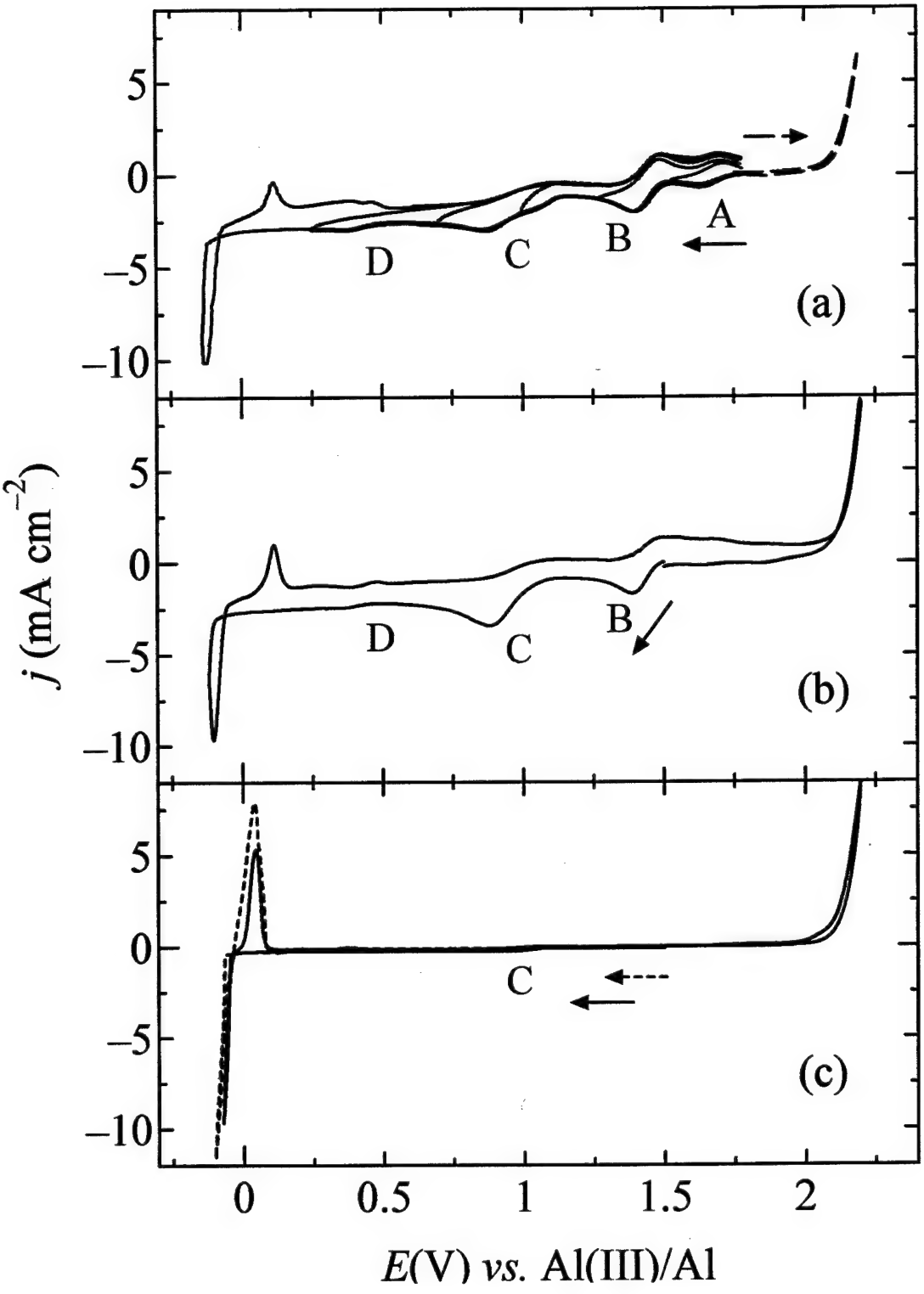
5
0
−5
−10
A
B
C
D
(a)
(b)
(c)
0
0.5
1
1.5
2
j (mA cm^{-2})
E(V) *vs.* Al(III)/Al

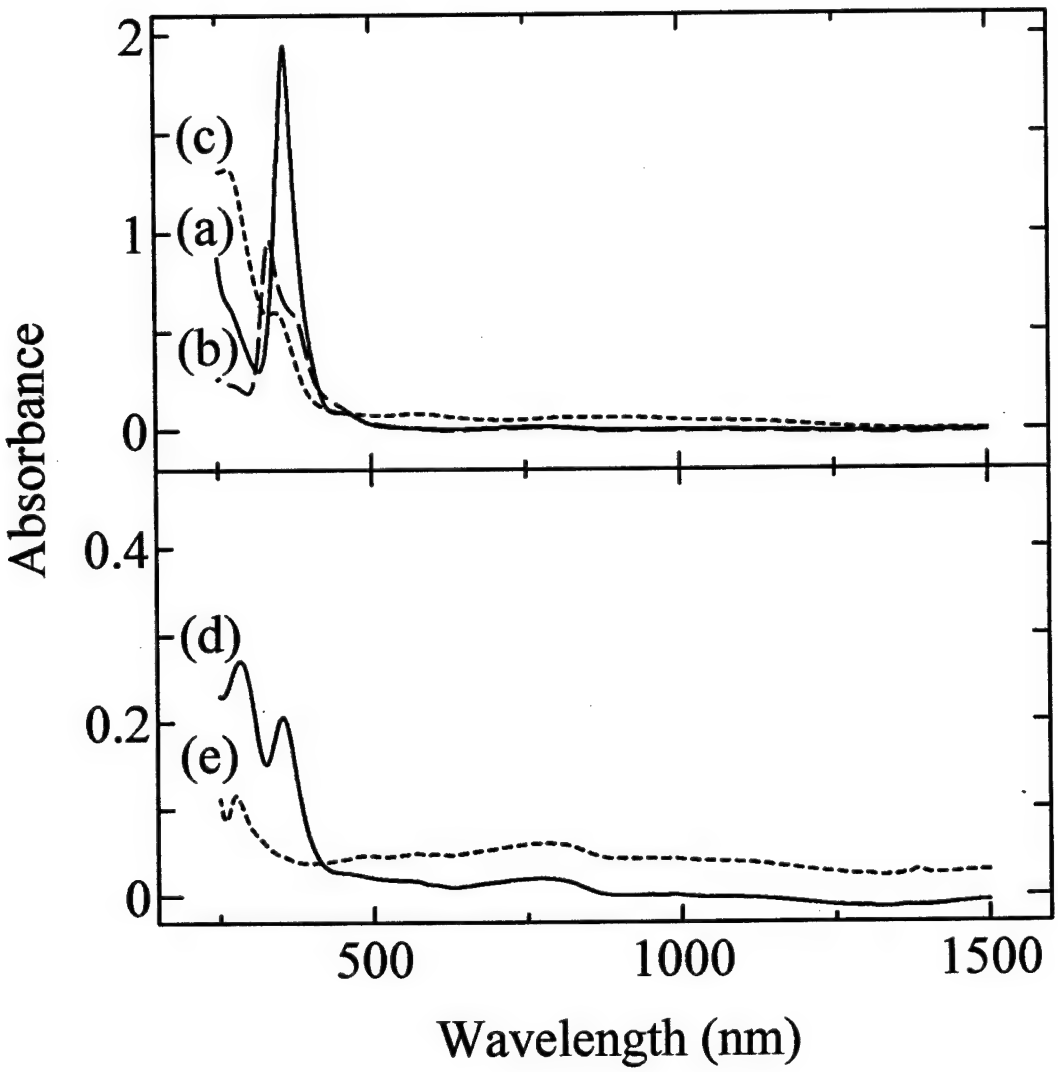
2
1
0
0.4
0.2
0
(c)
(a)
(b)
(d)
(e)
Absorbance
500
1000
1500
Wavelength (nm)

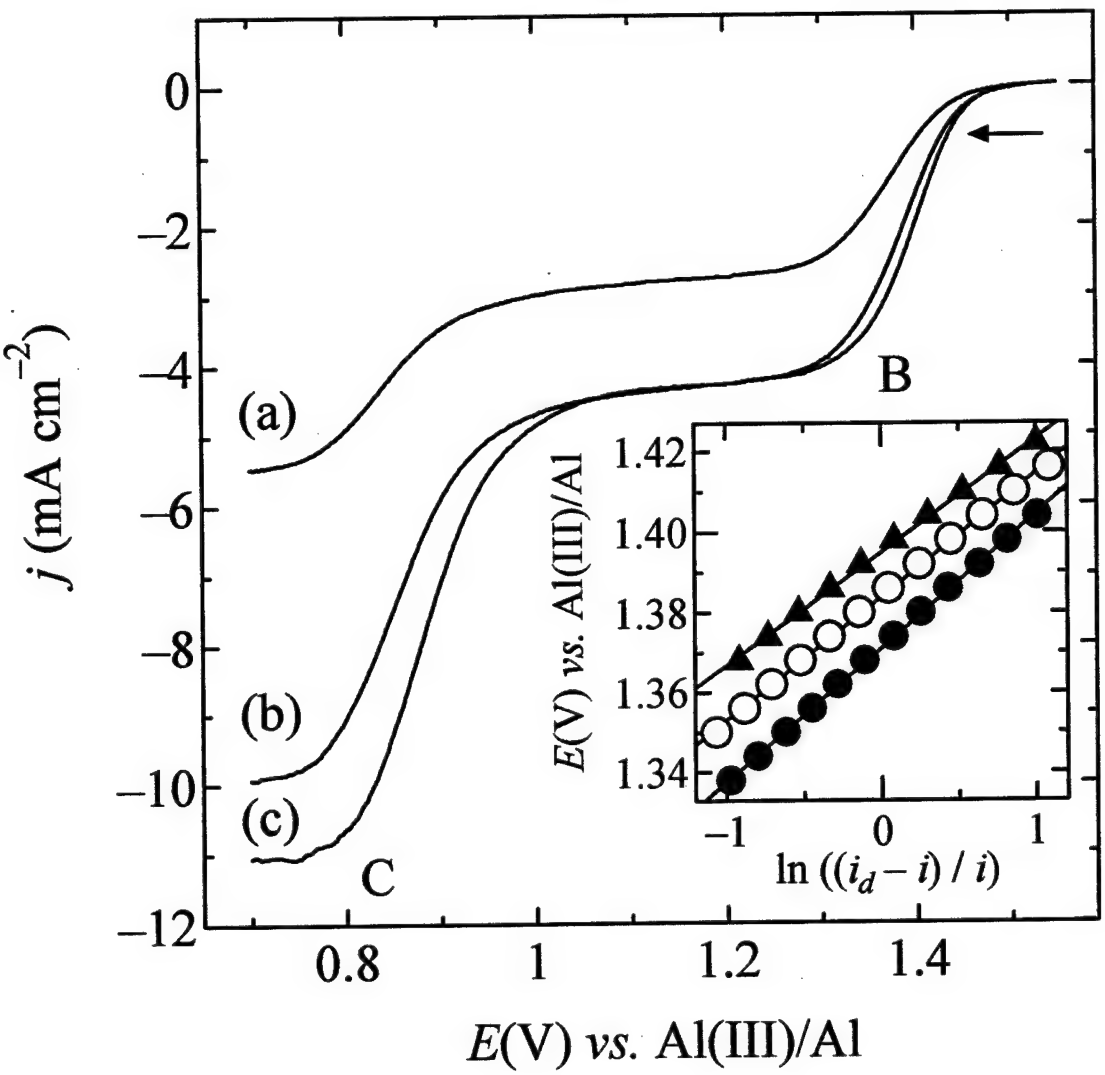
0
−2
−4
−6
−8
−10
−12
0.8
1
1.2
1.4
j (mA cm−2)
E(V) vs. Al(III)/Al
(a)
(b)
(c)
B
C
1.42
1.40
1.38
1.36
1.34
−1
0
1
E(V) vs. Al(III)/Al
ln ((id − i) / i)

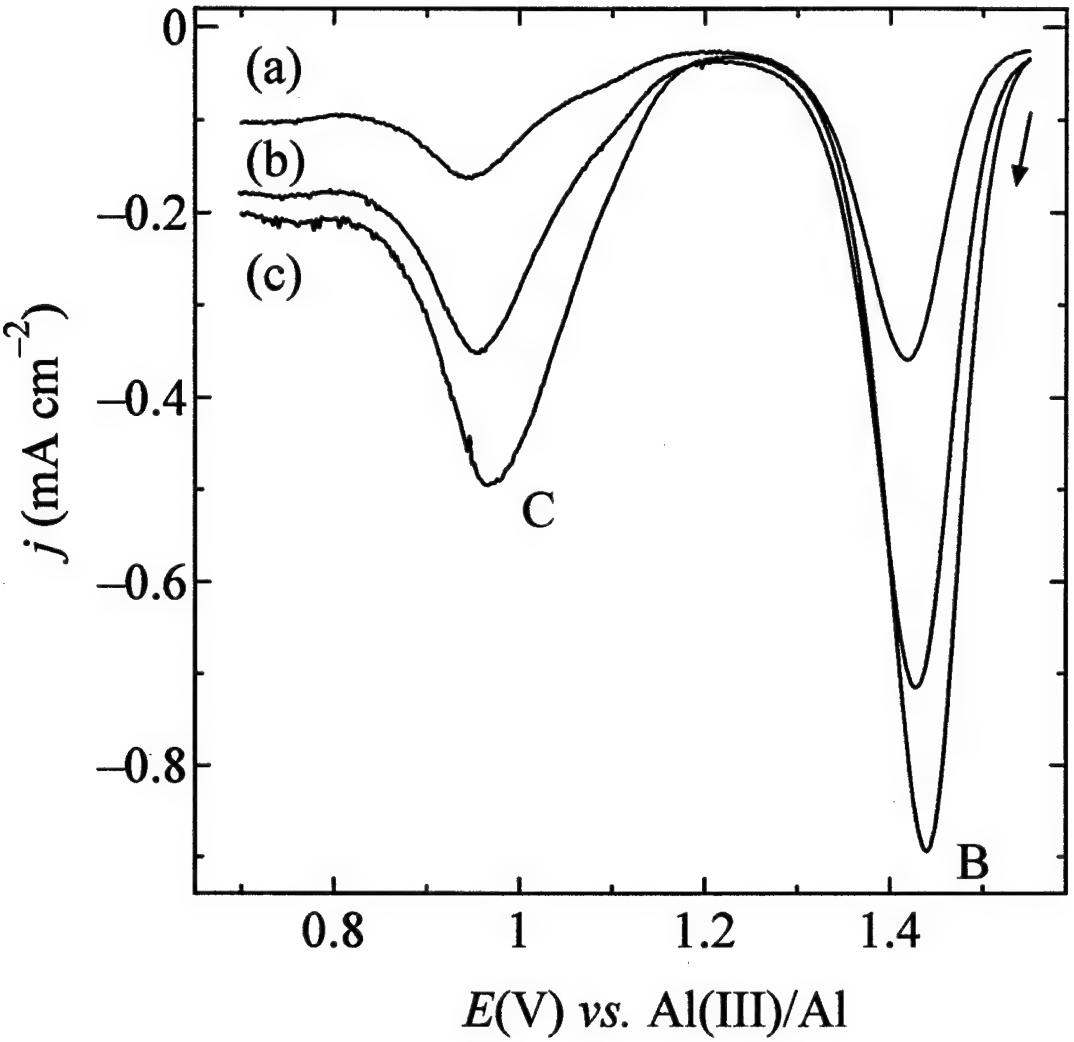
0
–0.2
–0.4
–0.6
–0.8
(a)
(b)
(c)
C
B
0.8
1
1.2
1.4
j (mA cm−2)
E(V) vs. Al(III)/Al

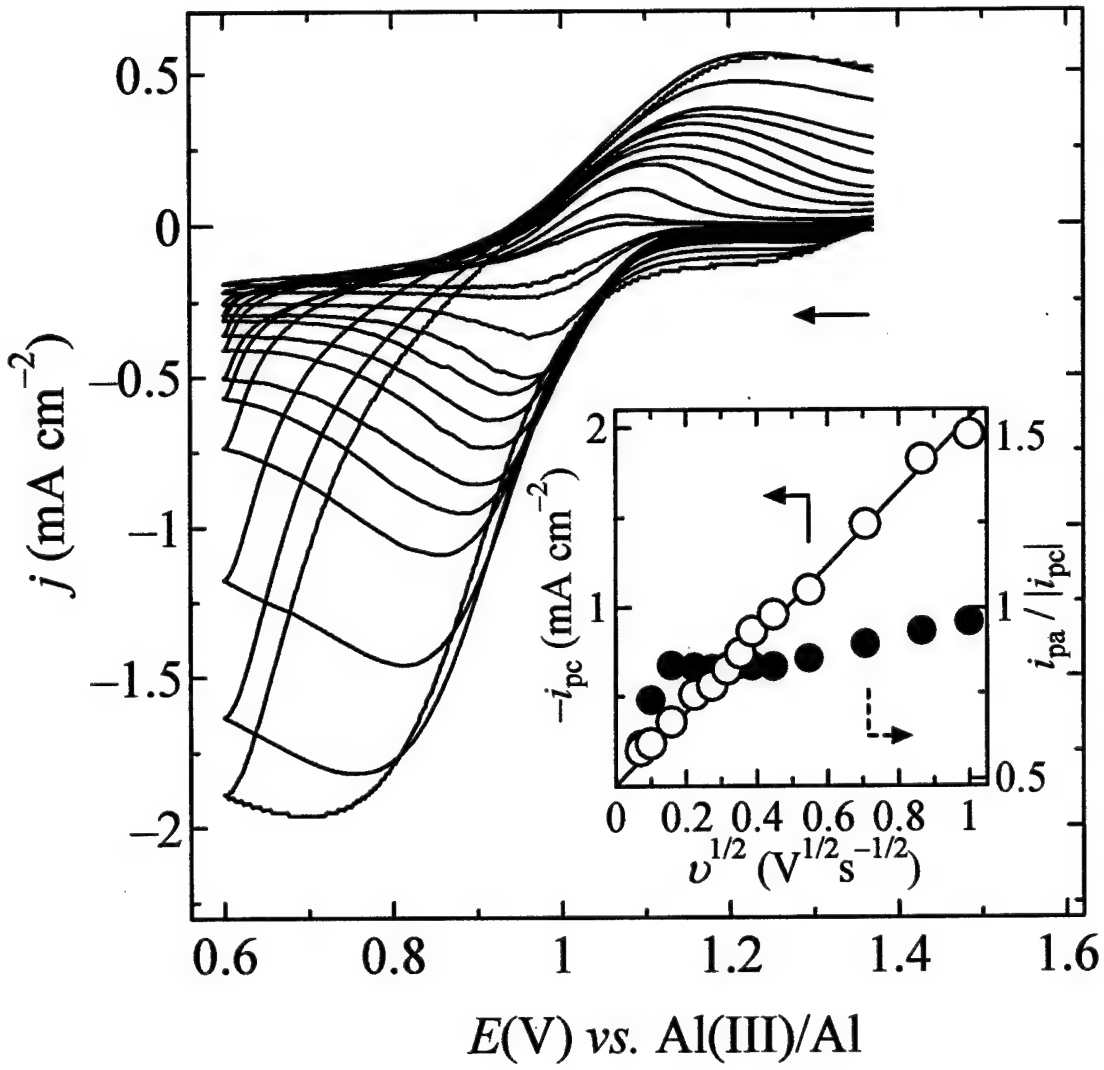
0.5
0
−0.5
−1
−1.5
−2
j (mA cm−2)
0.6
0.8
1
1.2
1.4
1.6
E(V) vs. Al(III)/Al
2
1
−ipc (mA cm−2)
1.5
1
0.5
ipa / |ipc|
0 0.2 0.4 0.6 0.8 1
υ1/2 (V1/2s−1/2)

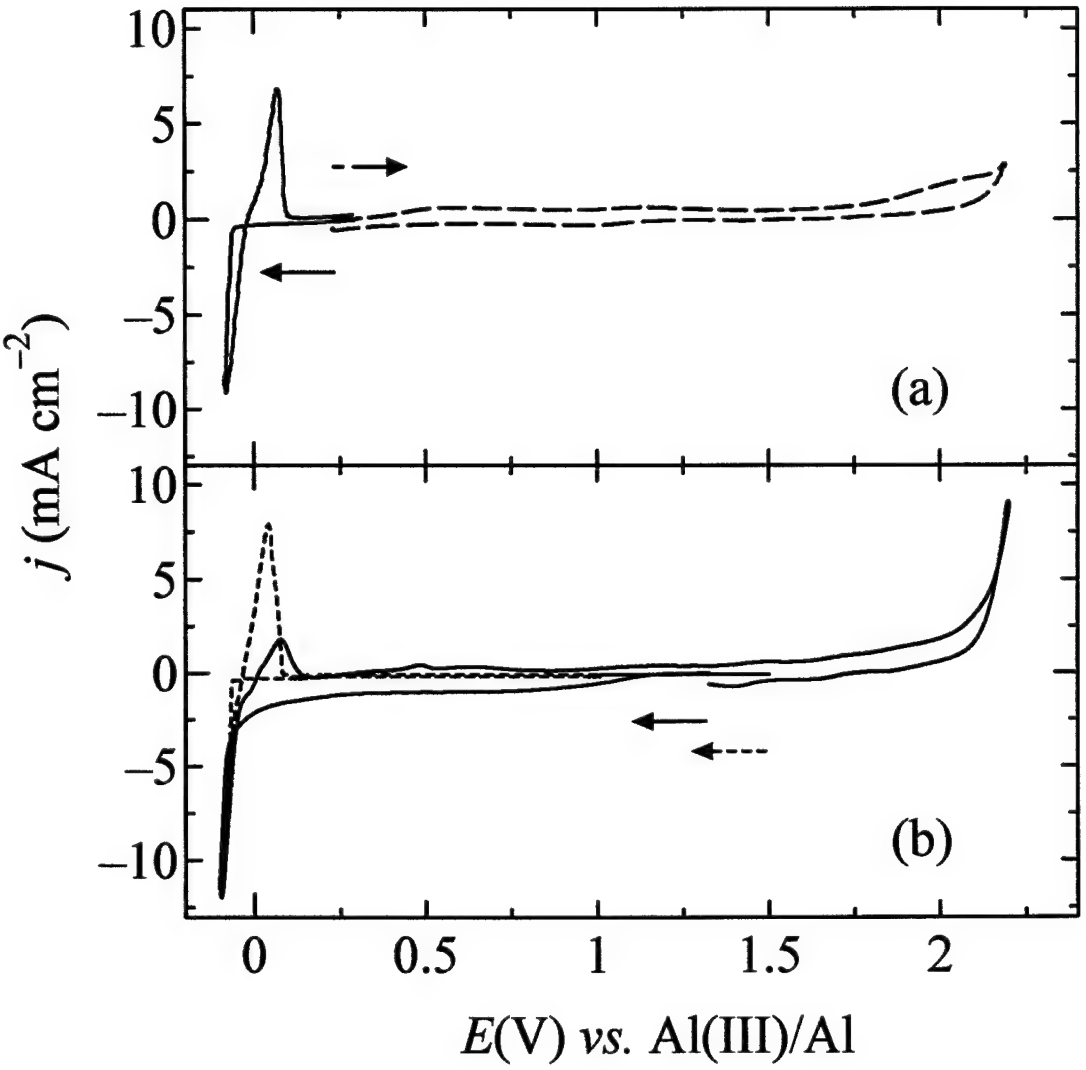
10
5
0
−5
−10
(a)
10
5
0
−5
−10
(b)
0
0.5
1
1.5
2
j (mA cm−2)
E(V) vs. Al(III)/Al

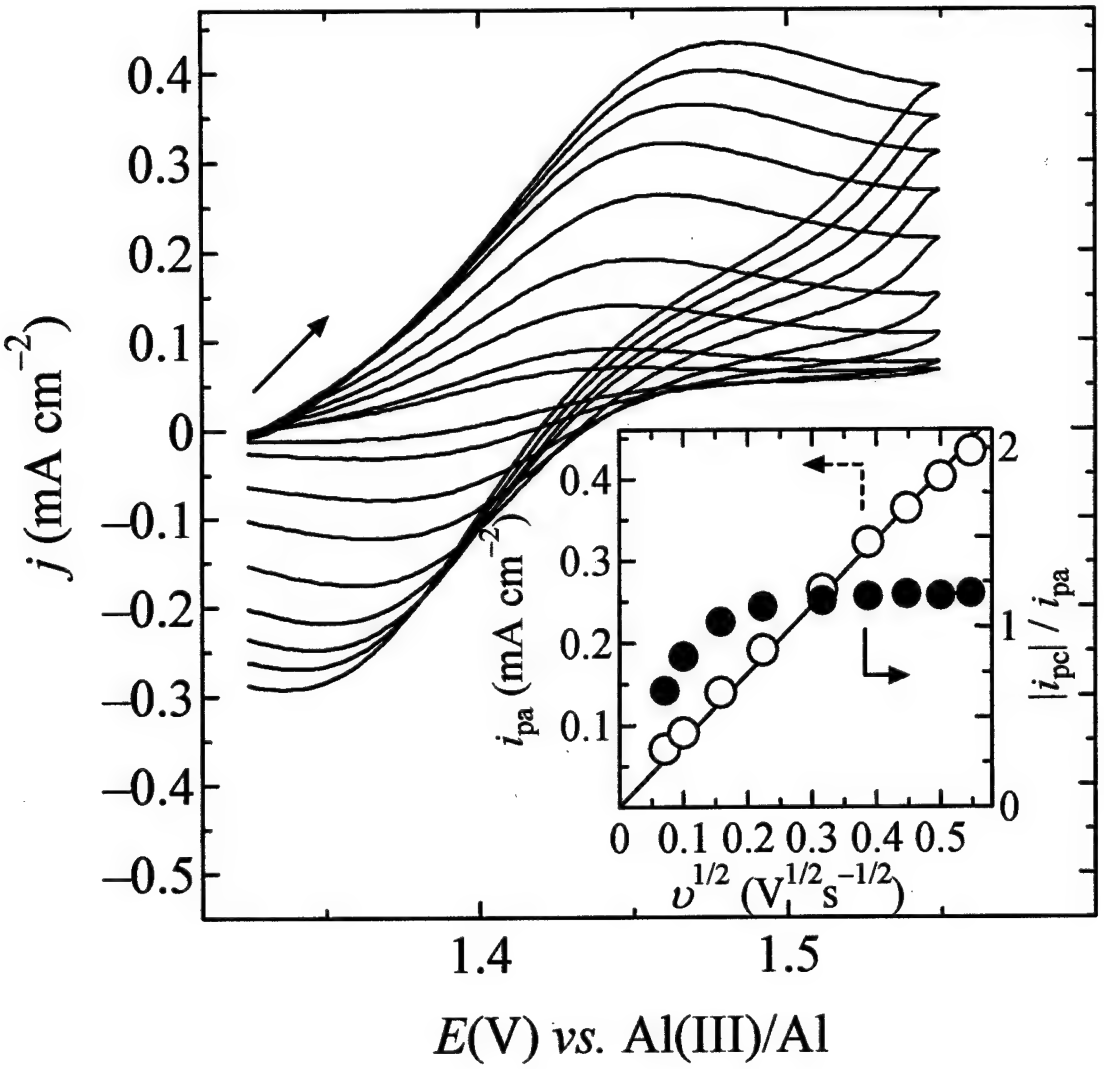
0.4
0.3
0.2
0.1
0
–0.1
–0.2
–0.3
–0.4
–0.5
j (mA cm^{-2})
1.4
1.5
E(V) vs. Al(III)/Al
0.4
0.3
0.2
0.1
i_pa (mA cm^{-2})
0 0.1 0.2 0.3 0.4 0.5
υ$^{1/2}$ (V$^{1/2}$s$^{-1/2}$)
2
1
0
|i_pc| / i_pa

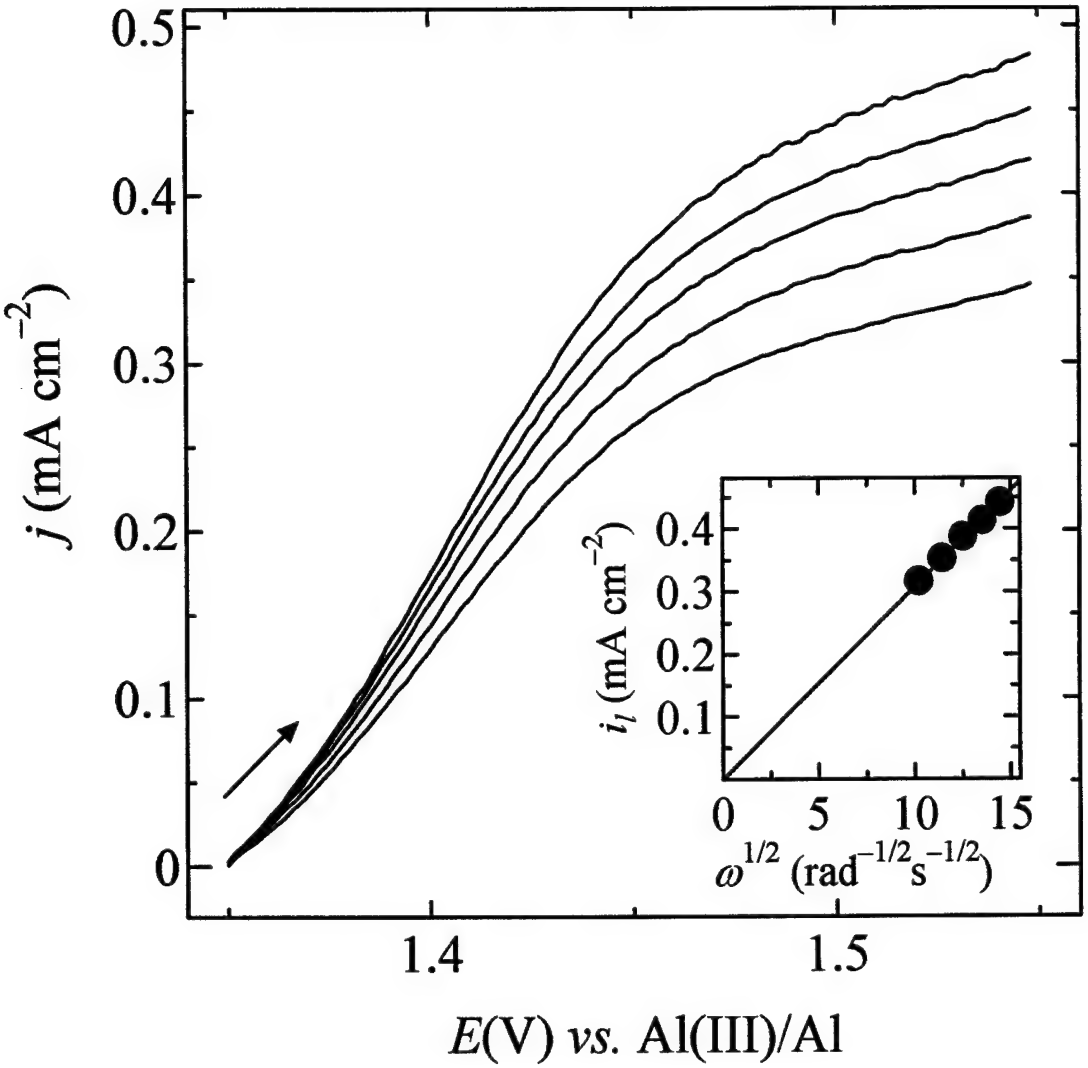
0.5
0.4
0.3
0.2
0.1
0
j (mA cm−2)
1.4
1.5
E(V) vs. Al(III)/Al
0.4
0.3
0.2
0.1
il (mA cm−2)
0
5
10
15
ω1/2 (rad−1/2s−1/2)

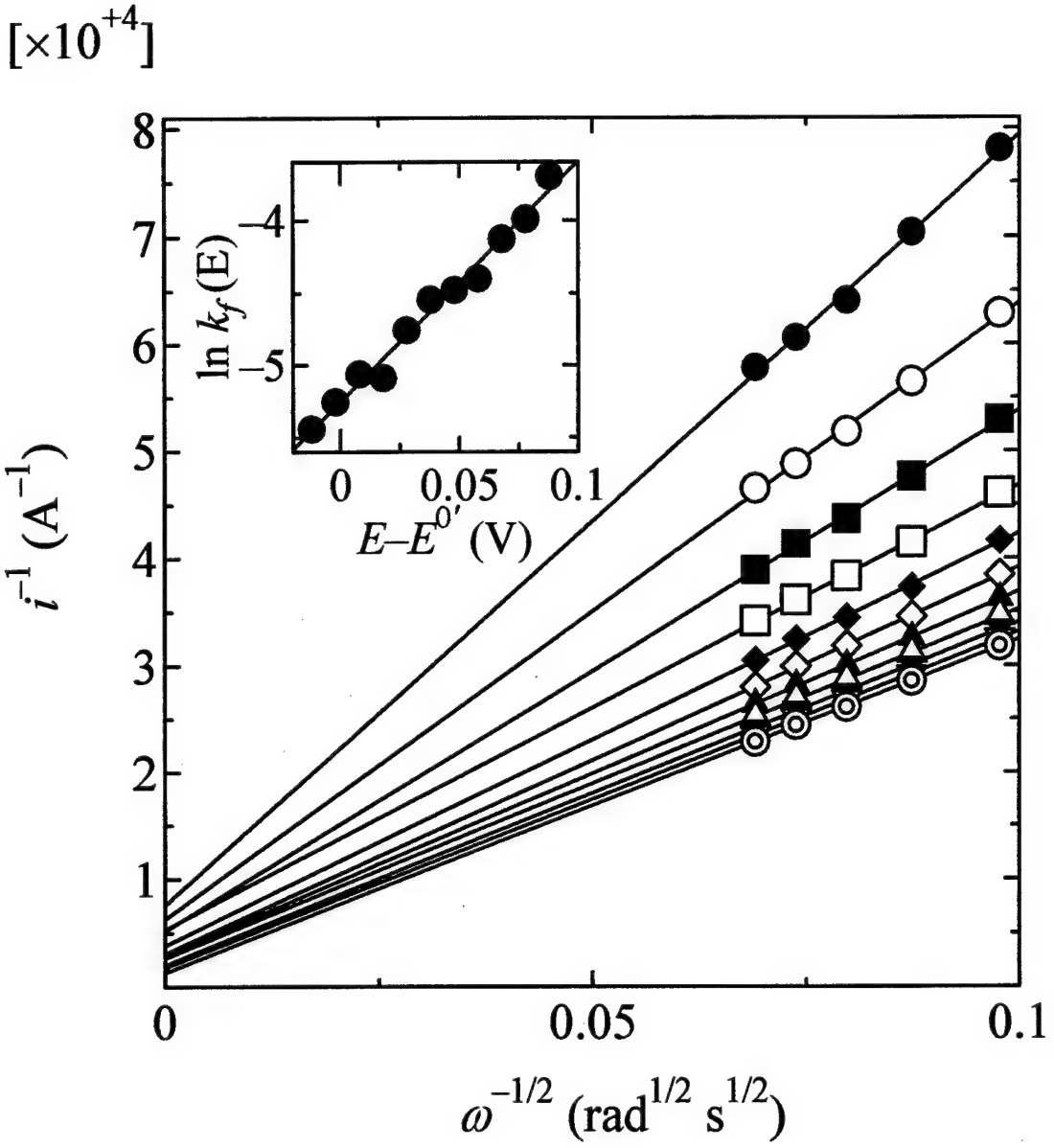
[×10+4]
8
7
6
5
4
3
2
1
0
0.05
0.1
i-1 (A-1)
ω-1/2 (rad1/2 s1/2)
ln kf(E)
−4
−5
0
0.05
0.1
E–E0′ (V)

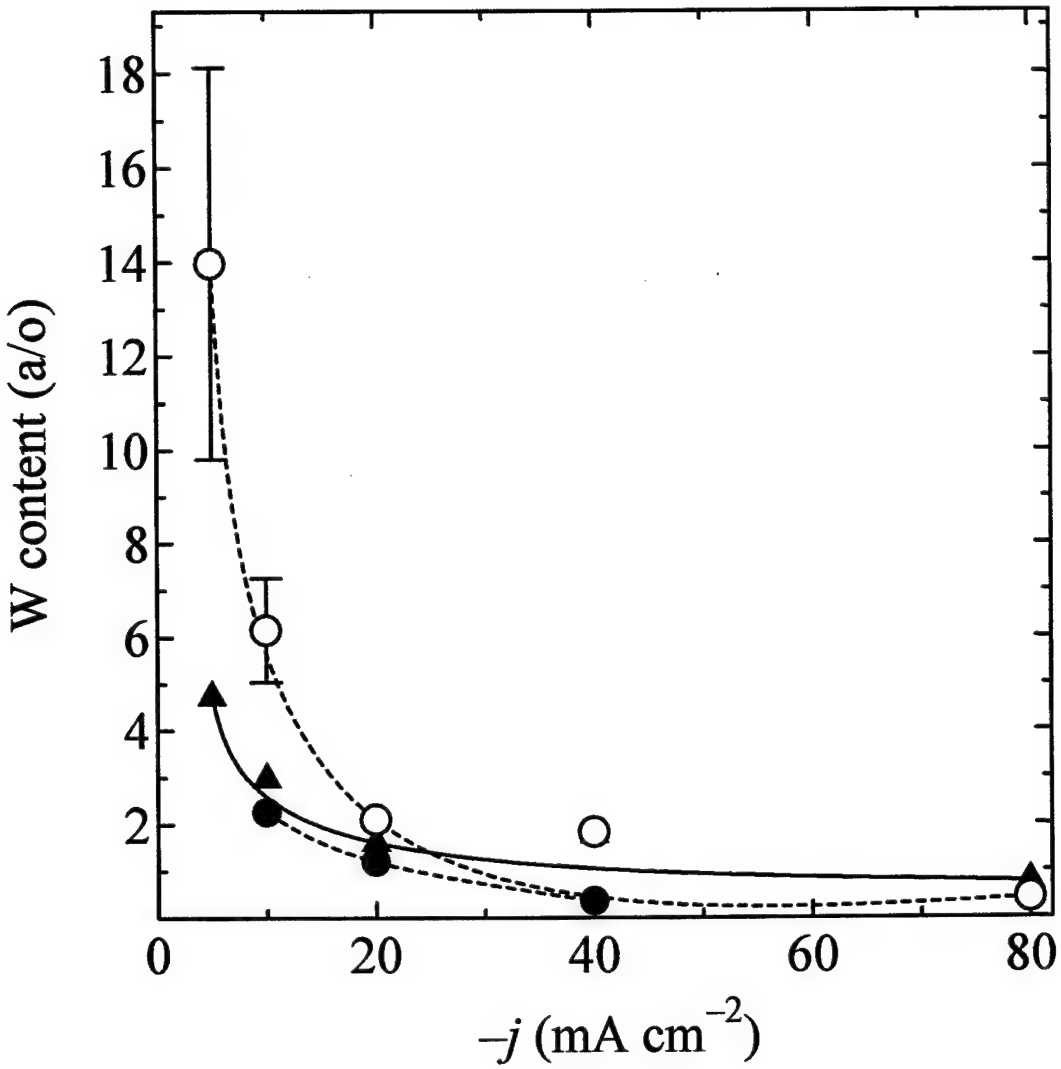
W content (a/o)
18
16
14
12
10
8
6
4
2
0
20
40
60
80
–j (mA cm–2)

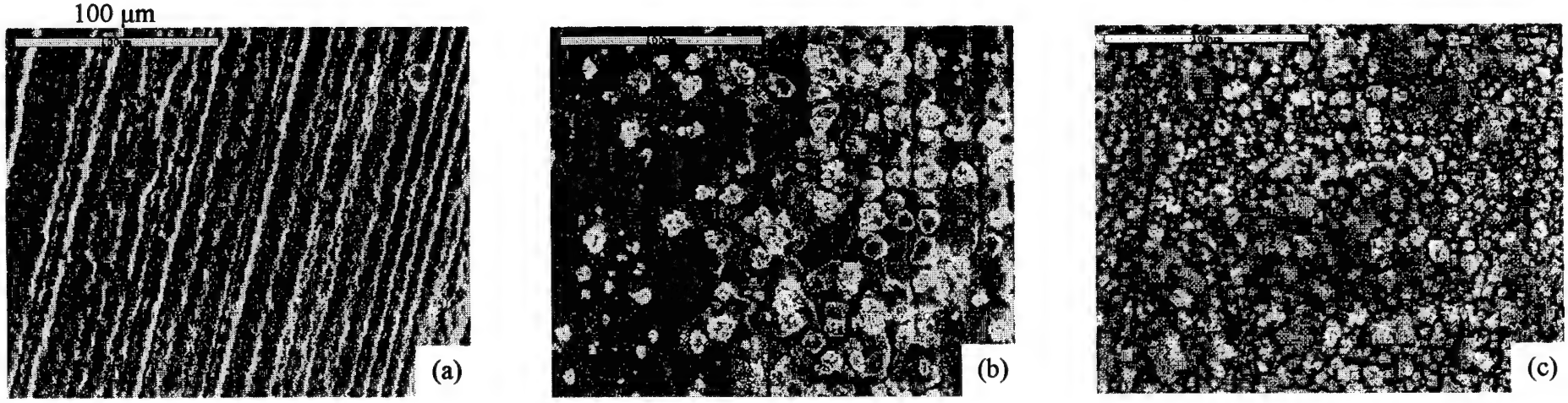
100 µm
(a)
(b)
(c)

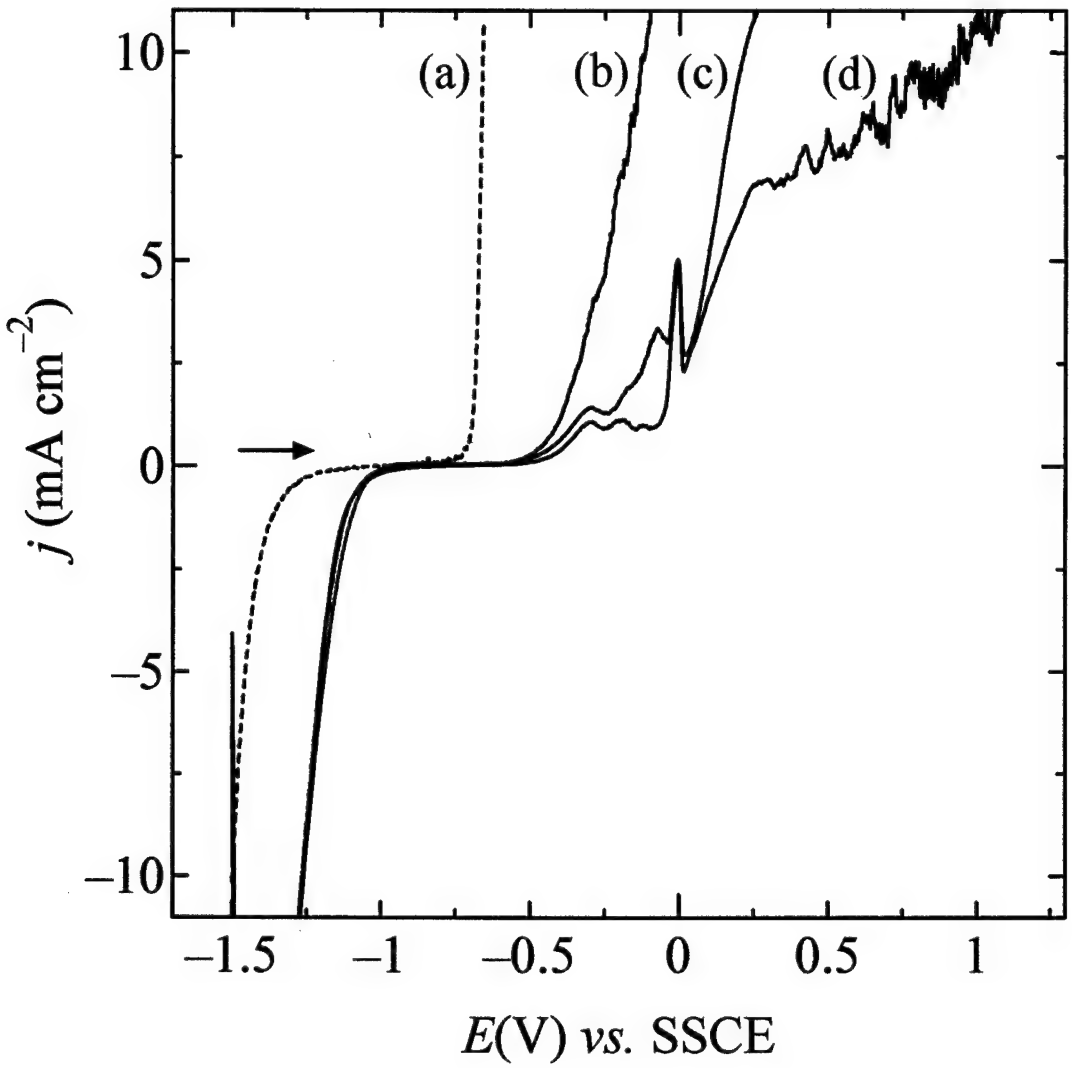
10
5
0
−5
−10
(a)
(b)
(c)
(d)
−1.5
−1
−0.5
0
0.5
1
j (mA cm−2)
E(V) vs. SSCE

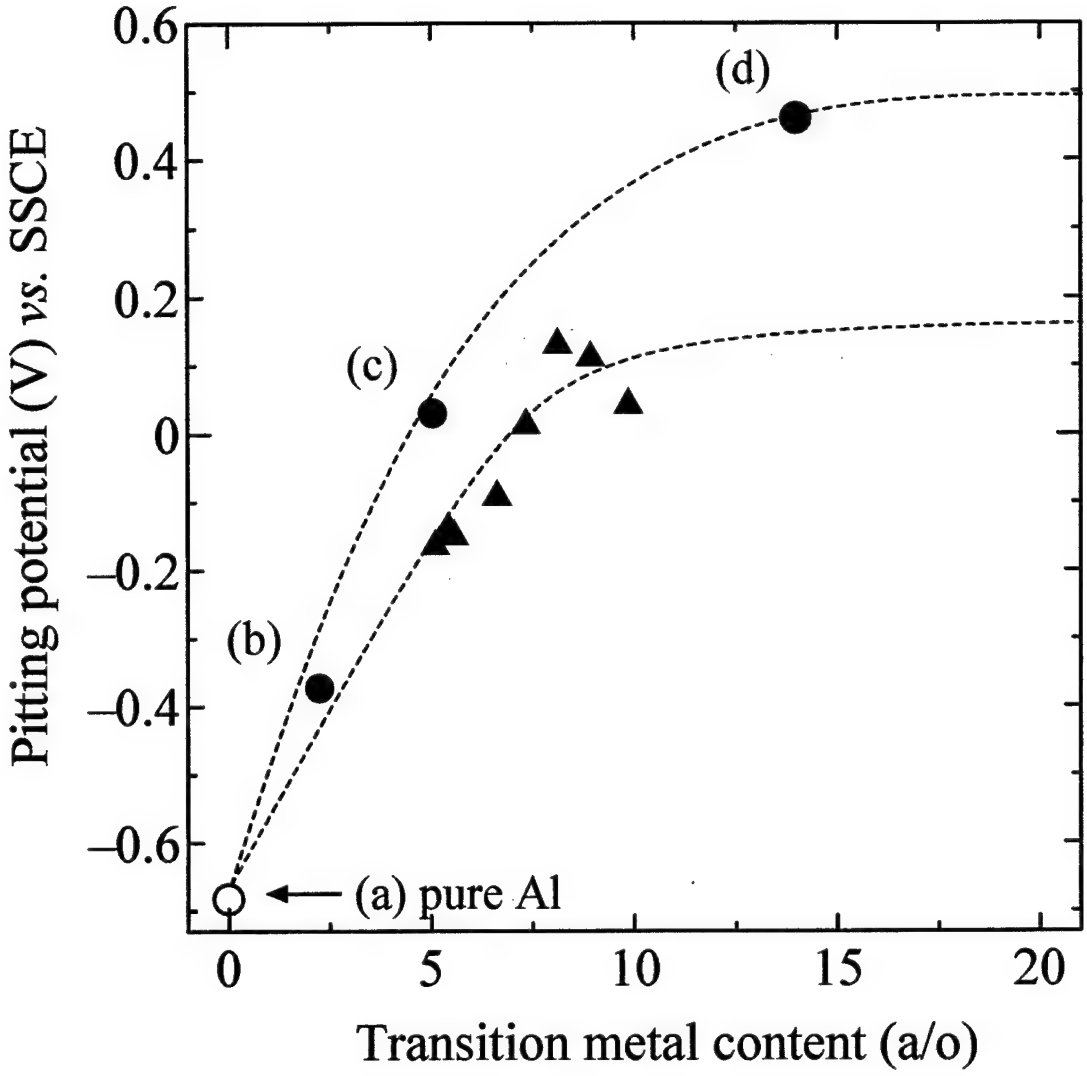
0.6
0.4
0.2
0
–0.2
–0.4
–0.6
Pitting potential (V) *vs.* SSCE
(d)
(c)
(b)
(a) pure Al
0
5
10
15
20
Transition metal content (a/o)

APPENDIX V

T. Tsuda, C. L. Hussey, and G. R. Stafford, "Electrodeposition of Aluminum-Manganese-Molybdenum Alloy from the Lewis Acidic Aluminum Chloride-1-Ethyl-3-methylimidazolium Chloride Melt," (Draft manuscript for submission to *Electrochimica Acta*)

Electrodeposition of Aluminum-Manganese-Molybdenum Alloy from the Lewis Acidic Aluminum Chloride-1-Ethyl-3-methylimidazolium Chloride Melt

Tetsuya Tsuda,[a] Charles L. Hussey,[a,*] and Gery R. Stafford[b]

[a]*Department of Chemistry and Biochemistry, The University of Mississippi, P.O. Box 1848, University, Mississippi 38677, USA*

[b]*Materials Science and Engineering Laboratory, National Institutes of Standards and Technology, Gaithersburg, Maryland 20899, USA*

ABSTRACT

The electrodeposition of aluminum-manganese-molybdenum alloy was examined in the Lewis acidic 66.7-33.3 mole percent (m/o) aluminum chloride-1-ethyl-3-methylimidazolium chloride ($AlCl_3$-EtMeImCl) molten salt containing $MnCl_2$ and $(Mo_6Cl_8)Cl_4$ under various conditions. The ratio of these two components in the melt strongly affected both the electrodeposition behavior and the surface morphology of the resulting Al-Mn-Mo alloys. The addition of Mo to the Al-Mn alloy resulted in a considerable improvement in its resistance to chloride-induced pitting corrosion. The pitting potential of the Al-Mn-Mo alloys shifted to approximately +500 and +800 mV against $Al_{95.8}Mn_{4.2}$ alloy and pure Al, respectively, and depended on the total Mo content. This increased resistance to chloride-induced pitting corrosion is comparable to that found for pure Al-Mo alloys electrodeposited from the 66.7 m/o melt. Thus, the addition of Mo into the Al-Mn alloy is an effective method to improve its chloride-induced pitting potential and may have other beneficial effects as well

Keyword: Al-Mn, Al-Mn-Mo, Pitting potential, Room temperature molten salt, Chloroaluminate melt.
* Corresponding author; E-mail: chclh@chem1.olemiss.edu

INTRODUCTION

Al-Mn is a typical example of a "stainless" Al alloy that has been prepared by electrodeposition from chloroaluminate melts [1-20]. The electroplating of this alloy from chloroaluminate melts is a promising method for surface finishing because the resulting alloy coatings exhibit good metallic brightness and a reasonably good resistance to chloride-induced pitting corrosion (< *ca.* +400 mV against pure Al). Recently, we have succeeded in preparing Al-Mo alloy coatings in the 66.7-33.3 mole percent (m/o) $AlCl_3$-EtMeImCl melt containing $(Mo_6Cl_8)Cl_4$ that show excellent corrosion resistance[21]. This alloy forms a metallic glass if the Mo content exceeds *ca.* 10 atomic percent (a/o). In this case, the chloride induced-pitting potential of the alloy shifts to approximately +800 mV versus pure Al [12, 21]. Therefore, we investigated the simultaneous co-deposition of Al, Mo, and Mn from the 66.7-33.3 m/o $AlCl_3$-EtMeImCl melt containing dissolved $MnCl_2$ and $(Mo_6Cl_8)Cl_4$ in order to ascertain whether the resulting ternary Al-Mn-Mo alloy would be more corrosion resistant than either of the related binary alloys, i.e., Al-Mn or Al-Mo.

EXPERIMENTAL*

Preparation of the plating bath.- The procedures used for the synthesis of EtMeImCl, the purification of $AlCl_3$ by sublimation, and the preparation and purification of the $AlCl_3$-EtMeImCl molten salt were identical to those described in previous articles [22-24]. Anhydrous manganese (II) chloride of 99.999 % purity (Aldrich) and anhydrous molybdenum (II) chloride, $(Mo_6Cl_8)Cl_4$, of 99.5 % purity (Cerac) were used as received. These compounds were dissolved in the $AlCl_3$–EtMeImCl molten salt in order to prepare the plating bath. All experiments were carried out in a nitrogen gas-filled glove box (VAC Atmospheres NEXUS system) with an O_2 and H_2O content < 5 ppm.

Electrochemical and spectroscopic experiments.- Electrochemical experiments were conducted using a three-electrode cell. A Pine Instruments Teflon-sheathed platinum disk electrode with a geometrical area of 0.099 cm^2 was used as the working electrode for voltammetry experiments. Coils of 0.10 cm diameter aluminum wire (Alfa Aesar, 99.999 %) were used for the counter and reference electrodes. These electrodes were immersed in melt with the same composition as the bulk melt, but were separated from the bulk melt by a porosity E glass frit (Ace Glass). The aluminum electrodes were cleaned with a mixture of concentrated H_2SO_4, HNO_3, and H_3PO_4, rinsed with distilled H_2O, and dried under vacuum before use. Alloy samples of approximately 10 μm thickness were plated from the solution described above onto working electrodes consisting of a length of 1.25 mm diameter copper wire, which was rotated at a fixed rate with a Pine Instruments AFMSRX electrode rotator. At the conclusion of each, the alloy-plated substrate was removed from the glove box and cleaned with distilled water.

* Certain trade names are mentioned for experimental information only, in no case does it imply a

Electrochemical experiments were conducted by using an EG&G Model 263A potentiostat/galvanostat. This potentiostat was controlled with an EG&G PARC Model 270 software. Electrodeposition of the Al-Mn-Mo alloy was performed with an EG&G PARC Model 173 potentiostat/galvanostat equipped with a Model 179 digital coulometer plug in module. Potentiodynamic pitting measurements were carried out on these alloy samples at room temperature in a 0.1 mol L^{-1} solution of NaCl in distilled H_2O. This solution was deaerated with nitrogen gas for more than 6 hours before each experiment. The reference electrode for these measurements was a sodium-saturated calomel electrode (SSCE), and the counter electrode was a large surface area platinum wire coil. A know length of the plated Cu wire was exposed to the NaCl solution by using a heat-shrink tubing mask, and the sample was scanned at 0.5 mV s^{-1} by using linear staircase voltammetry. UV-visible spectroscopic measurements were obtained by using a Varian CARY 5 spectrometer. Samples were contained in Wilmad No. 107-7 closed-type quartz cells with a 0.10 cm optical path length.

Characterization of the Al-Mn-Mo electrodeposits.- The crystal structure of the Al-Mn-Mo electrodeposits was examined with standard X-ray diffraction (XRD) techniques by using a Siemens D-500 X-ray diffractometer at NIST. This instrument was operated in the θ-2θ scan mode and employed Cu-Kα radiation. The lattice parameters of the fcc Al phase in the alloy deposits were accurately determined by employing the copper substrate reflections as an internal standard. A minimum of five well-resolved reflections were required for lattice parameter refinement. Surface morphology and elemental analysis of the alloy samples were performed with a JEOL JSM-6100 (The University of Mississippi) or JEOL JXA-840 (NIST) scanning electron microscopes (SEM). Alloy

---

recommendation or endorsement by NIST.

composition was measured with energy dispersive X-ray spectroscopy (EDS) on the as-deposited surfaces with pure Al, Mn, and Mo as standards.

RESULTS AND DISCUSSION

Absorption spectroscopy.- Manganese (II) chloride, $MnCl_2$, and Molybdenum (II) chloride, $(Mo_6Cl_8)Cl_4$, dissolved readily in the 66.7 m/o melt to produce a transparent and a yellow solution, respectively. Because the coordination/solvation of dissolved $(Mo_6Cl_8)Cl_4$ is unknown, we will refer to the dissolved Mo(II) entity by its core structure, $\{Mo_6Cl_8\}^{4+}$ or as Mo(II). Electronic absorption spectra of these solutions are shown in Fig. 1. A spectrum for $(Mo_6Cl_8)Cl_4$ is identical to that reported in a previous article [21]. No absorption spectrum was observed in the solution of Mn(II), indicating that any absorption bands for this species must occur below the UV cut-off of the melt at about 250 nm.

Effect of $MnCl_2$ and $(Mo_6Cl_8)Cl_4$ on the electrodeposition of aluminum.- Figure 2(a) shows cyclic staircase voltammograms recorded at a Pt stationary disk electrode in the 66.7 m/o melt after addition of Mn(II) as $MnCl_2$ or Mo(II) as $(Mo_6Cl_8)Cl_4$. To record these voltammograms, the potential scan was initiated from a rest potential to a potential sufficiently cathodic to initiate the electrodeposition of Al. The scan was then reversed until it reached the positive limit of the melt at +2.2 V and was finally returned to the initial potential. The negative and positive potential limits of the Lewis acidic $AlCl_3$-EtMeImCl molten salt arises from the reduction of the unsaturated $Al_2Cl_7^-$ ion to Al metal and to the oxidation of $AlCl_4^-$ ion to chlorine gas, respectively:

$$4Al_2Cl_7^- + 3e^- \rightleftharpoons Al + 7AlCl_4^- \quad (1)$$

$$2AlCl_4^- \rightleftharpoons Al_2Cl_7^- + 1/2\ Cl_2^- + e^- \quad (2)$$

The general appearance of these voltammograms was the same as reported previously [18, 19, 21] in that the stripping waves attributed to Al in pure melt are shifted to more positive potentials because they now correspond to the oxidation of Al-Mn or Al-Mo alloys. In melt containing both Mn(II) and Mo(II), the voltammetric behavior varied significantly with the Mn(II)/Mo(II) concentration ratio, $C_{Mn(II)}/C_{Mo(II)}$. When $C_{Mn(II)}/C_{Mo(II)}$ is < 1, the voltammogram exhibits only a single stripping wave and is similar to that seen in the voltammogram recorded in a melt solution containing only Mo(II) (Fig. 2b); however, the current for this stripping wave decreases as the Mn(II) concentration is increased. When $C_{Mn(II)}/C_{Mo(II)}$ is adjusted to four, the current density for the stripping wave characteristic of Al-Mo is greatly diminished and several other poorly defined oxidation waves become apparent (Fig. 2(c)). As described below, these voltammetric results are due to the effects of $C_{Mn(II)}/C_{Mo(II)}$ and current density on the Al-Mn-Mo alloy composition.

Electrodeposition of Al-Mn-Mo alloys.- Controlled-current techniques were used to prepare alloy samples for detailed compositional and morphological analysis. Bulk deposition experiments were conducted at a rotating copper wire substrate as noted in previous articles [21, 25]. Figure 3 shows the Mn and Mo content of electrodeposited Al-Mn-Mo alloys as a function of the applied current density and the concentration of Mn(II) and Mo(II). The plot that simply decreases with increase of the applied current densities remains basically unchanged when the ratio of Mn(II) and Mo(II) in the melt, $C_{Mn(II)}/C_{Mo(II)}$, is less than one. This is similar to the result given in the 66.7 m/o melt containing only $(Mo_6Cl_8)Cl_4$ [21]. This behavior is typically observed when the transition metal electrodeposition reaction begins at or about the same potential as the reaction in Eq. (1) [21, 25-29]. However, if the $C_{Mn(II)}/C_{Mo(II)}$ exceeds one, the behavior is quite different, especially at high applied current densities. In order to better understand this behavior, we plotted the

Mn and Mo content of the samples individually in Fig. 4. In all cases, the Mo content decreases with the applied current density, as was observed during Al-Mo alloy deposition [21]. In addition, at a fixed current density, the Mo content of the alloy decreases with an increase in the Mn(II) concentration in the plating bath. The latter is expected because the fraction of the total current density corresponding to the reduction of Mo(II) decreases as the fraction of the total current due Mn(II) reduction increases. On the other hand, the Mn content increases with the applied current density, and this tendency is enhanced if $C_{Mn(II)}/C_{Mo(II)}$ exceeds one. That is, the electrodeposition behavior is similar to that of the Al-Mo system until $C_{Mn(II)}/C_{Mo(II)}$ exceeds one. In this case, the electrodeposition of Mn predominates. This result is in accord with the variations of the voltammograms shown in Fig. 2.

Characterization of the Al-Mn-Mo alloy deposits.- Figure 5 shows SEM images of some typical bulk Al-Mn and Al-Mn-Mo alloy samples that were prepared under a variety of deposition conditions. The deposition charge used to prepare these samples was sufficient in theory to produce an atomically smooth layer of pure Al that was 10 μm in thickness. All of the alloy deposits prepared during this investigation were chloride-free. The alloy samples depicted in Figs. 5a and 5b are pure Al-Mn alloys. At the Mn content of these samples, the deposit is known to exhibit a crystal structure consistent with fcc solid solutions [1, 9, 10, 14, 16, 17, 19]. As a result, the surface morphology changed with the applied current density like pure Al electrodeposits [30]. Theoretically, this result is expected [31].

Figures 5c and 5d show the surface morphology of the electrodeposited ternary Al-Mn-Mo alloy produced when $C_{Mn(II)}/C_{Mo(II)} < 1$. The surface morphologies of the alloys are almost the same even if the Mn and Mo content of the samples is varied

considerably, and the morphologies depend only on the applied current density. The sample deposited at the lowest current density (-10 mA cm^{-2}) exhibits a surface features consisting mainly of spherical or cone-shaped nodules that are 5-15 μm in diameter. However, the deposit obtained at high current density (-40 mA cm^{-2}) is very smooth, being covered only with very small crystals. Figure 6 shows that when $C_{Mn(II)}/C_{Mo(II)}$ exceeds one, the deposit surface is covered with spherical nodules that are 5-10 μm in diameter and coalesce as the applied current density is increased. This results in an Al-Mn-Mo electrodeposit with a nearly specular surface.

Pitting potential measurements.- The pitting potentials of the electrodeposited Al-Mn-Mo alloys described above were determined by carrying out potentiodynamic anodic polarization experiments in a deaerated aqueous NaCl. Some examples of the resulting potentiodynamic current-potential curves resulting from these experiments are shown in Fig. 7. As noted for some other electrodeposited stainless aluminum alloys, e.g., Al-Mn [12, 20] and Al-Mo [21], the Al-Mn-Mo alloys are spontaneously passive at the rest potential of the solution. During anodic polarization, they display a stable passive region characterized by a very small potential-independent current followed by a sudden rise in current at the pitting potential. The variation of the pitting potential with alloy composition is shown in Fig. 8 along with data recorded for the Al-Mo alloy [21]. The top axis represents the concentration of Mn + Mo. The alloy obtained by adding 4.2 a/o Mn to pure Al exhibits a pitting potential about +300 mV more positive than that for Al alone. This data coincides with the pitting potential data reported by Moffat et al [20]. If ~ 4 a/o Mo is added to this $Al_{95.8}Mn_{4.2}$ alloy, the pitting potential of the resulting ternary alloy shifts to +500 mV versus the $Al_{95.8}Mn_{4.2}$ alloy. The increase in the pitting potential afforded by the addition of Mo to the Al-Mn alloy is comparable to that found for Al-Mo alloys electrodeposited from this same melt [21],

except that less Mo is required to attain the same pitting potential as found for the binary Al-Mo alloy. Thus, the addition of small amounts of Mo to Al-Mn alloys is an effective method for improving the chloride-induced pitting potential of these materials.

Acknowledgment

The research was supported by the Air Force Office of Scientific Research, Grant No, F49620-00-1-0123.

References

[1] G.R. Stafford and C.L. Hussey, "Electrodeposition of Transition Metal-Aluminum Alloys from Chloroaluminate Molten Salts," in Advances in Electrochemical Science and Engineering, R.C. Alkire and D.M. Kolb, Editors, Vol. 6, P.275, Wiley-VCH Verlag GmbH, Weinheim, (2002).

[2] L.W. Austin, M.G. Vucich, and E.J. Smith, Electrochem. Technol. 1 (1963) 269.

[3] H.J. Read and D.A. Shores, Electrochem. Technol. 4 (1966) 526.

[4] T. Hayashi, Proc. Int. Symp. Molten Salt Chem. (1983) 53.

[5] G.R. Stafford, J. Electrochem. Soc. 136 (1989) 635.

[6] B. Grushko and G.R. Stafford, Scripta Metall. 23 (1989) 557.

[7] B. Grushko and G.R. Stafford, Scripta Metall. 23 (1989) 1043.

[8] B. Grushko and G.R. Stafford, Metall. Trans., A, 20A (1989) 1351.

[9] B. Grushko and G.R. Stafford, Metall. Trans., A, 21A (1990) 2869.

[10] J. Uchida, A. Shibuya, T. Tsuda, Y. Yamamoto, and H. Seto, The Sumitomo Search 44 (1990) 126.

[11] A. Shibuya, J. Uchida, Y. Yamamoto, H. Seto, and T. Tsuda, Materials Science Forum 73-75 (1991) 577.

[12] T.P. Moffat, G.R. Stafford, and D.E. Hall, J. Electrochem. Soc. 140 (1993) 2779.

[13] G.R. Stafford, B. Grushko, and R.D. McMichael, J. Alloys and Compounds 200 (1993) 107.

[14] J. Uchida, T. Tsuda, Y. Yamamoto, H. Seto, M. Abe, and A. Shiuya, ISIJ International 33 (1993) 1029.

[15] B. Grushko and G.R. Stafford, Scripta Metall. 31 (1994) 1711.

[16] T. Takayama, H. Seto, J. Uchida, and S. Hinotani, J. Appl. Electrochem. 24 (1994) 131.

[17] J. Uchida, T. Hirayama, M. Abe, H. Seto, Y. Yamamoto, T. Tsuda, and A. Shibuya, Current Japanese Materials Research 16 (1996), 145.

[18] H.C. De Long, J.A. Mitchell, and P.C. Trulove, High Temp. Material Processes 2 (1998) 507.

[19] P.C. Trulove, J.A. Mitchell, P.L. Hagans, R.T. Carlin, G.R. Stafford, and H.C. De Long, in Twelfth International Symposium on Molten Salts, P.C. Trulove, H.C. De Long, G.R. Stafford, and S. Deki, Eds., PV 99-41, p. 517, The Electrochemical Society, (2000).

[20] Q. Zhuxian, S. Shuping, W. Ying, C. Songzhu, and S. Yang, Aluminum 76 (2000) 1028.

[21] T. Tsuda, C.L. Hussey, and G.R. Stafford, J. Electrochem. Soc. in printing.

[22] B.J. Tierney, W.R. Pitner, J.A. Mitchell, C.L. Hussey, and G.R. Stafford, J. Electrochem. Soc. 145 (1998) 3110.

[23] X.-H. Xu and C.L. Hussey, J. Electrochem. Soc. 140 (1993) 1226.

[24] T. Tsuda and C.L. Hussey, J. Min. and Metall., B, 39 (2003) 3.

[25] T. Tsuda, C.L. Hussey, G.R. Stafford, and J.E. Bonevich, J. Electrochem. Soc. 150 (2003) C234.

[26] T. Tsuda, C.L. Hussey, G.R. Stafford, and O. Kongstein, J. Electrochem. Soc. in printing.

[27] T. Tsuda, C.L. Hussey, and G.R. Stafford, Electrochim. Acta to be submitted.

[28] T. Tsuda, W.E. Cleland, Jr., C.L. Hussey, and G.R. Stafford, J. Electrochem. Soc. to be submitted.

[29] M. Matsunaga, M. Morimitsu, M. Nagano, and T. Tsuda, Molten Salt Forum 5-6 (1998) 601.

[30] Y. Kato, M. Tatano, and S. Takahashi, Nisshin Seikou Gihou 61 (1989) 44 (in Japanese).

[31] D. Pletcher, Industrial Electrochemistry, Chapman and Hall, London (1984).

Figure Captions

Figure 1. UV-visible spectra recorded in the 66.7-33.3 m/o $AlCl_3$-EtMeImCl melt containing: (a) 36.2 mmol L^{-1} Mo(II), (b) 36.2 mmol L^{-1} Mn(II), and (c) 36.2 mmol L^{-1} Mo(II) and 72.5 mmol L^{-1} Mn(II). The spectra were recorded at room temperature in 0.10 cm path length cells.

Figure 2. Cyclic voltammograms recorded at a stationary Pt disk electrode in the 66.7-33.3 m/o $AlCl_3$-EtMeImCl melt: (a) (- - -) pure melt; (——) 35.5 mmol L^{-1} Mn(II); (– – –) 35.5 mmol L^{-1} Mn(II); (b) (——) 35.5 mmol L^{-1} Mo(II) + 17.8 mmol L^{-1} Mn(II), (- - -) 35.5 mmol L^{-1} Mo(II) + 35.5 mmol L^{-1} Mn(II); (c) (——) 35.5 mmol L^{-1} Mo(II) + 71.0 mmol L^{-1} Mn(II), (- - -) 35.5 mmol L^{-1} Mo(II) + 142.5 mmol L^{-1} Mn(II). The temperature was 328 K, and the scan rate was 10 mV s^{-1}

Figure 3. Relationship between the applied current density and the total Mo + Mn content of Al-Mn-Mo electrodeposits prepared in the following solutions: (●)17.8 mmol L^{-1} Mn(II) + 35.5 mmol L^{-1} Mo(II); (○)35.5 mmol L^{-1} Mn(II) + 35.5 mmol L^{-1} Mo(II); (▲)71.0 mmol L^{-1} Mn(II) + 35.5 mmol L^{-1} Mo(II); (△)142.5 mmol L^{-1} Mn(II) + 35.5 mmol L^{-1} Mo(II).

Figure 4. Relationship between the applied current density and the Mo and Mn content of the deposits in Fig. 3. (a) 35.5 mmol L^{-1} Mn(II) + 35.5 mmol L^{-1} Mo(II): (●) Mn, (○) Mo; (b) 35.5 mmol L^{-1} Mo(II) + 17.8 mmol L^{-1} Mn(II): (◆) Mn, (◇) Mo; (c) 35.5 mmol L^{-1} Mo(II) + 35.5 mmol L^{-1} Mn(II): (▲) Mn, (△) Mo; (d) 35.5 mmol L^{-1} Mo(II) + 71.0 mmol

L^{-1} Mn(II), (▼) Mn, (▽) Mo; (e) 35.5 mmol L^{-1} Mo(II) + 142.5 mmol L^{-1} Mn(II): (■) Mn, (□) Mo.

Figure. 5. SEM images of electrodeposited A-Mn and Al-Mn-Mo alloys: (a) $Al_{97.4}Mn_{2.6}$, -10 mA cm^{-2}; (b) $Al_{94.3}Mn_{5.7}$, -40 mA cm^{-2}; (c) $Al_{89.7}Mn_{2.3}Mo_{8.0}$, -10 mA cm^{-2}; and (d) $Al_{92.4}Mn_{5.4}Mo_{2.2}$, -40 mA cm^{-2}.

Figure. 6. SEM images of electrodeposited Al-Mn-Mo alloys: (a) $Al_{88.8}Mn_{6.3}Mo_{4.9}$, -10 mA cm^{-2}; and (b) $Al_{85.2}Mn_{13.2}Mo_{1.6}$, -40 mA cm^{-2}.

Figure 7. Anodic polarization curves recorded in a deaerated 0.1 mol L^{-1} aqueous NaCl solution: (a) Al (99.999 %), (b) $Al_{95.8}Mn_{4.2}$, (c) $Al_{90.8}Mn_{3.7}Mo_{5.5}$, and (d) $Al_{87.9}Mn_{4.5}Mo_{7.6}$. The scan rate was 0.5 mV s^{-1}.

Figure 8. Pitting potentials of Al-Mn-Mo alloys: (a) $Al_{90.8}Mn_{3.7}Mo_{5.5}$, (b) $Al_{87.9}Mn_{4.5}Mo_{7.6}$, and (c) $Al_{91.0}Mn_{6.5}Mo_{2.5}$.

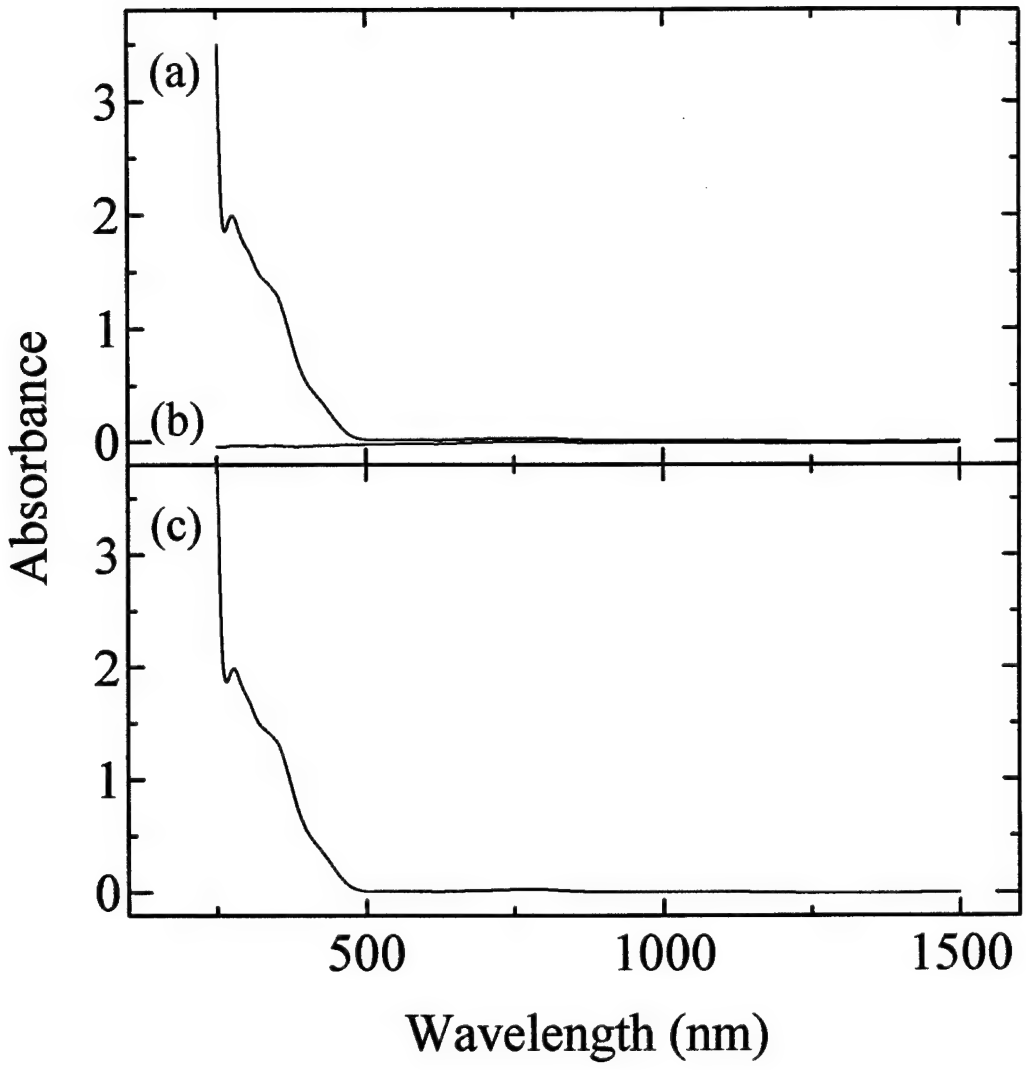
(a)
(b)
(c)
Absorbance
0
1
2
3
500
1000
1500
Wavelength (nm)

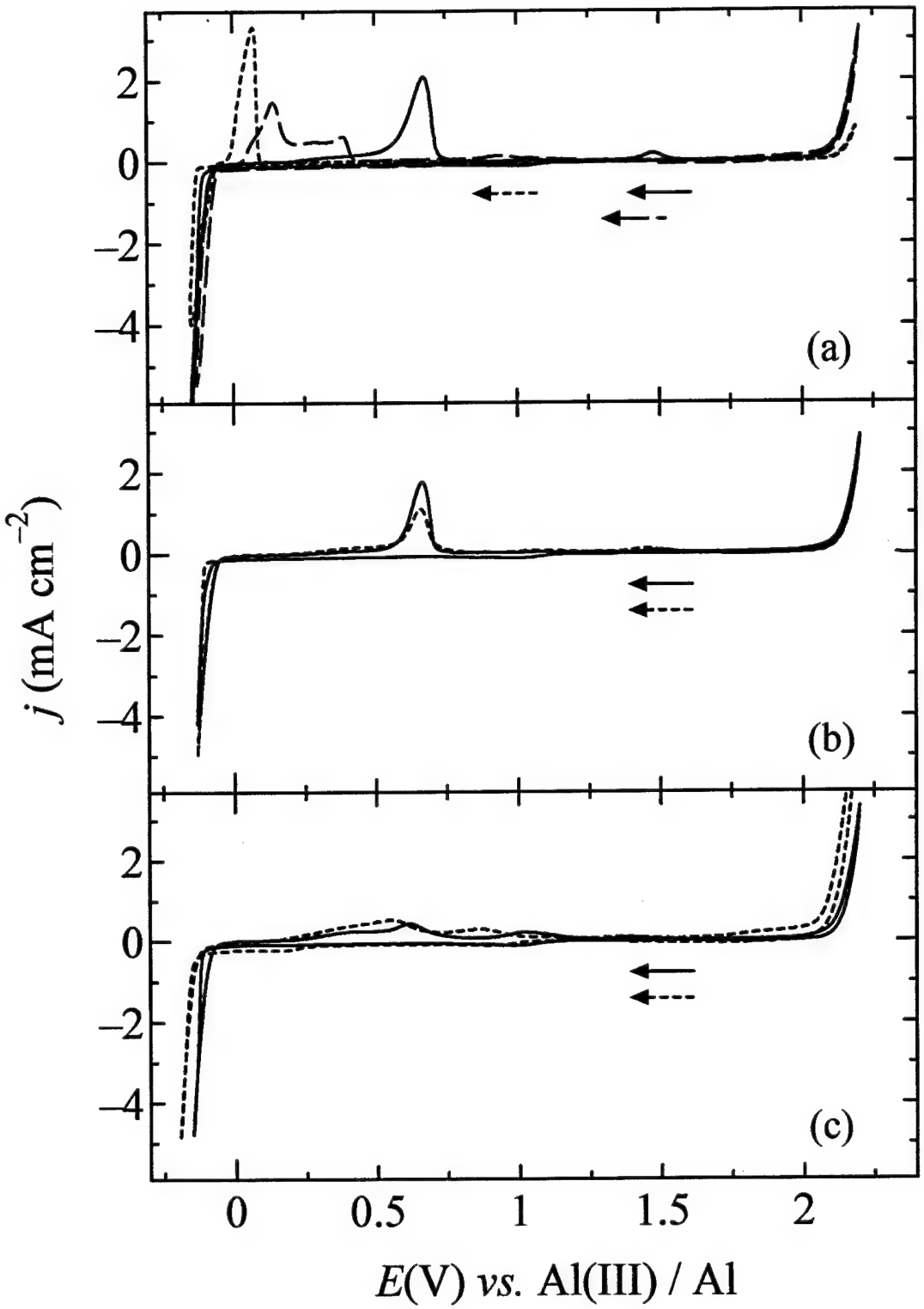
2
0
−2
−4
(a)
(b)
(c)
0
0.5
1
1.5
2
j (mA cm^{-2})
E(V) *vs.* Al(III) / Al

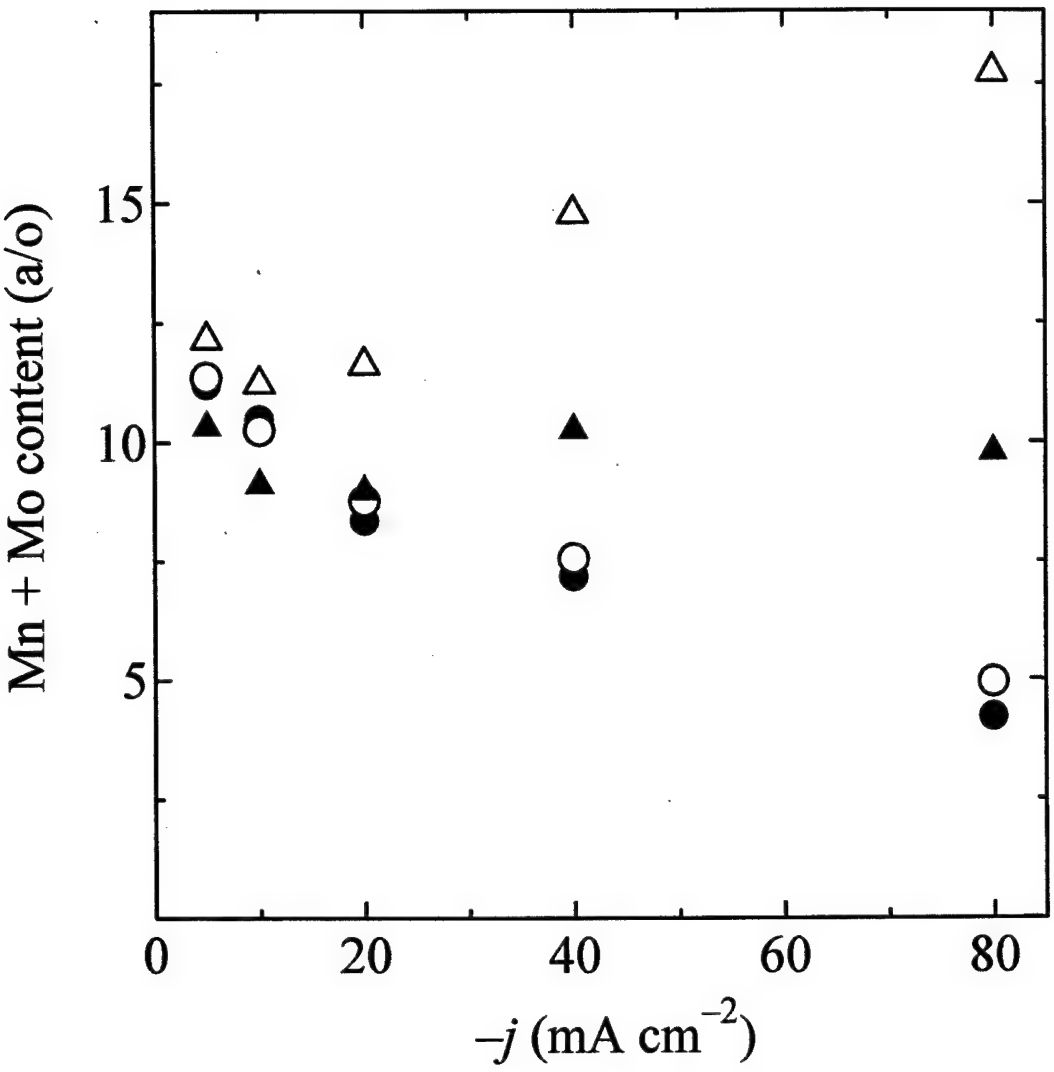
Mn + Mo content (a/o)
15
10
5
0
20
40
60
80
–j (mA cm–2)

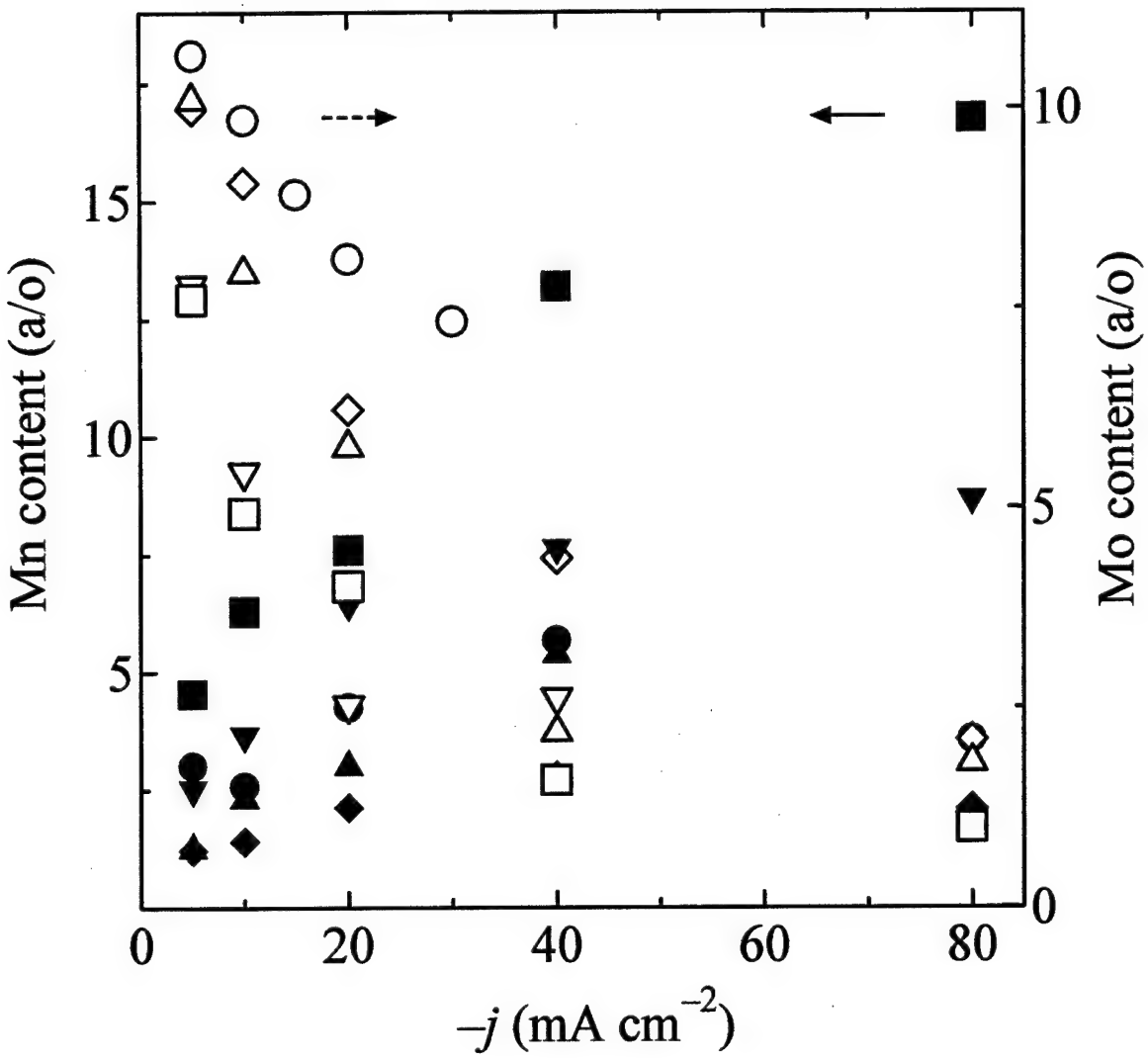
Mn content (a/o)
Mo content (a/o)
–j (mA cm–2)
0
20
40
60
80
5
10
15
0
5
10

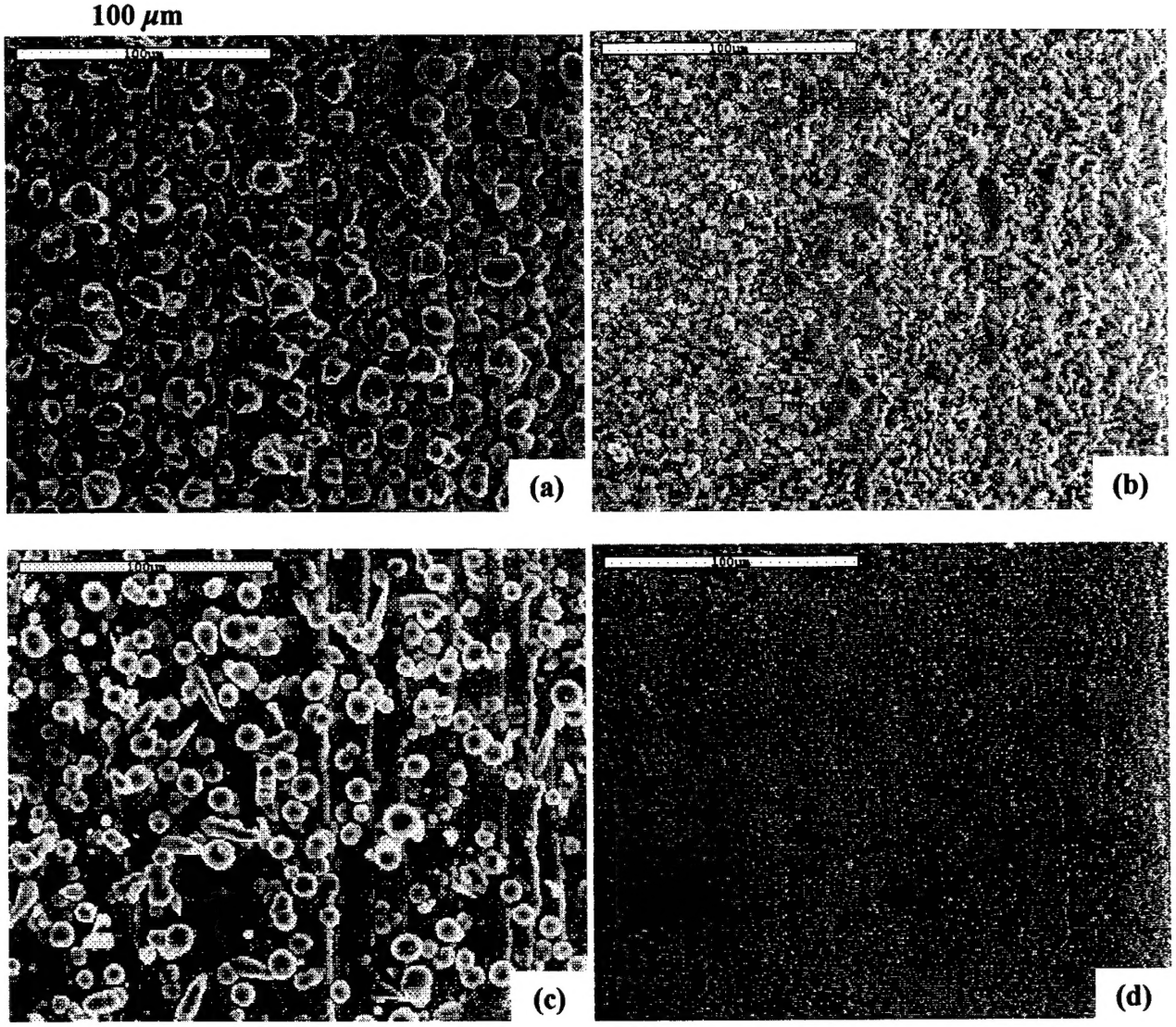
100 μm
100μm
(a)
100μm
(b)
100μm
(c)
100μm
(d)

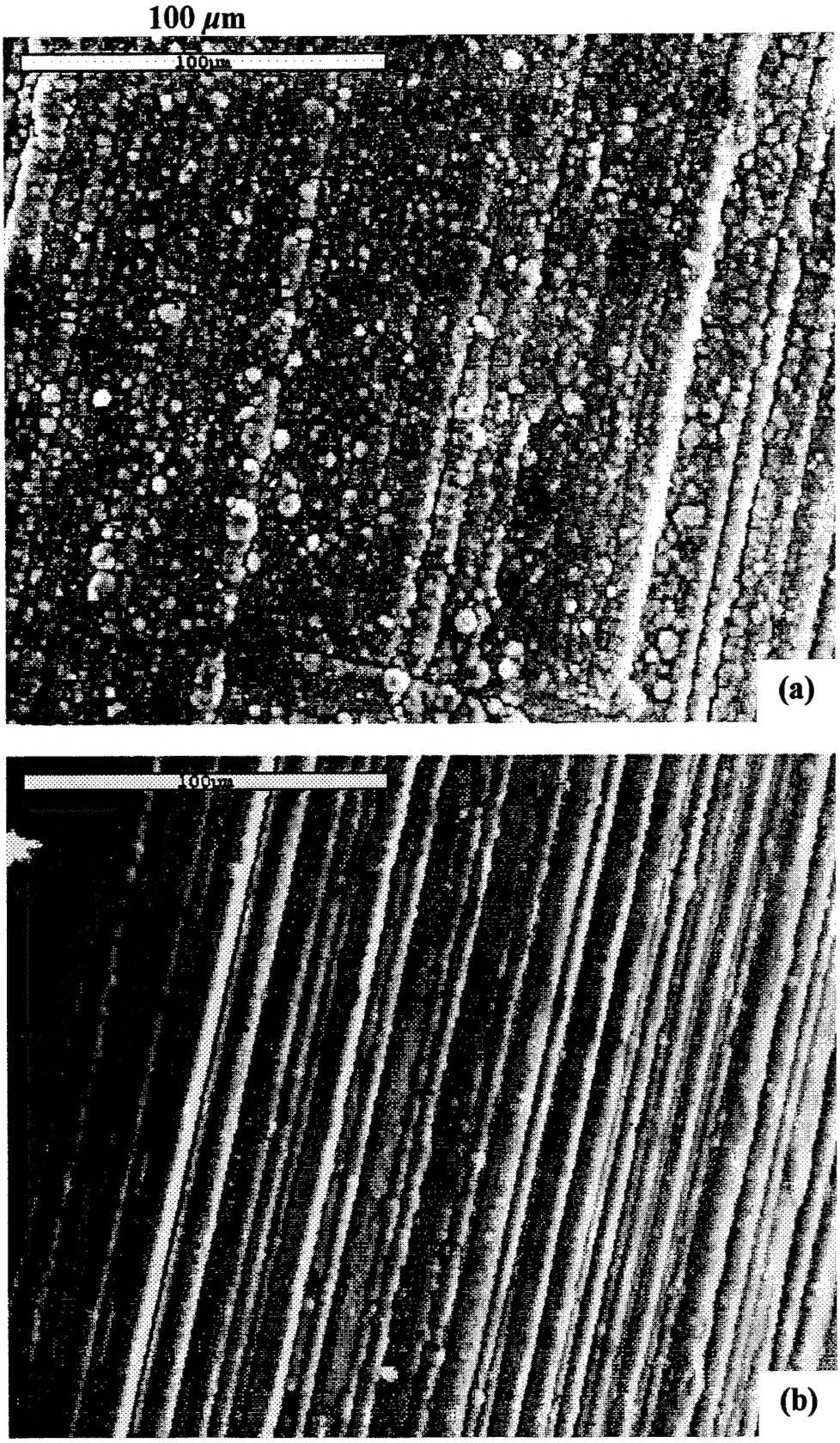
100 μm
100μm
(a)
100μm
(b)

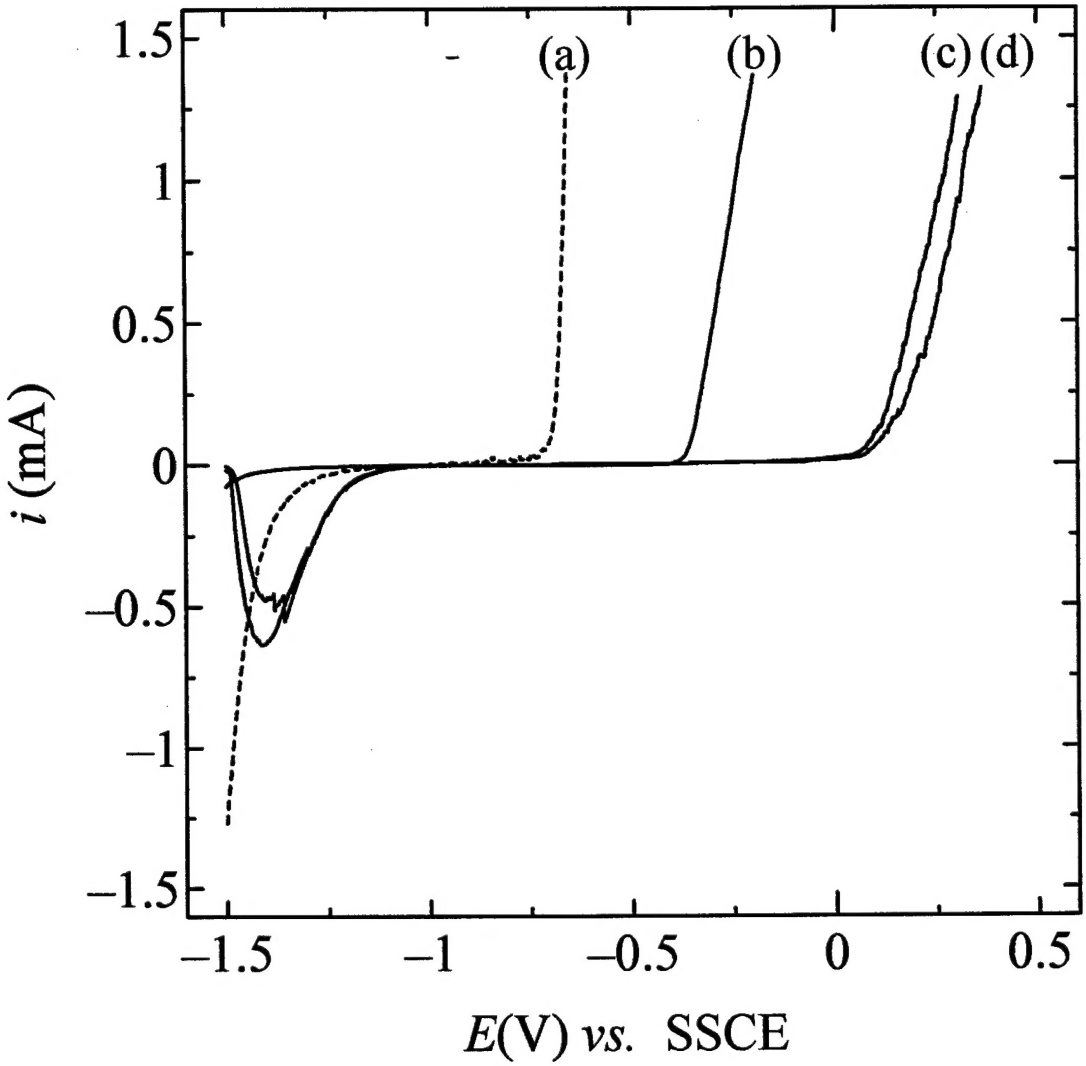
1.5
1
0.5
0
–0.5
–1
–1.5
i (mA)
(a)
(b)
(c)
(d)
–1.5
–1
–0.5
0
0.5
E(V) vs. SSCE

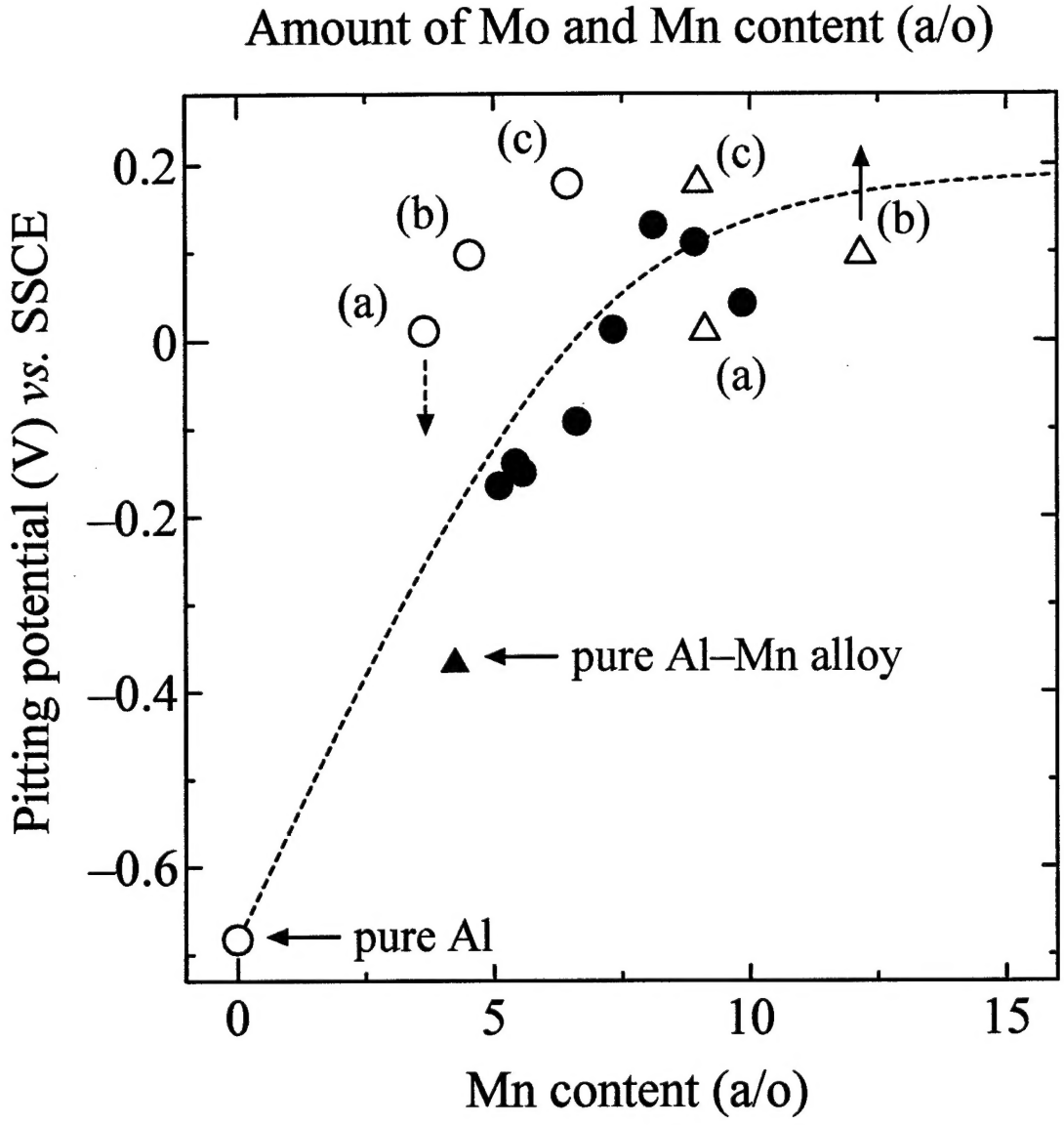
Amount of Mo and Mn content (a/o)
Pitting potential (V) vs. SSCE
0.2
0
–0.2
–0.4
–0.6
0
5
10
15
Mn content (a/o)
(a)
(b)
(c)
(a)
(b)
(c)
pure Al
pure Al–Mn alloy